



LUND UNIVERSITY

Theoretical Developments for the Real-Time Description and Control of Nanoscale Systems

Hopjan, Miroslav

2018

Document Version:

Publisher's PDF, also known as Version of record

[Link to publication](#)

Citation for published version (APA):

Hopjan, M. (2018). *Theoretical Developments for the Real-Time Description and Control of Nanoscale Systems*. [Doctoral Thesis (compilation), Mathematical Physics]. Lund University, Faculty of Science, Department of Physics, Division of Mathematical Physics.

Total number of authors:

1

Creative Commons License:

CC BY-NC-ND

General rights

Unless other specific re-use rights are stated the following general rights apply:

Copyright and moral rights for the publications made accessible in the public portal are retained by the authors and/or other copyright owners and it is a condition of accessing publications that users recognise and abide by the legal requirements associated with these rights.

- Users may download and print one copy of any publication from the public portal for the purpose of private study or research.
- You may not further distribute the material or use it for any profit-making activity or commercial gain
- You may freely distribute the URL identifying the publication in the public portal

Read more about Creative commons licenses: <https://creativecommons.org/licenses/>

Take down policy

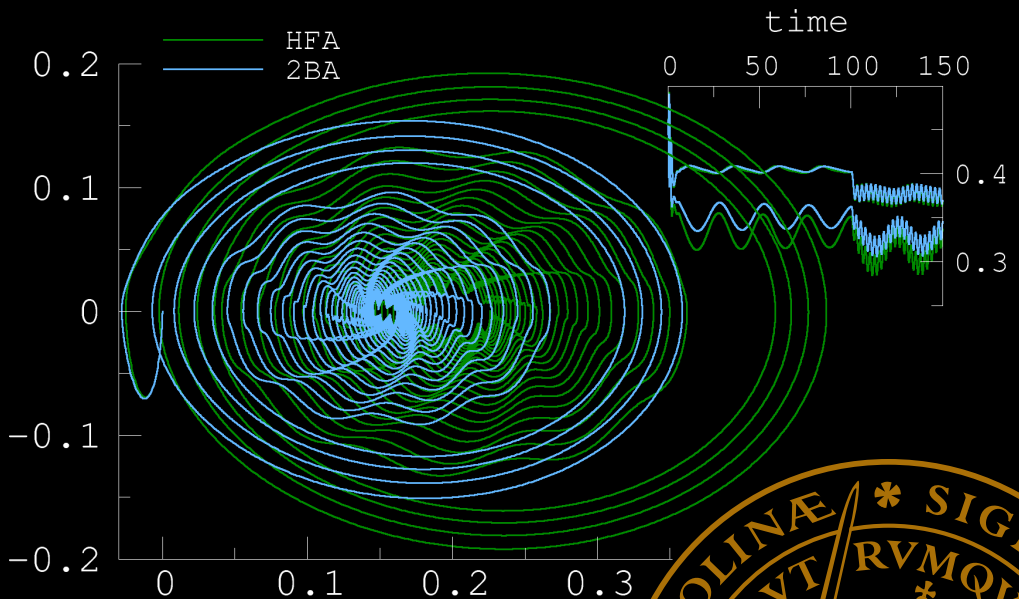
If you believe that this document breaches copyright please contact us providing details, and we will remove access to the work immediately and investigate your claim.

LUND UNIVERSITY

PO Box 117
221 00 Lund
+46 46-222 00 00

Theoretical Developments for the Real-Time Description and Control of Nanoscale Systems

MIROSLAV HOPJAN | DEPARTMENT OF PHYSICS | LUND UNIVERSITY 2018



Theoretical Developments for the Real-Time Description and
Control of Nanoscale Systems

Theoretical Developments for the Real-Time Description and Control of Nanoscale Systems

by Miroslav Hopjan



LUND
UNIVERSITY

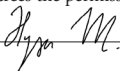
Thesis for the degree of Doctor of Philosophy
Thesis advisor: Assoc. Prof. Claudio Verdozzi
Faculty opponent: Prof. Michael Bonitz

To be presented, with the permission of the Faculty of Science of Lund University, for public criticism in the Rydberg lecture hall (Rydbergsalen) at the Department of Physics on Friday, the 23th of February 2018 at 13:15.

Organization LUND UNIVERSITY Department of Physics Box 118 SE-221 00 LUND Sweden	Document name DOCTORAL DISSERTATION
Author(s) Miroslav Hopjan	Date of disputation 2018-02-23 Sponsoring organization
Title and subtitle Theoretical Developments for the Real-Time Description and Control of Nanoscale Systems	
Abstract In this thesis we focus on improvements of the description of the electron-electron correlation effects in nonequilibrium nanosystems. We mainly focus on developments of two nonequilibrium methods, namely the formalism of <i>Nonequilibrium Green's Function</i> and <i>Time Dependent Density Functional Theory</i> and we explore the possibility to improve existing approximations in these theories. A smaller part of the thesis is devoted to the <i>Exact Diagonalization</i> method which provides a numerically exact description of small systems. Paper I: We review the current methods for description of correlated materials in nonequilibrium and their connection to pump-probe spectroscopy. Paper II: We propose a hybrid method for the real time dynamics of strongly correlated materials which includes memory effects beyond the adiabatic local density approximation. Paper III: We study the dynamics of desorption of a molecule from a surface with different levels of approximation for both the nuclear and the electronic part. We compare a full quantum mechanical treatment to the Ehrenfest approximation for the molecule and perturbative approximations for the electrons. Paper IV: We develop a theory of current-induced forces within Adiabatic Ehrenfest Dynamics which includes effects of electron-electron interactions. We study a dependence of the electronic friction on interaction strength. We also benchmark it against nonadiabatic Ehrenfest dynamics. Paper V: We study the competition of interaction and disorder in systems with steady state currents - in transport and ring geometries. We exactly define the exchange-correlation screening of the disorder by the interaction effects via Kohn-Sham construction of DFT. Paper VI: We study a competition between Kondo and RKKY interaction in small clusters of Periodic Anderson Model (ring geometries), we construct a nonequilibrium Doniach-phase like diagram. We then determine an optimal pulse to induce transitions with the highest fidelity.	
Key words Green's Function, DFT, TDDFT, Hubbard Model, Many-Body Perturbation Theory, Strongly Correlated Systems, Quantum Transport, Disorder, Ehrenfest Dynamics, Electronic Friction, Exact Diagonalization, Periodic Anderson Model	
Classification system and/or index terms (if any)	
Supplementary bibliographical information	Language English
ISSN and key title	ISBN 978-91-7753-499-0 (print) 978-91-7753-500-3 (pdf)
Recipient's notes	Number of pages 186 Security classification
	Price

Distribution by Miroslav Hopjan, Division of Mathematical Physics, Department of Physics, Box 118, SE-22100 LUND.

I, the undersigned, being the copyright owner of the abstract of the above-mentioned dissertation, hereby grant to all reference sources the permission to publish and disseminate the abstract of the above-mentioned dissertation.

Signature 

Date 2018-01-22

Theoretical Developments for the Real-Time Description and Control of Nanoscale Systems

by Miroslav Hopjan



LUND
UNIVERSITY

A doctoral thesis at a university in Sweden takes either the form of a single, cohesive research study (monograph) or a summary of research papers (compilation thesis), which the doctoral student has written alone or together with one or several other author(s).

In the latter case the thesis consists of two parts. An introductory text puts the research work into context and summarizes the main points of the papers. Then, the research publications themselves are reproduced, together with a description of the individual contributions of the authors. The research papers may either have been already published or are manuscripts at various stages (in press, submitted, or in draft).

Cover illustration front: The time evolution of a “molecular motor”. Phase space (p, x) characterisation and the density profile at the motor orbitals. (Adapted from paper IV.)

© 2018 Miroslav Hopjan

Paper I © 2014 Springer-Verlag Berlin Heidelberg

Paper II © 2016 American Physical Society

Paper III published 2016 under licence (CC-BY) by IOP Publishing Ltd

Paper IV © 2017 The Authors

Paper V © 2017 The Authors

Paper VI © 2018 The Authors

Faculty of Science, Department of Physics

ISBN: 978-91-7753-499-0 (print)

ISBN: 978-91-7753-500-3 (pdf)

Printed in Sweden by Media-Tryck, Lund University, Lund 2018



Contents

List of publications and author's contributions	v
Acknowledgements	ix
Popular summary in English	xi
I Background	I
1 Introduction	3
2 Strong electron-electron correlation and hybrid method	7
2.1 Hubbard model	8
2.2 NEGF on a lattice	9
2.3 DFT on a lattice	10
2.4 TDDFT on a lattice	12
2.5 TDDFT and the construction of the adiabatic local density approximation (ALDA)	12
2.6 Hybrid method	14
2.7 Perturbative solutions of the homogeneous Hubbard model	15
2.8 Exchange correlation potentials	16
2.9 On the performance of the hybrid method	18
2.10 Outlook: hybrid method for continuum	19
3 Electron-nuclear interactions and Ehrenfest dynamics	23
3.1 Electron-nuclei models	24
3.2 Ehrenfest dynamics	26
3.3 Nonadiabatic Ehrenfest dynamics	27
3.4 Strictly adiabatic Ehrenfest dynamics	27
3.5 Adiabatic Ehrenfest dynamics	29
3.6 On the performance of ED and AED	32
4 Disorder vs. interactions and DFT characterization	35
4.1 Anderson Model and Anderson–Hubbard Model	35
4.2 Solvers: steady-state KBE and exact diagonalization	37
4.3 DFT reconstruction procedure (reverse engineering)	38

4.4	Effect of disorder and disorder screening	40
5	Competing Kondo and RKKY interactions and optimal control	43
5.1	Single Kondo impurity and Kondo effect	43
5.2	Dense Kondo impurities and RKKY interaction	44
5.3	Single Impurity Anderson Model and Periodic Anderson Model	45
5.4	Kondo and RKKY physics in finite systems	45
5.5	Ground and equilibrium state	46
5.6	Time evolution and optimal control	48
	References	49
II	The papers	59
	Paper I: Probing Strongly Correlated Materials in Non-equilibrium: Basic Concepts and Possible Future Trends in First Principle Approaches	61
	Paper II: Merging Features from Green's Functions and Time Dependent Density Functional Theory: A Route to the Description of Correlated Materials out of Equilibrium?	101
	Paper III: Nonequilibrium Green's functions and atom-surface dynamics: Simple views from a simple model system	109
	Paper IV: Molecular Junctions and Molecular Motors: Including Electronic Correlations via Nonequilibrium Green's Functions	121
	Paper V: Systems with disorder, interactions, and out of equilibrium: The exact independent-particle picture from density functional theory	129
	Paper VI: Controlling Nonequilibrium Kondo-vs-RKKY Scenarios in Nanoclusters	137
III	Appendix	145
A	Derivation of gradient expansion rules	147
A.1	Derivative	147
A.2	Time integral	147
A.3	Multiplication	149
B	Generalized Kadanoff–Baym Ansatz	151
B.1	KBE - differential form	151
B.2	KBE - integral form	152
B.3	KBE - integral form - long-time limit	153
B.4	KBE - time-diagonal equation	153
B.5	GKBA - time-diagonal equation	155
B.6	Extended GKBA	156
B.7	GKBA - correlated ground state	158
B.8	GKBA - approximate correlated ground state	159
C	Selfenergy approximations for steady state KBE	161

C.1	Second Born approximation	161
C.2	T-matrix approximation	162
D	Gradient expansion	163
D.1	Retarded Green's function	163
D.2	Lesser Green's function	164
E	Optimal control - details	167

List of publications and author's contributions

This thesis is based on the following publications, referred to by their Roman numerals:

I Probing Strongly Correlated Materials in Non-equilibrium: Basic Concepts and Possible Future Trends in First Principle Approaches

M. Hopjan, C. Verdozzi

Topics Current Chemistry, 347: 347–384 (2014)

In this paper we review the current methods for description of correlated materials in nonequilibrium and their connection to pump-probe spectroscopy.

Contribution: I wrote a half of the first draft. I was part of the scientific discussions and the writing process.

II Merging Features from Green's Functions and Time Dependent Density Functional Theory: A Route to the Description of Correlated Materials out of Equilibrium?

M. Hopjan, D. Karlsson, S. Ydman, C. Verdozzi, and C.-O. Almbladh

Physical Review Letters, 116, 236402 (2016)

We propose a hybrid method for the real time dynamics of strongly correlated materials which includes memory effects beyond the adiabatic local density approximation.

Contribution: I constructed a program to compute double correction terms of exchange-correlation potentials. I conducted most of the simulations to test the method. I wrote the first draft. I was further part of the scientific discussions and the writing process.

III Nonequilibrium Green's functions and atom-surface dynamics: Simple views from a simple model system

E. Boström, **M. Hopjan**, A. Kartsev, C. Verdozzi, and C.-O. Almbladh
Journal of Physics: Conference Series 696 012007 (2016)

We study the dynamics of desorption of a molecule from a surface with different levels of approximation for both the nuclear and the electronic part. We compare a full quantum mechanical treatment to the Ehrenfest approximation for the molecule and perturbative approximations for the electrons.

Contribution: I computed a double correction terms of exchange-correlation potentials for the hybrid method. I implemented and tested the Ehrenfest dynamics in a Kadanoff–Baym code. I wrote half of the first draft. I was further part of the scientific discussions and the writing process.

IV Molecular Junctions and Molecular Motors: Including Electronic Correlations via Nonequilibrium Green's Functions

M. Hopjan, G. Stefanucci, E. Perfetto and C. Verdozzi
Draft submitted, arXiv:1712.08061 (2017)

We develop a theory of current-induced forces within Adiabatic Ehrenfest Dynamics which includes effects of electron-electron interactions. We study a dependence of the electronic friction on interaction strength. We also benchmark it against nonadiabatic Ehrenfest dynamics.

Contribution: Based on an idea and previous work of the coauthors, I formulated a new theory of current-induced forces in adiabatic Ehrenfest dynamics in presence of electron-electron interaction. I further implemented and tested the adiabatic Ehrenfest dynamics for the model system. I conducted simulations of nonadiabatic Ehrenfest dynamics within Kadanoff–Baym and Generalized Kadanoff–Baym Ansatz codes. I wrote the first draft. I was further part of the scientific discussions and the writing process.

v **Systems with disorder, interactions, and out of equilibrium: The exact independent-particle picture from density functional theory**

D. Karlsson, **M. Hopjan** and C. Verdozzi

Draft submitted, arXiv:1707.04216 (2017)

We study the competition of interaction and disorder in systems with steady state currents - in transport and ring geometries. We exactly define the exchange-correlation screening of the disorder by the interaction effects via Kohn–Sham construction of DFT.

Contribution: I provided an independent check of the transport geometry results and I conducted the simulations of the ring geometry with an exact diagonalization code. I was part of the scientific discussions and the writing process.

vi **Controlling Nonequilibrium Kondo-vs-RKKY Scenarios in Nanoclusters**

S. Ydman, **M. Hopjan** and C. Verdozzi

Draft to be submitted (2018)

We study a competition between Kondo and RKKY interaction in small clusters of Periodic Anderson Model (ring geometries), we construct a nonequilibrium Doniach-phase like diagram. We then determine an optimal pulse to induce transitions with the highest fidelity.

Contribution: I was part of the discussions of the optimal control implementation. I performed the calculations of the phase diagram and the optimal control. I wrote half of the first draft. I was part of the scientific discussions and the writing process.

All papers are reproduced with permission of their respective publishers.

Other publications, not included in this thesis:

Tunneling spectroscopy of superconducting nanospheres

M. Hopjan, P. Lipavský

Phys. Rev. B 89, 094507 (2014)

This paper is not included in the thesis since it results from my diploma work.

Acknowledgements

This thesis is a result of the last five years that I have spent in Lund. And, as almost always is the case, the way leading here was not straightforward. The thesis would not have been possible without the help of many people whom I met during these years. It is my pleasure to express here my gratitude to them.

Firstly, I would like to express biggest gratitude to my supervisor Claudio. Thank you for giving me the opportunity to do my doctoral studies in Lund. I particularly would like to thank you for offering me many interesting projects so I had the freedom to choose topics of my interest. I appreciate that you were always ready to help and discuss any matter, and that your door was always open to me. I have learned a lot from our long discussions and I have enjoyed working with you.

I am also grateful to current and former members of the research group for our common work on various projects. During my doctoral studies I had the opportunity to discuss my work with my co-supervisor Carl-Olof, always willing to share his insightful experience. My sincere thanks go to Daniel and Alexey for their nice work in the group which I also could built on. I am specially indebted to you Daniel for our common works and for the stimulating discussions whenever we meet. Emil, thank you for all your help and for exchanging ideas with me during the years. I would also like to acknowledge Simon for his effort in our common projects. Jeremie and Pernilla, it was nice to have you around and thank you for your help! I am also thankful to Gianluca and Enrico, our collaborators from Rome. Moreover, it was a pleasure to have interesting conversations with Ferdi, about a side project with him and Claudio, not included in this thesis. It was nice to work together with all of you. Finally, I wish to acknowledge Rei, Fredrik and Tor for discussions about the physics.

I am also grateful for beeing a member of the Mathematical Physics Division. My thanks go to the heads of our division, Sven and Peter, who always ensured a lively and stimulating environment. The division would not be the same without Cecilia and Katarina, thank you for creating a truly family atmosphere. Katarina, I specially thank you for all your help with every tiny practicality which made our everyday life easier. Let me also express my

gratitude to Florido and Lennart for their IT support.

My warm thanks go to my office mates Alexey, Ognjen, Jacob and Sara as well as short term visitors in our office, Stefano, Markus and Nastaran. Thank you all for brightening up our office, for all possible discussions enriching my cultural knowledge. I had a lot of fun during these years! I enjoyed having a good time with all members of the division on many occasions. I am particularly grateful to Elife, Francesc, Daniel, Ulrika, Gunnar, Fikeraddis, Sara, Bahareh, Yousef, David, Betül, Alex and Martin for organizing and attending most of the social events of our division.

Next, I want to express my sincere gratitude to people outside Lund who gave me additional support and encouragement during my doctoral studies. I always enjoy inspirational discussions with Pavel whenever I am in Prague. I am also thankful to Jakub, Filip and Jaromír for keeping in touch during the years. Finally, this thesis would not have been the same without Agnieszka and my family in Prague and Northern Moravia. Thank you for being with me, for your everyday support, patience and love.

Popular summary in English

In the age of miniaturization where the physical systems approach the nanoscale limit and where more complex materials are created there is necessity for understanding in terms of *quantum mechanics*. The understanding then opens and gives possibilities for manipulation and engineering of such systems and thus practical applications.

Quantum mechanics states that the electron cannot be characterized as a classical particle with a certain position and momentum. Instead the electron is described by the wave function, which gives the probability for the electron to be at certain space. The wave property of the electron then affects its behavior in nanoscale systems. In many electron systems the wave function concept becomes even more important.

In modern experiments, in order to learn more about the system, the strong and time-dependent external forces are often used to disturb the system out of its equilibrium state. One example is a pump-probe experiment where the strong electromagnetic pulse is used to transfer energy into the system and thus excite it into higher energy state. The second electromagnetic pulse can be used to probe the excited system and study relaxation processes taking place in the system.

Another experiment which can reveal the physical mechanism in a system is transport experiments where a central region is connected to leads which are electrically biased and an electric current is running through the central region. The leads are responsible for the excitation of the central region to higher energies but at the same time for the dissipation processes. Also, the magnetic field can be used to induce the nonequilibrium situation which can be useful for understanding the underlying physical processes. Ultimately the external time-dependent forces can also be used to manipulate with the system.

This brings us towards the main topic of the thesis. How to theoretically describe the influence of the external forces on a many electron system which cannot be longer described as a set of independent classical particles (in similar way as i.e. bouncing balls in classical gases)? In these systems quantum mechanics requires to construct a *many-body wave function* - an object which accounts for all possible effects of the interactions. The wave function

contains full information about the system from which one can access and possibly predict reduced quantities which can be measured.

However, to obtain the full many-body wave function and its time evolution is a difficult task, and the system size for which the wave function can be reached is limited. To bypass the computation of the full wave function alternative methods designed directly for the reduced quantities can be developed; among them, popular ones are the formalism of *Green's Function* and *Density Functional Theory*. These methods in principle account exactly for the many-body effects, however in practice the approximations are used. In addition, correspondingly to the experiment, the methods need to be extended to account for the nonequilibrium regime.

This thesis focus on improvements of the description of the electron-electron correlation effects in nonequilibrium nanosystems. We mainly focus on developments of two nonequilibrium methods, namely the formalism of *Nonequilibrium Green's Function* and *Time Dependent Density Functional Theory* and we explore the possibility to improve existing approximations in these theories. A smaller part of the thesis is devoted to the *Exact Diagonalization* method which provides a numerically exact description of small systems.

The outcome of the thesis will contribute to better understanding, improved description and consequently more efficient engineering of nanosystems where correlation effects are important. In particular, we consider the effect of i) strong electron-electron correlation, ii) electron-nuclear interactions, iii) disorder + interactions and iv) magnetic impurities.

Part I

Background

Chapter I

Introduction

A theoretical description of nanosystems usually requires the use of quantum mechanical formalism to account for effects beyond classical physics. Then in many cases we have to consider many particles (e.g. electrons) and their mutual interactions. The interactions between electrons have an impact on the behavior of a nanosystem and they induce interesting physical phenomena. To correctly account for such interactions is a challenging task, since usually there are several competing mechanisms at the same energy scale.

Before we attempt to manipulate nanosystems, we have to understand their dynamics while they are driven out of their equilibrium state. The out-of-equilibrium state, either steady or transient state, brings additional complications for a theoretical description. As a result a full understanding of nonequilibrium processes in realistic materials is still lacking.

As preliminary step to understand real materials, it is convenient to simplify our description and investigate model systems. Such model systems can still capture many features of the physical phenomena in real materials. In this thesis we consider a broad palette of physical phenomena: strong electron-electron interactions (correlations), electron-nuclear interactions, joint effects of disorder + interactions or competing magnetic correlations.

To describe such a variety of situations and systems we need to look for suitable methods. For small systems, and wherever possible, we use exact numerical methods: Exact Diagonalization and Time Dependent Density Renormalization Group (TDMRG). These methods can describe the exact dynamics, which is interesting in itself, but they also serve as our benchmark for approximate descriptions. For larger systems, due to the computational cost of the exact methods, one has to resort to approximations. For electrons we use Time Dependent Density Functional Theory (TDDFT) and Nonequilibrium Green's Function (NEGF). Each method is a reduced description of the full many-body problem (in principle exact), where further approximations are usually used. For heavy nuclei, the

quantum description can be approximated by the classical Ehrenfest dynamics.

To help the readers to orient themselves, we show a diagram in Fig.1.1, visualizing the connections between the methods and the different chapters of the thesis:

Strong electron-electron correlation and hybrid method. – In many modern complex materials and nanosystems, physical and chemical properties can be highly influenced by the electronic correlation. The Hubbard model is the simplest model capturing electron-electron correlations and the electron-driven Mott–Hubbard transition. Its time dynamics can be described by both TDDFT and NEGF methods, however only in limiting cases where particular approximations work. We present a new hybrid method which combines advantages of NEGF and TDDFT (and their approximations) for a better description of the time evolution of the electronic density.

Electron-nuclear interactions and Ehrenfest dynamics. – The electronic degrees of freedom are typically not isolated from others degrees of freedom, for example electrons can scatter on impurities and phonons. A local vibration mode can be especially important for small devices based on molecules. Here we consider models of interacting electrons coupled to heavy nuclear modes (atoms on surfaces, molecular motors) where in many instances one can leave the quantum regime of the nuclei and consider classical Ehrenfest dynamics. We include electron-electron interactions with the NEGF method and study the resulting classical-quantum dynamics.

Disorder vs. interactions and DFT characterization. – The Anderson–Hubbard model describes how disorder affects systems with electron-electron interactions. In fact disorder is inevitable in all realistic systems and for example a strong disorder can induce insulating behavior. Disorder can compete with the electron-electron interactions if they are of the same order. Then the effect of the disorder can be screened by the interactions. We use TDDFT to unambiguously define and quantify the screening of the disorder caused by interaction.

Competing Kondo and RKKY interaction and optimal control. – The Periodic Anderson Model (PAM) describes localized impurities with electron-electron interaction coupled to conduction electrons and as such may represent a model of a heavy fermion material. The single Anderson impurity is known to capture the Kondo effect – screening of localized electron spin by conduction electrons. If there is more than one impurity the localized electrons can mutually interact via conduction electrons. In the case of dense impurities (e.g. the PAM) the localized spin can be correlated either with the spin of the conduction electrons or with the neighbor localized spins – there is a competition of spin (magnetic) ordering. We will investigate small ring-shaped clusters which can be represent by the PAM, and how the magnetic ordering is influenced by a nonequilibrium steady-state current. We adapt optimal control theory to exact Lanczos propagation in order to find the best pulse to optimally manipulate the system between the two regimes.

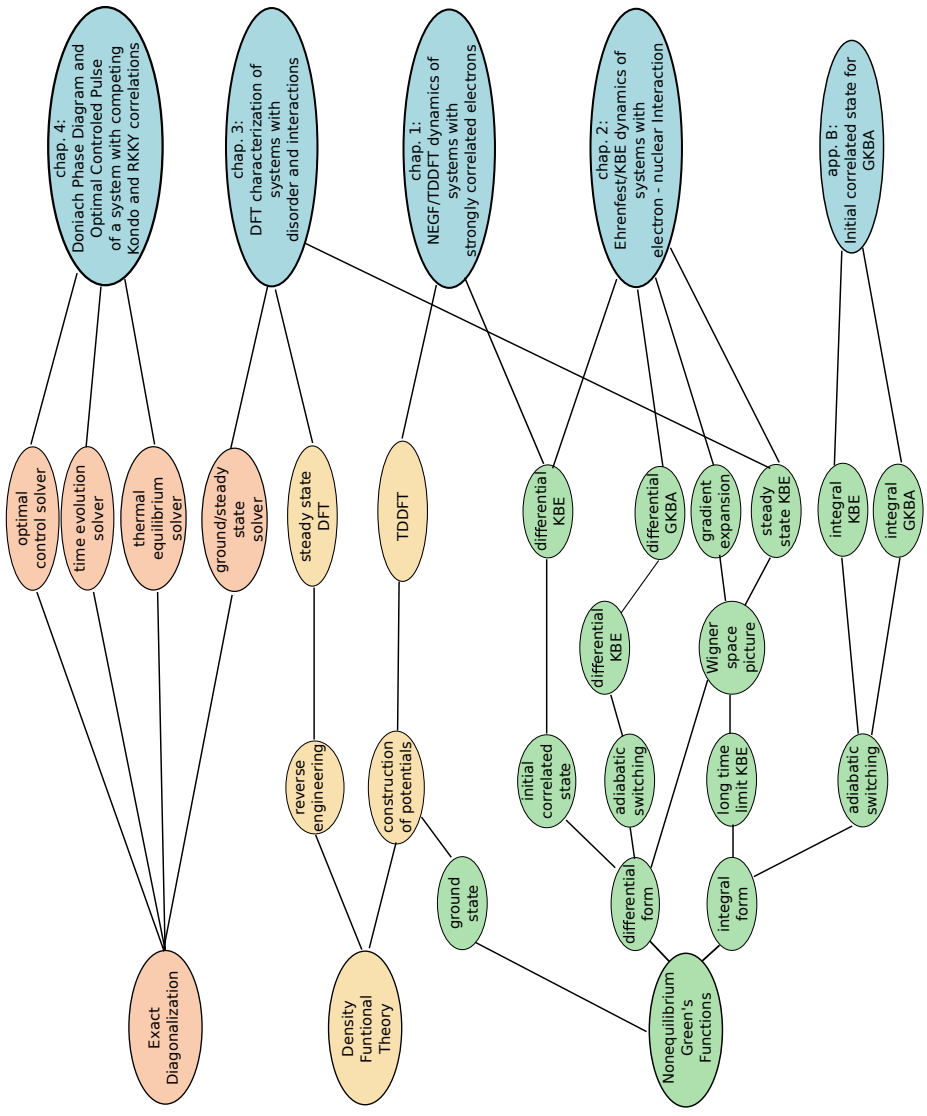


Figure 1.1: A diagram showing the methods discussed in this thesis and their connection to the chapters of the thesis. In the diagram the following acronyms are used: Density Functional Theory (DFT), Time Dependent Density Functional Theory (TDDFT), Nonequilibrium Green's Function (NEGF), Kadanoff-Baym Equations (KBE), Generalized Kadanoff-Baym Ansatz (GKBA) and Ruderman-Kittel-Kasuya-Yosida (RKKY).

Chapter 2

Strong electron-electron correlation and hybrid method

The theoretical description of electron-electron correlations can become problematic if the applied approximations are away from their region of validity. For example, standard methods such as Hartree–Fock or Density Functional Theory [1, 2] (DFT) in the so-called Local Density Approximation (LDA) are not performing well when strong electron-electron correlations are present. On the other hand, Dynamical Mean Field Theory [3] (DMFT) is successful for systems with strong electron-electron correlations at the localized orbitals and on lattices with high connectivity, but might be incorrect for systems with delocalized electrons and on low-connected lattices. From the examples it is clear that for systems outside the regions of validity, more advanced methods have to be used. Then, occasionally, the theoreticians resort to merge already existing methods and combine their strengths.

An example of such combination can be the LDA method merged with the Hubbard on-site interaction U , the so-called LDA+ U method [4]. It was created to be the appropriate method for description of strongly correlated Mott insulators regime. Another sophisticated scheme is to combine the LDA with the DMFT [5], sometimes known as LDA++ [6]. The main feature of this approach is that it takes into account the energy dependence of the electron selfenergy, with the momentum dependence being neglected. However, usually in such combined theories, a problem of double counting is naturally generated. To avoid the Hubbard interaction parameters and the double counting terms inherent to conventional “LDA+DMFT,” a hybrid “GW+DMFT” was proposed in 2003 [7]. The method combines the DMFT with the GW¹ method [8] and it captures the local correlations effects by DMFT with the nonlocal correlation effects by the GW. The careful choice of double

¹Here, the letter G stands for the Green’s Function and the letter W for the screened Coulomb interaction.

counting corrections in the GW+DMFT approach can lead for example to a reconsideration of the correlation effects in cubic perovskite SrVO₃ [9].

In this chapter, we generalize this idea for the groundstate calculations to the time domain. We are interested in the real-time evolution of the electron density in systems with strong electronic correlations after an external field is applied. The evolution of the electron density can be described with either the Nonequilibrium Green's Function (NEGF) method or Time Dependent Density Functional Theory (TDDFT). The performance of the methods, which were implemented for the Hubbard model, was reviewed in paper I [10]. It was concluded that the regime of very strong correlations and the strong nonadiabatic perturbations is not captured by any of the methods. The adiabatic TDDFT misses nonadiabatic effects, in the standard NEGF a breakdown of the perturbative approximations to the selfenergy can be observed. To overcome this problem we combine the strengths of the two methods and approximations, and illustrate the implementation on the Hubbard model. However, the idea is general and we also give an outlook for continuum systems. This chapter presents the background for the content of paper II (development of the hybrid method).

2.1 Hubbard model

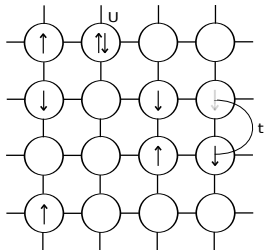


Figure 2.1: The 2D Hubbard model at quarter-filling.

The tight binding model is an effective description of electrons, mutually noninteracting, which are moving across a system with localized atomic orbitals that can be represented by the lattice. It has a simple form, in the standard notation of the second quantization:

$$\hat{H} = -t \sum_{\langle i,j \rangle, \sigma} \hat{c}_{i\sigma}^\dagger \hat{c}_{j\sigma} + \sum_{i, \sigma} v_i \hat{c}_{i\sigma}^\dagger \hat{c}_{i\sigma}, \quad (2.1)$$

where \hat{c}^\dagger creates the electron, \hat{c} annihilates the electron, σ is the spin index, t is the hopping parameter, $\langle \dots \rangle$ denotes nearest neighbor sites and v_i is the on-site energy at site i . The Hubbard model [11] represents the simplest extension of the tight binding model capturing correlation effects among electrons. It can be written as

$$\hat{H} = -t \sum_{\langle i,j \rangle, \sigma} \hat{c}_{i\sigma}^\dagger \hat{c}_{j\sigma} + \sum_{i, \sigma} v_i \hat{c}_{i\sigma}^\dagger \hat{c}_{i\sigma} + U \sum_i \hat{c}_{i\uparrow}^\dagger \hat{c}_{i\uparrow} \hat{c}_{i\downarrow}^\dagger \hat{c}_{i\downarrow}, \quad (2.2)$$

where the first part is the tight binding Hamiltonian and the latter term accounts for the on-site interaction between two electrons with strength U . The ratio $\frac{U}{t}$ relates to the strength of the correlations in the system. We keep $t = 1$ as our energy unit. We consider only the spin compensated one band Hubbard model, so the density n of each site can vary from 0 to 2 with half-filling at $n = 1$.

2.2 NEGF on a lattice

The time evolution of the density on a lattice can be described via nonequilibrium Green's function evolution [12, 13]. The lattice Green's function is defined as

$$G(1, 2) = -iT r[\hat{\rho} \mathbf{T}\{\hat{c}^\dagger(1)\hat{c}(2)\}], \quad (2.3)$$

where $1 = (i_1, \sigma_1, t_1)$ is a collective index of the lattice site (position), spin and time, $T r$ denotes the trace over the complete set of initial many-body states, \mathbf{T} is the contour time ordering operator and ρ is the statistical weight of the initial many-body states (equilibrium Gibbs distribution). The density is obtained from the relation

$$n(i_1, t_1) = \sum_{\sigma} (-i)G(1, 1^+), \quad (2.4)$$

where the time on the time contour is ordered as $t_{1^+} > t_1$. The Green's function can be evolved with the Kadanoff–Baym equation for the time t_1 (and similarly for t_2)

$$[i\partial_{t_1} - \hat{t} - v_H(1) - v_{ext}(1)]G(1, 2) = \delta(1, 2) + \int_{\gamma} d3(\Sigma_{emb} + \Sigma_{xc})(1, 3)G(3, 2), \quad (2.5)$$

where the integral runs over the Schwinger–Keldysh contour γ [15, 16], \hat{t} is the kinetic energy, v_H is the Hartree field and v_{ext} is a time-dependent external field. The embedding selfenergy Σ_{emb} describes the effect of noninteracting leads and the exchange correlation (XC) selfenergy Σ_{xc} is the key element which accounts for many-body effects beyond the Hartree field.

Examples of standard approximations of the XC selfenergy are depicted in Fig. 2.2 in terms of Feynman diagrams. We choose approximations which can be represented by diagrams

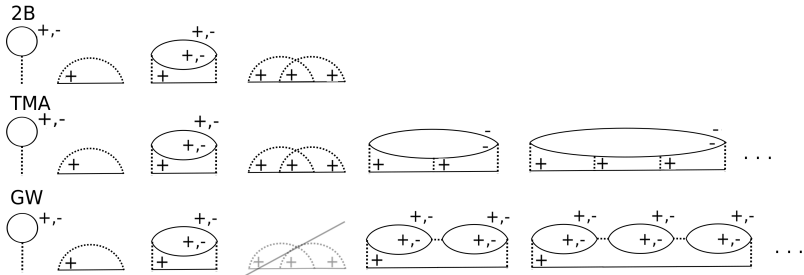


Figure 2.2: Taken from [14] with the agreement of the author. Standard many-body approximations in terms of diagrams; the 2B in the top, the TMA in the middle and the GW in the bottom. The 2B approximation consists of all diagrams up to second order. In the TMA ladder diagrams up to infinite order are included. The GW approximation is constructed from polarization electron-hole “bubbles”. The spin projections are denoted by “+” and “-”.

constructed from the dressed Green's function, hence assuring the conservation laws of Baym and Kadanoff [17]. Thus we work within the second Born (2B) approximation, T-matrix (TMA) approximation [18] and the screened potential GW approximation [8], see Fig.2.2.

The time evolution of the Hubbard model with such selfenergies has already been tested elsewhere [19, 20] and here we only summarize the main aspects. For weak interactions the 2B and TMA approximations perform rather well. For low filling, the TMA works well even for strong interactions. However the perturbative nature of the approximations does not allow for a good description around half-filling ($n=1$) and for strong interactions. The dynamics with the perturbative selfenergies Σ_{xc}^{PT} written as

$$[i\partial_{t_1} - \hat{t} - v_H(1) - v_{ext}(1)]G(1, 2) = \delta(1, 2) + \int_{\gamma} d\mathcal{B}(\Sigma_{emb} + \widehat{\Sigma_{xc}^{PT}})(1, 3)G(3, 2), \quad (2.6)$$

can well describe nonlocal and nonadiabatic effects, but only in the weakly correlated limit. To describe the effects of strong correlations one need to construct a nonperturbative double time selfenergy $\Sigma_{xc}^{np}(1, 2)$. A possible approach could be to use the nonequilibrium extension of DMFT [21]. An alternative way to introduce the effects of strong correlations is to use TDDFT, which will be introduced in the next sections.

2.3 DFT on a lattice

In the first DFT paper [1] Hohenberg and Kohn prove that there is a one to one correspondence between the ground state density n and the external potential which shapes the density and the ground state wave function $|\Psi_n\rangle$. One starts by constructing the universal functional $F[n]$:

$$F[n] = \langle \Psi_n | \hat{T} + \hat{U} | \Psi_n \rangle, \quad (2.7)$$

where \hat{T} is the kinetic energy operator and \hat{U} the interaction term operator. The energy functional is constructed by adding the interaction of the density with the external potential

$$E_{v_{ext}}[n] = \int v_{ext}(r)n(r)dr + F[n], \quad (2.8)$$

which can be seen as Legendre transform of $F[n]$. The energy functional $E_{v_{ext}}[n]$ is finally minimized for the ground state density and the problem is thus formulated in a variational manner. However to find the exact $F[n]$ is notoriously difficult.

In order to proceed with the construction of $F[n]$, Kohn and Sham [2] proposed to replace the interacting system with an auxiliary noninteracting one in some effective potential. The

potential acts such that it reproduces the ground state density of the interacting system. The functional $F[n]$ can be written as

$$F[n] = T[n] + U[n] = T_0[n] + E_H[n] + E_{xc}[n], \quad (2.9)$$

where $T[n]$ is the kinetic energy functional of the interacting system, $U[n]$ is the electron-electron interaction energy functional, $T_0[n]$ is the kinetic energy of the noninteracting system, $E_H[n]$ is the Hartree energy functional and $E_{xc}[n]$ is the exchange correlation functional. The latter contains all the intricacies of the construction (notice that $E_{xc}[n]$ accounts for part of T ;) and needs to be approximated for the purpose of any practical applications. Using the variational principle, the variation of the functional $F[n]$ in the noninteracting system leads to the Kohn–Sham equations, which are

$$(\hat{t} + v_{\text{KS}})\phi_\kappa = \epsilon_\kappa\phi_\kappa, \quad (2.10)$$

where the form of the kinetic energy operator is known for the independent particles $\hat{t} = -\frac{1}{2}\nabla^2$. The Kohn–Sham potential v_{KS} is defined as

$$v_{\text{KS}} = v_{\text{ext}} + \frac{\delta E_H}{\delta n} + \frac{\delta E_{xc}}{\delta n} = v_{\text{ext}} + v_H + v_{xc}, \quad (2.11)$$

where v_{ext} is the external potential, v_H the Hartree potential, and v_{xc} the XC potential. The density is constructed from the Kohn–Sham orbitals ϕ_κ

$$n_{\text{KS}} = 2 \sum_{\kappa}^{\text{occ}} |\phi_\kappa|^2, \quad (2.12)$$

where the factor 2 comes from a sum over spin. The set of equations (2.10) and (2.12) is solved iteratively until self-consistency is reached.

DFT on a lattice was for the first time introduced in Ref. [22] and further rigorously developed in the series of papers [23, 24, 25]. In lattice DFT the density is defined at the lattice points similarly to a continuum

$$n_{\text{KS}}(i) = 2 \sum_{\kappa}^{\text{occ}} |\phi_\kappa(i)|^2, \quad (2.13)$$

and is accordingly determined by the lattice Kohn–Sham equations

$$(\hat{t} + v_{\text{KS}})\phi_\kappa(i) = \epsilon_\kappa\phi_\kappa(i), \quad (2.14)$$

where \hat{t} is written as a matrix and ϕ as a vector. The problem is solved by diagonalization which is repeated until selfconsistency is reached.

2.4 TDDFT on a lattice

Time dependent DFT was firstly introduced in Ref. [26] where the one to one correspondence between the time-dependent density and the time-dependent potential was proven within what is now known as the Runge–Gross theorem. The uniqueness of the potential allows us to write the time evolution of the corresponding Kohn–Sham system

$$(\hat{t} + (v_H + v_{ext} + v_{xc})(t))\phi_\kappa(t) = i\partial_t\phi_\kappa(t), \quad (2.15)$$

where the time-dependent Kohn–Sham density

$$n_{\text{KS}}(t) = 2 \sum_{\kappa}^{\text{occ.}} |\phi_\kappa(t)|^2, \quad (2.16)$$

reproduces the density of the original system. The ground state is solved first and then the time evolution is performed.

The lattice version for TDDFT was first introduced a decade ago in Ref. [27], while the questions of uniqueness was solved only very recently [28]. Thus we can write the time-dependent Kohn–Sham equations for the orbitals defined at the lattice points i

$$(\hat{t} + (v_H + v_{ext} + v_{xc})(i, t))\phi_\kappa(i, t) = i\partial_t\phi_\kappa(i, t), \quad (2.17)$$

where the time-dependent density is

$$n(i, t) = 2 \sum_{\kappa}^{\text{occ.}} |\phi_\kappa(i, t)|^2. \quad (2.18)$$

The equations of lattice TDDFT above can be reformulated in terms of a Kohn–Sham nonequilibrium Green’s function as

$$[i\partial_{t_1} - \hat{t} - v_H(1) - v_{ext}(1) - v_{xc}(1)]G_{\text{KS}}(1, 2) = \delta(1, 2) + \int_{\gamma} d3 \Sigma_{emb}(1, 3)G_{\text{KS}}(3, 2). \quad (2.19)$$

with the connection $n(i_1, t_1) = \sum_{\sigma} (-i)G_{\text{KS}}(1, 1^+)$ to Eq. (2.18). Notice that in the Kohn–Sham Green’s function formulation we can naturally include the effects of the leads (if present) via the embedding selfenergy.

2.5 TDDFT and the construction of the adiabatic local density approximation (ALDA)

The XC potential is a functional of the density: $v_{xc}[n](i, \sigma, t)$, and is the key ingredient of TDDFT. A general shape for the functional is unknown, therefore certain simplification

should be used. The functional is usually approximated by the Adiabatic Local Density Approximation (ALDA). In ALDA the functional at lattice site i and time t is constructed solely from the density $n(i, t)$ at site i and time t . The value of the functional is defined by a homogeneous reference system with a uniform density matching $n(i, t)$. More formally for the spin compensated system

$$v_{xc}[n](i, \sigma, t) \approx v_{xc,\text{ref.}}(n(i, t)). \quad (2.20)$$

For the homogeneous system the functional derivative becomes a partial derivative

$$v_{xc,\text{ref.}}(n) = \frac{\partial}{\partial n} e_{xc,\text{ref.}}(n), \quad (2.21)$$

where $e_{xc,\text{ref.}} = \lim_{L \rightarrow \infty} \frac{E_{xc,\text{ref.}}}{L}$ is the XC energy per site (L is a number of sites). Further $e_{xc,\text{ref.}}(n) = e_{\text{tot.},\text{ref.}}(n) - t_0(n) - e_H(n)$ are the total energy per site, the non-interacting kinetic energy per site and the Hartree energy per site, respectively.

Since we are focusing on lattice TDDFT, a suitable reference system for short range interaction is the d -dimensional homogeneous Hubbard model. If we are able to find an exact solution for the ground state energy, we will be able to construct an optimal ALDA. In this respect the 1D Hubbard model benefits from its analytical solution via the Bethe–Ansatz [29]. The optimal LDA for the 1D Hubbard model constructed from the Bethe–Ansatz is usually denoted as BALDA [29]. This approximation, rigorously introduced in Ref. [24] and further discussed in Ref. [25], was benchmarked against the Monte Carlo method and successfully used to describe Mott plateaus in cold gas [30]. This is a consequence of the lattice XC potential having a discontinuity at half-filling. In 3D the solution of the paramagnetic ground state energy for the homogeneous case can be successfully approximated by DMFT [31] and this also allows us to use an optimal ALDA. For the 3D Hubbard model [31], the discontinuity of the XC potential appears only above a certain critical value $U = U_{cr.}$ of the interaction strength, i.e. a manifestation of the Mott–Hubbard transition along the interaction U .

With the optimal XC potentials in the ALDA $v_{xc,\text{ref.}}^{np}$, the evolution of the Kohn–Sham Green’s function is then governed by

$$\begin{aligned} & \text{local adiabatic} \\ & \text{strongly correlated} \\ & [i\partial_{t_1} - \hat{t} - v_H(1) - v_{ext}(1) - \overbrace{v_{xc,\text{ref.}}^{np}}(n(i_1, t_1))] G_{\text{KS}}(1, 2) = \delta(1, 2) + \int_{\gamma} d3 \Sigma_{emb}(1, 3) G_{\text{KS}}(3, 2). \end{aligned} \quad (2.22)$$

The above equation can well describe strong correlation effects, but only in the local and adiabatic limit. Such evolution misses memory effects and for more rapid changes of the densities it breaks down [32, 10]. In the next section we describe how to overcome this limitation.

2.6 Hybrid method

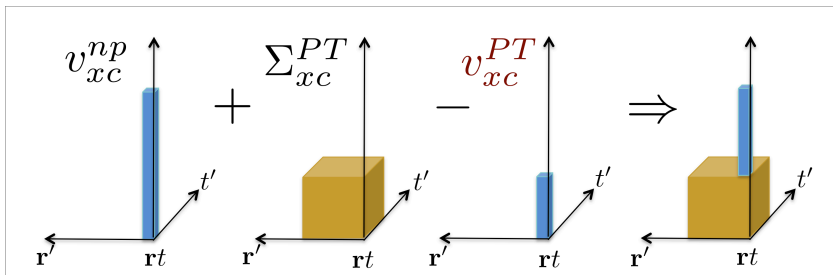


Figure 2.3: Schematic representation of locality in time and space and level of description of correlations in the hybrid method. The nonperturbative XC potential v_{xc}^{np} plus the perturbative XC selfenergy Σ_{xc}^{PT} double counts the local perturbative effects. The perturbative XC potential v_{xc}^{PT} is then subtracted to avoid the double counting. (The hybrid method still misses the nonlocal and nonadiabatic effects which are beyond the perturbative level.)

In the previous sections we presented the NEGF and TDDFT methods. In each method, there was the key ingredient which needed to be approximated; this was the XC selfenergy in NEGF and the XC potential in TDDFT. The approximations have their pros and cons. NEGF can describe nonadiabatic and nonlocal effects but only in the weakly correlated limit and TDDFT can describe strong correlation effects but only in the local and adiabatic limit. One step forward is to take advantage of both methods. The combination of both needs to be done carefully to avoid double counting, see Fig. 2.3.

The basic equation of our approach is

$$[i\partial_{t_1} - h_H(1, 2) - \overbrace{(v_{xc,ref.}^{np} - v_{xc,ref.}^{PT})}^{\text{strongly correlated double counting correction}}(n(i_1, t_1))]G(1, 2) = \delta(1, 2) + \int_{\gamma} d\mathcal{B}(\Sigma_{emb} + \overbrace{\Sigma_{xc}^{PT}}^{\text{nonlocal nonadiabatic}})G, \quad (2.23)$$

where $h_H(1, 2) = \hat{t} + v_H(1) + v_{ext}(1)$. The equation contains both key ingredients, the nonperturbative XC potential $v_{xc,ref.}^{np}$ and the perturbative XC selfenergy Σ_{xc}^{PT} . Additionally a perturbative XC potential $v_{xc,ref.}^{PT}$ is included.

The perturbative XC potential is an important ingredient because it corrects double counting of the local correlations, see Fig. 2.3. The perturbative XC potential must be of the same kind as the perturbative selfenergy. This corresponds to computing the ground state energy, for the reference system - the homogeneous Hubbard model, via the Green's function with a selfenergy containing the corresponding diagrams. In the next section we examine in details how to compute the ground state Green's function and the ground state energy.

2.7 Perturbative solutions of the homogeneous Hubbard model

At equilibrium, where the Green's function depends only on the difference of the coordinates ($i_1 - i_2, t_1 - t_2$), it is natural to perform calculations in frequency and momentum space (ω, \mathbf{k}). For the approximations based on the selfconsistently dressed diagrams, the total energy per site and spin can be computed with the Galitskii–Migdal formula [33]

$$\frac{e_{tot,ref.}}{2} = \frac{-1}{(2\pi)^{d+1}} \int_{-\infty}^{\infty} \int_{BZ} d\omega d\mathbf{k} (\omega + \epsilon(\mathbf{k})) \text{Im} G^R(\omega, \mathbf{k}) f(\omega), \quad (2.24)$$

where G^R is the retarded Green's function and f is the Fermi function. The corresponding density per site and spin can be computed as

$$\frac{n}{2} = \frac{-2}{(2\pi)^{d+1}} \int_{-\infty}^{\infty} \int_{BZ} d\omega d\mathbf{k} \text{Im} G^R(\omega, \mathbf{k}) f(\omega), \quad (2.25)$$

and is fixed by the chemical potential in the Fermi function. In practice one scans values of the chemical potential and looks at the resulting density and energy values.

To solve for the Green's function, we use the Dyson equation

$$G^{-1}(\omega, \mathbf{k}) = G_0^{-1}(\omega, \mathbf{k}) - v_H - \Sigma_{xc,ref.}^{appr.}(\omega, \mathbf{k}), \quad (2.26)$$

where $G(\omega, \mathbf{k})$ is the time ordered propagator v_H is the Hartree potential and $\Sigma_{xc,ref.}^{appr.}(\omega, \mathbf{k})$ is the XC selfenergy. To compute $\Sigma_{xc,ref.}^{appr.}(\omega, \mathbf{k})$ we use the many-body approximations as in Fig. 2.2 which can be written with help of the time ordered Green's function:

- For the 2B approximation (HXC stands for Hartree exchange correlation)

$$\begin{aligned} \Sigma_{Hxc,ref.}^{2B}(\omega, \mathbf{k}) &= \frac{U}{(2\pi)^{(d+1)}} \int_{-\infty}^{\infty} \int_{BZ} d\omega' d\mathbf{k}' (-i) G(\omega', \mathbf{k}') + \\ &+ \frac{U^2}{(2\pi)^{2(d+1)}} \int_{-\infty}^{\infty} \int_{-\infty}^{\infty} \int_{BZ} \int_{BZ} d\omega' d\omega'' d\mathbf{k}' d\mathbf{k}'' \\ &\times G(\omega', \mathbf{k}') G(\omega'', \mathbf{k}'') G(\omega - \omega' + \omega'', \mathbf{k} - \mathbf{k}' + \mathbf{k}''). \end{aligned} \quad (2.27)$$

- To obtain TMA approximation one first constructs a particle-particle propagator

$$\mathcal{G}(\omega, \mathbf{k}) = \frac{1}{(2\pi)^{(d+1)}} \int_{-\infty}^{\infty} \int_{BZ} d\omega' d\mathbf{k}' G(\omega', \mathbf{k}') G(\omega - \omega', \mathbf{k} - \mathbf{k}'), \quad (2.28)$$

and then a partial summation to infinite order of the particle-particle propagator

$$\mathcal{T}(\omega, \mathbf{k}) = -iU + iU\mathcal{G}(\omega, \mathbf{k})\mathcal{T}(\omega, \mathbf{k}), \quad (2.29)$$

which gives the T-matrix $\mathcal{T}(\omega, \mathbf{k})$. The selfenergy is constructed as

$$\Sigma_{Hxc, \text{ref.}}^{TMA}(\omega, \mathbf{k}) = \frac{1}{(2\pi)^{(d+1)}} \int_{-\infty}^{\infty} \int_{BZ} d\omega' d\mathbf{k}' G(\omega', \mathbf{k}') \mathcal{T}(\omega + \omega', \mathbf{k} + \mathbf{k}'). \quad (2.30)$$

where $\Sigma_{Hxc, \text{ref.}}^{TMA}(\omega, \mathbf{k}) = v_H + \Sigma_{xc, \text{ref.}}^{TMA}(\omega, \mathbf{k})$ already contains the Hartree contribution.

- For the GW approximation one first constructs the polarization particle-hole bubble

$$\mathcal{P}(\omega, \mathbf{k}) = -2i \frac{1}{(2\pi)^{(d+1)}} \int_{-\infty}^{\infty} \int_{BZ} d\omega' d\mathbf{k}' G(\omega', \mathbf{k}') G(\omega + \omega', \mathbf{k} + \mathbf{k}'), \quad (2.31)$$

and then a partial summation to infinite order of the polarization particle-hole bubbles

$$\mathcal{W}(\omega, \mathbf{k}) = U + U\mathcal{P}(\omega, \mathbf{k})\mathcal{W}(\omega, \mathbf{k}), \quad (2.32)$$

which gives a screened potential $\mathcal{W}(\omega, \mathbf{k})$. The screened potential is then used to construct the selfenergy

$$\begin{aligned} \Sigma_{Hxc, \text{ref.}}^{GW}(\omega, \mathbf{k}) &= \frac{U}{(2\pi)^{(d+1)}} \int_{-\infty}^{\infty} \int_{BZ} d\omega' d\mathbf{k}' (-2i) G(\omega', \mathbf{k}') + \\ &+ \frac{1}{(2\pi)^{(d+1)}} \int_{-\infty}^{\infty} \int_{BZ} d\omega' d\mathbf{k}' G(\omega - \omega', \mathbf{k} - \mathbf{k}') \mathcal{W}(\omega', \mathbf{k}'). \end{aligned} \quad (2.33)$$

In practice we then use the Langreth–Wilkins rules [34] to obtain equations in terms of the retarded G^R , advanced G^A , lesser $G^<$ and greater $G^>$ Green's functions. Further, the fluctuation-dissipation relations $G^< = -2\text{Im}G^R f$ and $G^> = 2\text{Im}G^R(1 - f)$ and the relation $G^A = (G^R)^\dagger$ are used to rewrite the selfenergies in terms of only G^R . The selfenergies are constructed with help of the Fourier transform and the Dyson equation is then iterated until self-consistency is reached.

2.8 Exchange correlation potentials

In this section the exchange correlation potentials from the approximate solutions of the reference homogeneous Hubbard model are presented and, where possible, they are compared to exact solutions. We investigate mainly the behavior of the potentials with respect to the dimensionality of the lattice. In Fig. 2.4 the potentials for 1D, 2D and 3D are displayed.²

²Fig.2.4 is taken from [14] with the author's permission. Some of the potentials from Fig.2.4 are originally published elsewhere. In 1D the BALDA and 2B are taken from Ref. [35], and the TMA for $U = 4$ is published in Ref. [36]. In 3D the DMFT-LDAs shown in Ref. [31] and the 2B as well as the TMA for $U = 24$ are reported in Ref. [36].

In 1D we compare the potentials coming from the approximate perturbative solutions with the exact BALDA potential by Lieb and Wu [29]. The BALDA potential displays a discontinuity at half-filling, which is the signature of Mott physics. The discontinuity persists for all non-zero interaction strengths; such feature reflects the absence of Mott–Hubbard transition in 1D. Among the approximate potentials, none exhibits the discontinuity at half-filling which, seems to be a natural behavior for the perturbative potentials. We note that also non-selfconsistent perturbation theory, e.g. the non-selfconsistent second Born approximation [24, 37], predicts a continuous potential. Besides, we can also observe that all potentials drop to zero at zero density n , which is generally expected.

Next, we investigate the quality of the approximate potentials. At the density range (0-0.3 and 1.7-2.0), the low and the high filling, the TMA potential performs the best compared to the exact BALDA potential. Here, the 2B and GW potentials are overestimated. Moreover, in the density range (0.3-0.5), although the TMA potential starts to deviate from the BALDA potential, the TMA and the BALDA potentials keep the same sign of their derivatives. The 2B and GW potentials manifest the opposite behavior. We can conclude that the TMA potential outperforms the 2B and GW potentials also in the density ranges (0.3-0.5 and 1.5-1.7). Finally, for the density range (0.5-1.5) the perturbative potentials are rather inaccurate.

In 3D, we compare potentials of the approximate perturbative solutions with a virtually exact DMFT potential. Within the DMFT [3], the paramagnetic ground state energy

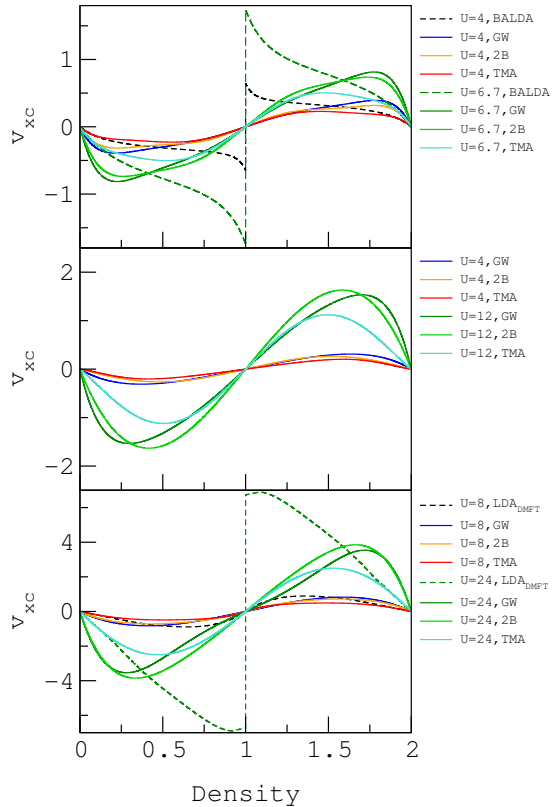


Figure 2.4: Exchange correlation potential v_{xc} , as a function of the total density per site, for different U -values. The panel shows 1D, the mid panel is 2D and the bottom panel is 3D.

of the 3D Hubbard model is obtained by mapping a 3D cubic lattice onto a single impurity Anderson model [31]. Here, for certain critical interaction strength U_{cr} , the system undergoes the Mott–Hubbard transition. The transition is reflected in the DMFT potential where a discontinuity appears. If we look at the quality of the perturbative potentials the situation is similar to the 1D Hubbard model: the TMA potentials again outperforms the 2B and GW potentials. For low and high densities, the TMA potential approaches the DMFT potential. Ultimately, none of the approximate potentials is able to generate the discontinuity at the half filling, not even for high interaction strengths.

In 2D, a potential which could serve as the benchmark to the perturbative potentials is missing due to the lack of exact solutions [38]. However, we can still examine the mutual behavior of the approximate potentials and learn about their quality. From Fig. 2.4, it is apparent that the mutual behavior of the potentials is very similar to the 1D and 3D cases. This allows us to “interpolate” to 2D the behavior of the approximate potentials with respect to the exact one. Thus we expect that even in 2D the TMA potential outperforms the 2B and GW potentials and it is the closest potential to the exact one in the low and high density regimes.

2.9 On the performance of the hybrid method

In the previous section we presented the exchange correlation potentials for 1D, 2D and 3D. In this section we want to discuss the hybrid method and its performance. This can be done only in 1D and 3D for which we have both the nonperturbative $v_{xc,ref}^{np}$ and the perturbative $v_{xc,ref}^{PT}$ exchange correlation potential, see Eq.(2.23). For the 2D Hubbard model an accurate nonperturbative method for obtaining the ground state energy and $v_{xc,ref}^{np}$ is still lacking [38]. This prevents at present an implementation of the hybrid method in 2D.

In paper II the hybrid method is tested against exact results in Hubbard-type systems, with respect to interaction strength, speed and inhomogeneity of the perturbation, and dimensionality and size of the system. In many regimes, we find significant improvement over adiabatic TDDFT or second Born NEGF approximations. The main conclusion of the paper is that if the speed of the perturbation is not too fast or its inhomogeneity in space is not too strong, but already beyond the adiabatic regime (i.e. where ALDA fails) the perturbative, nonadiabatic and nonlocal effects are sufficient for the description of the evolution.

An example (not presented in paper II) of such an evolution is shown in Fig. 2.5 where a linear 1D chain of 8 sites, where the interactions are present at the 5th site, is disturbed by an external potential. Comparing to the exact solution one can observe the dephasing of the ALDA (nonadiabatic regime) and the density and phase discrepancy of the 2B NEGF.

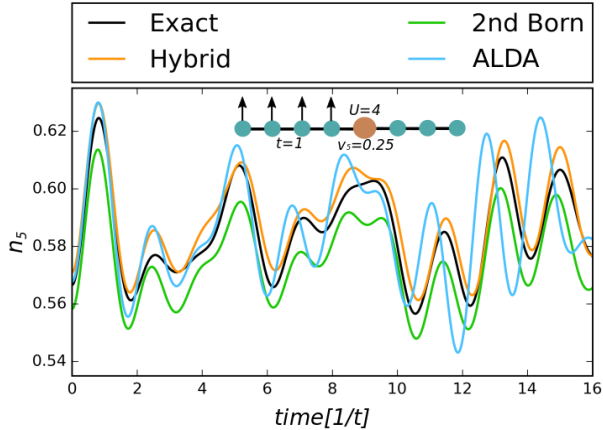


Figure 2.5: Adapted from Ref. [39] with the agreement of the author. Total electron density given by different approximations benchmarked against the Exact Diagonalization (black line). A finite tight binding chain with eight sites, where the fifth site represents the Anderson impurity with $U = 4$, is considered. We perturb the system by a potential $V_{\text{ext}} = 0.5\theta(t)$, on one half of the chain (see inset).

In the hybrid method, the phase keeps with the exact solution, and this is a general feature of the proposed approach.

In paper II only selected systems (small clusters and the Anderson impurity in transport setup) were treated, as they could be solved with exact methods and thus they could be benchmarked. It would be interesting to study larger lattice systems with the hybrid method, for example, the expansions of a fermion cloud in an optical lattice in 1D and 3D, as they were studied by ALDA [40] and pure NEGF [41, 42].

2.10 Outlook: hybrid method for continuum

In the previous sections we presented and discussed the hybrid method as formulated for the lattice Hubbard model. The question is how to extend it to the case of the continuum, where the collective index denotes $1 = (\mathbf{r}_1, \sigma_1, t_1)$. In the continuum, the strongly correlated regime can be described by a strictly correlated electron (SCE) limit [43] of the Hohenberg–Kohn energy density functional. The corresponding Kohn–Sham scheme called the restricted Kohn–Sham scheme, and denoted KS SCE scheme, was proposed in Ref. [44].

In the continuum the implementation of the hybrid method needs to be adapted, since

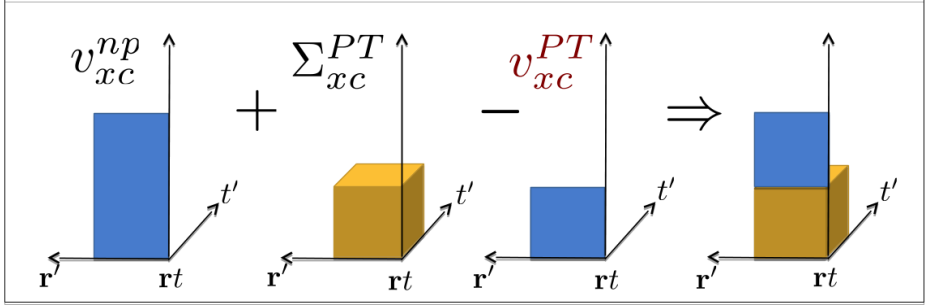


Figure 2.6: Schematic representation of locality in time and space and level of description of correlations in the hybrid method for the continuum case. In this case the nonperturbative XC potential $v_{xc}^{np} = v_{Hxc}^{SCE} - v_H$ accounts for the nonlocal effects.

the Hartree exchange correlation potential³ (HXC) of the KS SCE scheme is inherently nonlocal, so the idea to use a local adiabatic approximation is improper. Thus, for the ground (initial) state, the hybrid method does not add anything to $v_{Hxc}^{SCE}[n_{eq}(\mathbf{r})]$ since the non locality is already taken into account, and there is no use for a perturbative equilibrium correction. The advantage of the hybrid method in this case is to account for the memory effects, which can be included at the perturbative level as shown in Fig. 2.6.

For an isolated system (i.e. no need for $\Sigma_{emb.}$) the dynamical equation becomes

$$[i\partial_{t_1} - b(1, 2) - (v_{Hxc}^{SCE} - v_{xc}^{PT})[n(\mathbf{r}_1, t_1)]]G(1, 2) = \delta(1, 2) + \int_{\gamma} d3 \Sigma_{xc}^{PT}(1, 3)G(3, 2), \quad (2.34)$$

where $[n]$ emphasizes the non-local dependence in space. The v_{Hxc}^{SCE} is then used in the adiabatic approximation, i.e. there is a procedure giving v_{Hxc}^{SCE} and which takes the density $n(\mathbf{r}_1, t_1)$ as input. For the Hubbard model one was able to come up with a general (albeit numeric) expression for v_{xc}^{PT} as function of n . Here, instead, due to the non locality of the problem, the functional form of v_{xc}^{PT} is not known, and we consider a modified protocol.

The procedure to obtain v_{xc}^{PT} is the following: let us assume we know the density $n(\mathbf{r}, t)$. We then consider the time-dependent Hamiltonian at time t , and solve for its instantaneous equilibrium (ground) state density $n^{eq}(\mathbf{r}, t)$ according to

$$(\omega - h_H(1, 2) - \tilde{v})G_{PT}(\omega, \mathbf{r}_1, \mathbf{r}_2) = \delta(\mathbf{r}_1, \mathbf{r}_2) + \int d\mathbf{r}_3 \Sigma_{xc}^{PT}(\omega, \mathbf{r}_1, \mathbf{r}_3)G_{PT}(\omega, \mathbf{r}_3, \mathbf{r}_2), \quad (2.35)$$

where we have switched to the equilibrium ω -representation. The potential \tilde{v} is fixed by ensuring that $n^{eq}(\mathbf{r}, t) = n(\mathbf{r}, t)$. This can be seen as a reverse-engineering procedure for the pair $(n(\mathbf{r}, t), \tilde{v})$.

³We consider systems of finite size.

Under the same conditions and requirements of Eq. (2.35), we also solve for

$$(\omega - h_H(1, 2) - \tilde{v}) G_{\text{KS}}(\omega, \mathbf{r}_1, \mathbf{r}_2) = \delta(\mathbf{r}_1, \mathbf{r}_2). \quad (2.36)$$

This can also be seen as a reverse-engineering procedure, this time for the pair $(n(\mathbf{r}, t), \tilde{v})$. In the standard Kohn–Sham construction this potential \tilde{v} can be seen as a standard XC ground state potential but for a nonequilibrium density.

The meaning of Eqs. (2.35, 2.36) can be seen from the following. The equations for \tilde{v} and \tilde{v} can be rewritten in schematic notation as

$$G_{\text{KS}} = g_0 + g_0 \tilde{v} G_{\text{KS}}, \quad (2.37)$$

$$G_{PT} = g_0 + g_0 (\Sigma_{xc}^{PT} + \tilde{v}) G_{PT} \equiv G_{\text{KS}} + G_{\text{KS}} (\Sigma_{xc}^{PT} + \tilde{v} - \tilde{v}) G_{PT}. \quad (2.38)$$

where $g_0^{-1} = \omega - h_H$. Since G_{PT} and G_{KS} are tailored to give the same non-equilibrium density $n(\mathbf{r}, t)$, by taking the diagonal elements of the matrices in Eq. (2.38), we arrive at

$$\text{Diag}(G_{\text{KS}} (\Sigma_{xc}^{PT} + \tilde{v} - \tilde{v}) G_{PT}) = 0. \quad (2.39)$$

This gives the sought association

$$v_{xc}^{PT} \equiv \tilde{v} - \tilde{v}. \quad (2.40)$$

In fact we are using a Sham–Schlüter “technology” in disguise, but the direct reverse engineering of \tilde{v} and \tilde{v} should make the numerics easier than directly solving the Sham–Schlüter equation [45].

Chapter 3

Electron-nuclear interactions and Ehrenfest dynamics

In the previous chapter we focused on the strong electron-electron correlation induced by the electron-electron scattering. However, usually the electronic degrees of freedom are not isolated from other degrees of freedom, i.e. electron-electron scattering is also influenced by other mechanisms. In this chapter we focus on one such mechanism, namely the interaction of electrons with nuclei. We consider Ehrenfest dynamics - a mixed classical and quantum description (for nuclei and electrons, respectively). Specifically, we investigate how to describe the Ehrenfest dynamics of interacting electrons. Such a description requires us to include a quantum description of the interacting electrons, done here via the NEGF method.

We will consider two systems where the electron-nuclear interaction is important, presented in Fig. 3.1 - an adsorbate molecule on a surface where the distance between the molecule and the surface can be affected by electron dynamics, and a conducting molecular junction where currents can induce vibrations in the junction - a “molecular motor”. This chapter provides the background to paper III and paper IV.

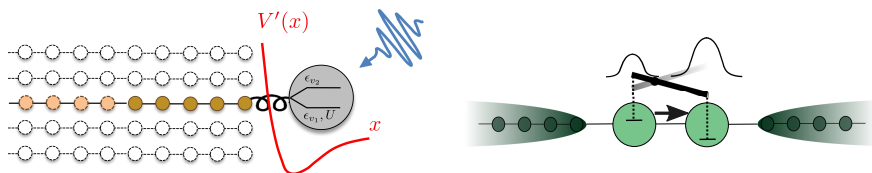


Figure 3.1: A model of an adsorbate molecule disturbed by a time-dependent electric field (left, taken from [35]) and a model of a “molecular motor” driven by currents (right).

3.1 Electron-nuclei models

Our goal is to describe the dynamics of the set of classical coordinates $\mathbf{x} = \{x_1, x_2, \dots, x_N\}$ moving in a classical potential $U_{\text{cl.}}(\mathbf{x})$, which are coupled to electronic degrees of freedom. The Hamiltonian for the classical coordinates reads

$$H_{\text{cl.}}(\mathbf{x}, \mathbf{p}) = \sum_{\nu}^N \frac{p_{\nu}^2}{2M_{\nu}} + U_{\text{cl.}}(\mathbf{x}). \quad (3.1)$$

where M_{ν} is the mass of the mode ν and p_{ν} is the canonical momentum. This Hamiltonian is coupled to electronic degrees of freedom so in general the electronic part of the Hamiltonian depends on the coordinates $H_{\text{el.}} \equiv H_{\text{el.}}(\mathbf{x}, t)$.

Adsorbate molecule dynamics. – Adsorption is the process of adhesion of atoms or molecules (from gas, liquid or plasma) to a surface. The process creates a layer of adsorbate on the surface, and the physical and chemical behavior of the adsorbate can be different from the free atom or molecule. The opposite process, when atoms or molecules leave the surface, is called desorption. Here we present a simple model to study the process of desorption which is induced by an external field. For the adsorbate molecule we consider one coordinate

$$H_{\text{cl.}}(x, p) = \frac{p^2}{2M} + \frac{\kappa}{x^4}, \quad (3.2)$$

coupled to the electronic part of the Hamiltonian

$$H_{\text{el.}}(x, t) = H_{\text{a}} + H_{\text{s}} + H_{\text{as}}(x) + H_{\text{ext}}(t), \quad (3.3)$$

where H_{a} describes the adsorbate molecule, H_{s} the surface and $H_{\text{ext}}(t)$ the external perturbation. The nuclear coordinate is coupled via the adsorbate-surface tunneling $H_{\text{as}}(x)$. Explicitly, the adsorbate molecule is described by the two level system

$$H_{\text{a}} = \sum_{v=v_1, v_2} \sum_{\sigma} \epsilon_v n_{v, \sigma} + U n_{v_1, \uparrow} n_{v_1, \downarrow}. \quad (3.4)$$

The operator $c_{v, \sigma}^{\dagger}$ creates an electron with spin σ and energy ϵ_v at the valence orbital v of the adsorbate and $n_{v, \sigma} = c_{v, \sigma}^{\dagger} c_{v, \sigma}$. In the adsorbate level v_1 , valence electrons mutually interact with interaction strength U . The surface is modeled as a non-interacting tight binding chain with one orbital per site

$$H_{\text{s}} = -V \sum_{\langle ij \rangle \in \alpha, \sigma} a_{i\sigma}^{\dagger} a_{j\sigma} + \sum_{i, \sigma} v a_{i\sigma}^{\dagger} a_{i\sigma}, \quad (3.5)$$

where $a_{i, \sigma}^{\dagger}$ creates an electron at site i with spin σ , V is the hopping parameter and v is the potential in the lead α . The adsorbate-surface interaction Hamiltonian H_{as} is given by

$$H_{\text{as}} = -g e^{-\lambda(x-1)} \sum_{v, \sigma} \left(c_{v, \sigma}^{\dagger} a_{S, \sigma} + h.c. \right), \quad (3.6)$$

where $ge^{-\lambda(x-1)} = V'(x)$ is a position dependent hopping parameter. The strength of correlation is given by the ratio U/V' . The time-dependent external perturbation $H_{\text{ext}}(t)$ is modeled by a dipole interaction term

$$H_{\text{ext}}(t) = \Lambda(t) \sum_{\sigma} a_{v_1\sigma}^{\dagger} a_{v_2\sigma} + h.c., \quad (3.7)$$

with the specific time profile $\Lambda(t)$, which could be e.g. Gaussian in shape. We define our central region as

$$h_{\text{el.}}(x, t) = H_{\text{a}} + H_{\text{as}} + \sum_{\sigma} v a_{1\sigma}^{\dagger} a_{1\sigma}, \quad (3.8)$$

so that the first site of the surface, see Fig. 3.1, is a part of the central region. In this way all the coupling on x is conveniently included in the central region and the rest of the system is independent of x .

Tunnel junction geometry. – A molecule coupled to macroscopic leads can serve as a molecular junction for the transport of electrons. The electrons can couple to local vibrational modes of the junction and thus induce forces in the junction. The current-induced forces can, in principle, be nonconservative allowing for molecular motors [46, 47]. The current-induced forces can be classified in the adiabatic regime where one can identify a steady-state, a friction and a Lorentz like force [48, 49]. Under general nonequilibrium conditions the friction can become positive. The positive friction gives a possibility for Van der Pol oscillations of the vibration coordinates [48, 49]. The forces can also eventually lead to effects such as run away modes [50, 51] or heating of nanojunctions [52].

Here we generalize a paradigmatic model [49] where we can study how the current-induced forces are influenced by electron-electron correlations. The electronic part of the Hamiltonian for a molecular motor is

$$H_{\text{el.}}(x, t) = H_{\text{cen.}}(x, t) + \sum_{\alpha} H_{\alpha}(t) + H_{\text{tun.}}, \quad (3.9)$$

where $H_{\text{cen.}}$ is the Hamiltonian of a central region, H_{α} represents the leads and $H_{\text{tun.}}$ describes the connections of the leads to the central region. More specifically, the leads are described by 1D tight binding semi-infinite chains

$$H_{\alpha}(t) = -V \sum_{\langle ij \rangle \in \alpha, \sigma} a_{i\sigma}^{\dagger} a_{j\sigma} + \sum_{i \in \alpha, \sigma} b_{\alpha}(t) a_{i\sigma}^{\dagger} a_{i\sigma}, \quad (3.10)$$

where $\alpha = \text{L, R}$ run over the left and right lead, V represents the hopping term in the leads, and $b_{\alpha}(t)$ is a time-dependent bias. The Hamiltonian for the central region is

$$H_{\text{cen.}}(x, t) = \sum_{ij, \sigma}^M h_{ij}(x, t) c_{i\sigma}^{\dagger} c_{j\sigma} + \sum_i U_i n_{i\uparrow} n_{i\downarrow}, \quad (3.11)$$

where $h_{ij}(x, t)$ is the single particle part with a coupling to the classical coordinates, and the rightmost term describes the effect of the on-site interactions with strength U_i . The central region is coupled to a lead α via the tunneling Hamiltonian

$$H_{\text{tun.}} = \sum_{\alpha} \left(\sum_{\langle i \in C, j \in \alpha \rangle, \sigma} V' (a_{j\sigma}^{\dagger} c_{i\sigma} + h.c.) \right), \quad (3.12)$$

where V' describes the tunneling from the surface site of the lead to one of the sites of the central region C . The central region for the model from Fig. 3.1 is

$$h_{\text{el.}}(x, t) = gx \sum_{\sigma} (n_{1\sigma} - n_{2\sigma}) + \sum_{\sigma} t (c_{1\sigma}^{\dagger} c_{2\sigma} + h.c.) + v_c (n_{1\sigma} + n_{2\sigma}), \quad (3.13)$$

where g is the coupling strength, t the cluster hopping and v_c the gate voltage.

3.2 Ehrenfest dynamics

In the limit of heavy masses \mathbf{M} , the wave function will be strongly localized around the classical coordinates \mathbf{x} that will be virtually equal to the quantum average value $\mathbf{x} \approx \langle \hat{\mathbf{x}} \rangle$. In this limit, the dynamics can be formulated within the classical description. The equation of motion for the classical coordinates \mathbf{x} can be formally derived by the path integral formalism [53, 54]. This leads to an equation of Langevin character

$$M \frac{d^2 x_{\nu}}{dt^2} + \frac{\partial U_{\text{cl.}}(\mathbf{x}(t))}{\partial x_{\nu}} \approx - \sum_{ij, \sigma} [\partial_{x_{\nu}} h_{\text{el.}}(\mathbf{x}(t))]_{ij} \rho_{ji}(t) + \xi_{\nu}(t), \quad (3.14)$$

where the first term on the right hand side is an electronic force and ξ_{ν} is a stochastic force which accounts for the quadratic fluctuations around the classical path $\approx (\hat{\mathbf{x}} - \langle \hat{\mathbf{x}} \rangle)^2$. The quantity $\rho_{ji}(t) = \langle \psi | c_{i\sigma}^{\dagger} c_{j\sigma} | \psi \rangle$ is the one-particle density matrix (here, the same for both spin channels). The density matrix and thus the electronic force can in general be nonadiabatic. Ignoring the stochastic forces ξ_{ν} corresponds to Ehrenfest dynamics (ED)

$$M \frac{d^2 x_{\nu}}{dt^2} + \frac{\partial U_{\text{cl.}}(\mathbf{x}(t))}{\partial x_{\nu}} \approx - \sum_{ij, \sigma} [\partial_{x_{\nu}} h_{\text{el.}}(\mathbf{x}(t))]_{ij} \rho_{ji}(t). \quad (3.15)$$

The density matrix can be computed if the wave function is evolved according to

$$i\partial_t |\psi\rangle = H(\mathbf{x}(t), t) |\psi\rangle. \quad (3.16)$$

and then constructing $\rho_{ji}(t) = \langle \psi | c_{i\sigma}^{\dagger} c_{j\sigma} | \psi \rangle$. However evolving the full wave function is computationally expensive and for an infinite system not possible. Instead we use the Nonequilibrium Green's Function method. The density matrix is connected to the double time Green function via its time diagonal $\rho_{ji}(t) = -iG_{ji}^<(t, t^+) = -iG_{ji}^<(t, t)$. The NEGF method is used to directly evolve the Green's function as will be discussed in the next section.

3.3 Nonadiabatic Ehrenfest dynamics

3.3.1 Kadanoff–Baym equations

The electron dynamics of the Green’s function is governed by the Kadanoff–Baym equation:

$$[i\partial_t - h_{HF}(\mathbf{x}, t)]G(t, t') = \delta(t, t') + \int_{\gamma} d\bar{t}(\Sigma_{emb} + \Sigma_c)(t, \bar{t})G(\bar{t}, t'), \quad (3.17)$$

where the explicit dependence on \mathbf{x} is contained in $h_{HF}(\mathbf{x}, t)$, which is the single-particle Hartree–Fock Hamiltonian of the central region; Σ_c contains the correlation effects beyond the HF selfenergy. The resulting classical-quantum Ehrenfest-KBE dynamics was tested in paper III against an exact solution. Recently a very similar approach was also reported in Ref. [55].

3.3.2 Generalized Kadanoff–Baym Ansatz

The Ehrenfest dynamics involves a slow nuclear time scale, so the resulting propagation time appears large at the electronic time scale. The propagation of the KBE on such time scales can be expensive so instead we could search for a reduced equation for the density matrix. Using the so-called Wigner space transform (appendix A), an exact equation directly for ρ can be derived (appendix B). The equation for ρ in the space matrix notation reads:

$$\partial_t \rho(t) + i[h_{HF}(\mathbf{x}, t), \rho(t)] = -(I^<(t, t) + h.c.), \quad (3.18)$$

where $\rho(t)$ is the density matrix, and $I^<(t, t)$ is a collision integral formally involving $G^{<,>,R,A}$ and $\Sigma^{<,>,R,A}$. To proceed with the collision integral an ansatz for the lesser Green’s function can be employed [12, 56, 57]

$$\tilde{G}^<(t, t') = -\tilde{G}^R(t, t')\rho(t') + \rho(t)\tilde{G}^A(t, t'), \quad (3.19)$$

which can be interpreted as having an “auxiliary” lesser Green’s function $\tilde{G}^<$. The closed equation for ρ is obtained by a further choice of an “auxiliary” retarded Green’s function \tilde{G}^R in terms of ρ . This can be either on the level of the HF approximation [57] or the so-called static-correlation approximation [58]. The cost of the evolution of the final equations is quadratic in propagation time as opposed to the cubic dependence of the full KBE [59]. Further discussion of these basic aspects is presented in appendix B.

3.4 Strictly adiabatic Ehrenfest dynamics

Under the assumption of a slow x-coordinate regime, where the electrons have time to adjust to the moving x-coordinates, (in this way they are in their instantaneous steady state), all

electronic quantities depends on time parametrically through $\mathbf{x}(t)$. In this so-called strictly adiabatic limit one replace the density matrix in eq. (3.20) by its steady state value

$$M_\nu \frac{d^2 x_\nu}{dt^2} = -\frac{\partial U_{\text{cl.}}(\mathbf{x}(t))}{\partial x_\nu} - \sum_{ij,\sigma} \frac{\partial h_{\text{el.}}^{ij}(\mathbf{x}(t))}{\partial x_\nu} \rho_{ji}^{\text{ss}}(\mathbf{x}(t)). \quad (3.20)$$

This evolution is called ‘‘strictly adiabatic Ehrenfest dynamics’’ and it can be identified as a steady-state Born-Oppenheimer approximation. The density matrix is determined from the steady state Green’s function

$$\rho_{ij}^{\text{ss}}(\mathbf{x}(t)) = \int \frac{d\omega}{2\pi} (-i) G_{ij}^{<,\text{ss}}(\mathbf{x}(t), \omega). \quad (3.21)$$

The steady state Green’s functions are determined from the steady state KBE equations, which have the form

$$\begin{aligned} G_{ij}^{R,\text{ss}} &= ((\omega - h - \Sigma^{R,\text{ss}})^{-1})_{ij}, \\ G_{ij}^{<,\text{ss}} &= \sum_{kl} G_{ik}^{R,\text{ss}} \Sigma_{kl}^{<,\text{ss}} G_{lj}^{A,\text{ss}}, \end{aligned} \quad (3.22)$$

where $h = h(\mathbf{x}(t))$ is fixed. All the functions are dependent only on ω since a time-independent steady state (but non-equilibrium) is assumed. Please note that the long time limit of the KBE dynamics has been assumed.

As seen in chapter 2 the selfenergy is usually divided into an embedding part, the Hartree part and the exchange-correlation part. However it is convenient for solving the steady-state KBE (for the Hubbard on-site interaction) to merge the Hartree part and the exchange part into the Hartree–Fock (HF) selfenergy:

$$\begin{aligned} \Sigma^{R,\text{ss}} &= \Sigma_{\text{emb}}^R + \Sigma_{\text{HF}}^{R,\text{ss}}[G^{\text{ss}}] + \Sigma_c^{R,\text{ss}}[G^{\text{ss}}], \\ \Sigma^{<,\text{ss}} &= \Sigma_{\text{emb}}^{<} + \Sigma_c^{<}[G^{\text{ss}}], \end{aligned} \quad (3.23)$$

where Σ_c^R contains the correlation effects beyond the HF selfenergy. The HF contribution is instantaneous, and so there is no lesser selfenergy. The Hartree–Fock and correlation parts are generally functionals of the Green’s function and the KBE must therefore be solved iteratively until selfconsistently is reached.

In the case of on-site interactions the HF selfenergy can be written as $(\Sigma_{\text{HF}}^{R,\text{ss}})_{ij} = \delta_{ij} U_i n_i^{\text{ss}}$ where U_i is the on-site interaction and n_i^{ss} the occupation belonging to one spin component. To proceed, one needs to specify the prescription for the correlation part. We choose to work mainly with the 2B and TMA approximations which have already been tested elsewhere [19, 20]. The equations for the correlation selfenergy for these approximations are presented in appendix C.

3.5 Adiabatic Ehrenfest dynamics

To go one step beyond the strictly adiabatic approximation, the first nonadiabatic correction needs to be taken into account. The correction linear in the nuclear velocity gives rise to a friction term. In this so-called adiabatic Ehrenfest dynamics (AED), the evolution of the system can be written as

$$M_\nu \frac{d^2 \mathbf{x}_\nu}{dt^2} = -\frac{\partial U_{\text{cl.}}(\mathbf{x}(t))}{\partial \mathbf{x}_\nu} - \sum_{ij,\sigma} \frac{\partial h_{\text{el.}}^{ij}(\mathbf{x}(t))}{\partial \mathbf{x}_\nu} \rho_{ji}^{\text{ss}}(\mathbf{x}(t)) - \sum_{\mu} \gamma_{\nu\mu} \dot{\mathbf{x}}_{\mu}. \quad (3.24)$$

At each step the long time limit of the electron dynamics is assumed. To derive the friction term we use the nonadiabatic density

$$\rho_{ij}(\mathbf{x}(t), t) = -iG_{ij}^<(\mathbf{x}(t), t, t) \quad (3.25)$$

represented as the time diagonal of the lesser Green's function. The reason for this representation is that we can expand the Green's function in the orders of derivatives of the position \mathbf{x} .

The expansion of the Green's function is formulated in the Wigner representation [60], defined through the transform

$$t = T + \frac{\tau}{2} \quad t' = T - \frac{\tau}{2} \quad \rightarrow \quad T = \frac{t+t'}{2} \quad \tau = t-t', \quad (3.26)$$

where the time difference τ is further Fourier transformed to ω . In the Wigner picture, the Green's function becomes a function of (T, ω) so that we can write $G(t, t') \rightarrow G(\omega, T)$. Note that for the physically interesting time diagonal $t = t'$, the central time T has the meaning of physical time t and we can write

$$\rho_{ij}(\mathbf{x}(t), t) = -iG_{ij}(\mathbf{x}(t), t, t^+) = \int \frac{d\omega}{2\pi} (-i)G_{ij}^<(\mathbf{x}(t), \omega, t), \quad (3.27)$$

where, as opposed to the strictly adiabatic approximation, the density matrix is explicitly dependent on time.

One way to find the function $G(\omega, T)$ is by the direct transform of $G(t, t')$ (the latter is found through the standard KBE). The second way is finding and solving the KBE (or the Dyson equation) written directly in the Wigner space

$$G(t, t') = \mathcal{F}[G(t, t')] \quad \rightarrow \quad G(\omega, T) = \mathcal{F}_{\mathbb{W}}[G(\omega, T)], \quad (3.28)$$

where $\mathcal{F}[G(t, t')]$ is the Dyson functional and $\mathcal{F}_{\mathbb{W}}[G(\omega, T)]$ is a functional form in the Wigner space. The functional has an exponential form, see appendix A, and the expansion

of an exponential has infinitely many terms. The expansion is usually cut in first order - i.e. we introduce the so-called gradient expansion. In the following we will discuss how to get the equations of motions in the Wigner space up to first order in derivatives of the position \mathbf{x} .

3.5.1 Wigner space gradient expansion rules

Derivative. – The first expression which appears in the KBE and needs to be transformed to Wigner space is the time derivative $-i\partial_{t'}$. In appendix A.1 we show that the derivative will be translated as

$$-i\partial_{t'} \rightarrow (-i/2\partial_T + \omega). \quad (3.29)$$

Time integral. – In the selfenergy part of the KBE we construct a two-time function from the collision integral

$$C(t, t') = \int d\bar{t} A(t, \bar{t}) B(\bar{t}, t'), \quad (3.30)$$

and, for this integral, the Wigner space picture reads

$$C(T, \omega) = e^{-\frac{i}{2}\frac{\partial}{\partial\omega'}\frac{\partial}{\partial T'} + \frac{i}{2}\frac{\partial}{\partial\omega}\frac{\partial}{\partial T'}} A(T, \omega) B(T', \omega')|_{\omega=\omega', T=T'}. \quad (3.31)$$

as shown in appendix A.2. In other words, the integral is translated to the exponent of the gradient operator, which is a bit impractical. However, for a slow perturbation in time it is sufficient to do the expansion up to first order

$$C(T, \omega) \approx A(T, \omega) B(T, \omega) + i/2[\partial_\omega A(T, \omega) \partial_T B(T, \omega) - \partial_T A(T, \omega) \partial_\omega B(T, \omega)]. \quad (3.32)$$

Multiplication. – A multiplication of a double-time function with a one-time function can be considered as an integral

$$A(t, t') b(t') = \int d\bar{t} A(t, \bar{t}) b(\bar{t}) \delta(\bar{t}, t'). \quad (3.33)$$

and thus using the rule for the gradient expansion of the integral in appendix A.3 the multiplication is translated to

$$A(t, t') b(t') \rightarrow A(T, \omega) b(T) + i/2\partial_\omega A(T, \omega) \partial_T b(T). \quad (3.34)$$

3.5.2 Gradient expansion - retarded and lesser Green's function

We start with the equation of motion for the retarded Green's function in the differential form

$$-i\partial_{t'} G^R(t, t') - G^R(t, t') b(t') = \delta(t - t') + \int dt_1 G^R(t, t_1) \Sigma^R(t_1, t'). \quad (3.35)$$

As shown in appendix D.1, we apply the gradient expansion rules presented above so that we end up with the expression

$$G^R \approx (\omega - h - \Sigma^R)^{-1} + i/2[\partial_\omega G^R \partial_T (h + \Sigma^R) G^R - G^R \partial_T (h + \Sigma^R) \partial_\omega G^R]. \quad (3.36)$$

which is the equation of motion up to first order in the time derivative.

Similarly we start with the equation of motion for the lesser Green's function in the integral form (note that we assume the long-time limit of the KBE)

$$G^<(t, t') = \int \int d\bar{t} d\bar{t}' \bar{t} G^R(t, \bar{t}) \Sigma^<(\bar{t}, \bar{t}') G^A(\bar{t}', t'), \quad (3.37)$$

By manipulating $G^<$ as shown in appendix D.2, we get a final expression which is exact up to first order

$$\begin{aligned} G^< \approx & (\omega - h - \Sigma^R)^{-1} \Sigma^< (\omega - h - \Sigma^A)^{-1} + i/2[\partial_\omega G^R \partial_T \Sigma^< G^A - \\ & - G^R \partial_T \Sigma^< \partial_\omega G^A + \partial_\omega G^R \partial_T (h + \Sigma^R) G^< - G^< \partial_T (h + \Sigma^A) \partial_\omega G^A + \\ & + \partial_\omega G^< \partial_T (h + \Sigma^A) G^A - G^R \partial_T (h + \Sigma^R) \partial_\omega G^<]. \end{aligned} \quad (3.38)$$

Equations (3.36) and (3.38) are equations of motions for $G^{R,<}$ and they need to be solved together with the selfenergies. Thus we have derived the functional $\mathcal{F}_W[G(\omega, T)]$ in (3.28) up to first order in the time derivative.

Assuming that $\partial_T \Sigma$ changes only due to the nuclear coordinates \mathbf{x} and that the coordinates vary slowly, meaning that $\partial_T \Sigma \approx \partial_{\mathbf{x}} \Sigma \cdot \dot{\mathbf{x}}$, one can further rewrite the Green's function as

$$\begin{aligned} G^< \approx & (\omega - h - \Sigma^R)^{-1} \Sigma^< (\omega - h - \Sigma^A)^{-1} + i/2 \sum_{\mu} \dot{x}_{\mu} [\partial_\omega G^R \partial_{x_{\mu}} \Sigma^< G^A - \\ & - G^R \partial_{x_{\mu}} \Sigma^< \partial_\omega G^A + \partial_\omega G^R \partial_{x_{\mu}} (h + \Sigma^R) G^< - G^< \partial_{x_{\mu}} (h + \Sigma^A) \partial_\omega G^A + \\ & + \partial_\omega G^< \partial_{x_{\mu}} (h + \Sigma^A) G^A - G^R \partial_{x_{\mu}} (h + \Sigma^R) \partial_\omega G^<]. \end{aligned} \quad (3.39)$$

This equation should in principle be solved selfconsistently, which however makes the procedure cumbersome. One can simplify the procedure if only the first iteration is considered as discussed in the next section.

3.5.3 First iteration and the friction coefficient

In the first iteration we solve Eq. (3.39) without the velocity corrections - this is equal to solving the steady-state KBE. In the next step we use the solution of the steady-state KBE in the velocity correction term of Eq. (3.39)

$$G^{<,(1)} \equiv (\omega - h - \Sigma^{R,ss})^{-1} \Sigma^{<,ss} (\omega - h - \Sigma^{A,ss})^{-1} + i/2 \sum_{\mu} \dot{x}_{\mu} [\dots]_{ss}. \quad (3.40)$$

We can identify the first term as the steady-state Green's function and write

$$G^{<, (1)} = G^{<, \text{ss}} + i/2 \sum_{\mu} \dot{x}_{\mu} [\dots] |_{\text{ss}}. \quad (3.41)$$

The first term in (3.41) leads to the steady-state force, which is already present in the strictly adiabatic Ehrenfest dynamics (3.21), and reads

$$F_{\nu}^{\text{ss}} = \int \frac{d\omega}{2\pi} -i2\mathcal{T}r[\partial_{x_{\nu}} h G_{\text{ss}}^{<}(T, \omega)], \quad (3.42)$$

where $\mathcal{T}r$ denotes the trace over the space indices, the factor 2 comes from spin sum and we note that $h = h(\mathbf{x}(T))$. The steady-state force is generally (for more than one nuclear coordinate) nonconservative in character [48, 49].

The second term is proportional to the velocities, and leads to the correction of the strictly adiabatic Ehrenfest dynamics (3.21). The evolution of the system (3.24) contains the friction coefficient $\gamma_{\nu\mu}$ which can be identified as

$$\begin{aligned} \gamma_{\nu\mu} = 2 \int \frac{d\omega}{4\pi} \mathcal{T}r \left[\partial_{x_{\nu}} h [\partial_{\omega} G_{\text{ss}}^R \partial_{x_{\mu}} \Sigma_{\text{ss}}^{<} G_{\text{ss}}^A - G_{\text{ss}}^R \partial_{x_{\mu}} \Sigma_{\text{ss}}^{<} \partial_{\omega} G_{\text{ss}}^A + \partial_{\omega} G_{\text{ss}}^R \partial_{x_{\mu}} (h + \Sigma_{\text{ss}}^R) G_{\text{ss}}^{<} - \right. \\ \left. - G_{\text{ss}}^{<} \partial_{x_{\mu}} (h + \Sigma_{\text{ss}}^A) \partial_{\omega} G_{\text{ss}}^A + \partial_{\omega} G_{\text{ss}}^{<} \partial_{x_{\mu}} (h + \Sigma_{\text{ss}}^A) G_{\text{ss}}^A - G_{\text{ss}}^R \partial_{x_{\mu}} (h + \Sigma_{\text{ss}}^R) \partial_{\omega} G_{\text{ss}}^{<} \right]. \end{aligned} \quad (3.43)$$

The symmetric part of tensor $\gamma_{\nu\mu}$ describes the friction in the system and the asymmetric part is a Lorentz-like force. We wish to stress that all these forces are automatically present in the full nonadiabatic Ehrenfest dynamics.

3.6 On the performance of ED and AED

Adsorbate dynamics. – In paper III we discuss the dynamics of the surface-adsorbate system as presented at the beginning of this chapter under a time-dependent laser pulse. For a surface of finite size we solve the model exactly both in the electronic and in the nuclear part (not presented in the thesis), treating the nuclear coordinate exactly with first quantization. The exact solution serves as a benchmark for the ED dynamics presented above.

To summarize the main finding about the quality of the ED: desorption can be described by the ED with good qualitative agreement to the exact solution in limiting cases: the exact result predicts either a very small (top panels of Fig. 3.2) or a very large desorption probability (right bottom panel of Fig. 3.2). In such limits the localized nuclear wave packet satisfies the assumption of the ED. In the intermediate case, when the nuclear wave packet

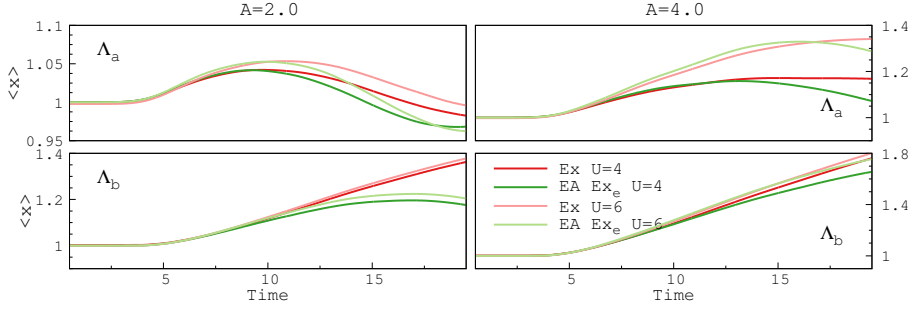


Figure 3.2: Taken from paper III. Comparisons between the full quantum description (red) and the Ehrenfest dynamics with the exact quantum description of the electrons (green) for a Gaussian pulse Λ_a and a modulated Gaussian pulse Λ_b of strengths $A = 2.0, 4.0$.

splits into a bound and a quasi-free part of the comparable weights, the Ehrenfest treatment fails to reproduce the exact results (left bottom panel of Fig. 3.2) .

In paper III we further benchmark the ED within the full KBE on the level of the 2B approximation (and also the hybrid NEGF/TDDFT approach) with the ED within the exact description of the electrons. Finally, the KBE allow us to also solve for the semi-infinite version of the surface. We find that the inclusion of a semi-infinite surface has a limited effect but predicts a slightly lower desorption probability (because of additional dissipative channels in the system).

Tunnel junction geometry. – In paper IV we present the AED including electron-electron correlation effects, which is numerically highly efficient, and we benchmark it against the

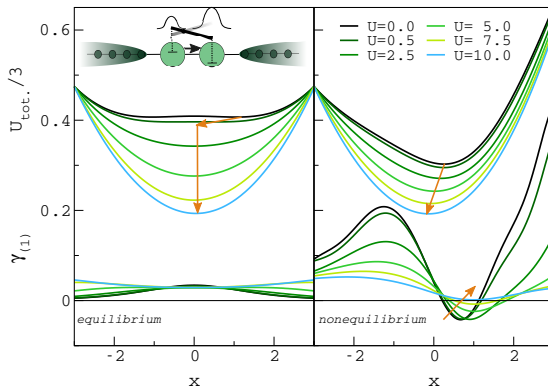


Figure 3.3: Taken from paper IV. The potential $U_{\text{tot.}}$ and the friction $\gamma_{(1)}$ within 2B approximation as a function of interaction strength U and position x .

full ED using the model described at the beginning of the chapter, see Fig.3.1.

One of the main findings is that for our model the electron-electron correlation within the 2B approximation reduce the possibility to have a negative friction and thus the possibility for a molecular motor. In Fig. 3.3 we plot the total potential $U_{\text{tot.}} = U_{\text{cl.}} + U_{\text{ss}}$ where $U_{\text{ss}} = -\int^x F_{\text{ss}} dx$ together with the first iteration of the friction γ . Looking at the friction coefficient in nonequilibrium and to the region of x with the negative friction, we see that the 2B approximation predicts a reduction of the region. Moreover, in paper IV we considered also other approximations - the HF approximation and the TMA approximation - with different levels of correlation treatment. We observe that the mean field HF approximation predicts the opposite trend than the 2B approximation while the TMA approximation is consistent with the 2B approximation. The results indicate the importance of the inclusion of correlation effects beyond mean field level. Further, in paper IV, the differences between the HF and the 2B approximations are illustrated in time domain, see also the cover of this thesis.

Using the full ED in the adiabatic limit and comparing it to the AED we have shown the consistency of the inclusion of the electron-electron interaction in the adiabatic expansion (see Fig. 3.4). We also discuss the AED beyond the regime of validity, primarily addressing the problem of explicit inclusion of the time-dependent bias switching. In this transient regime the full ED can be used instead to give an initial condition for the AED after the transient.

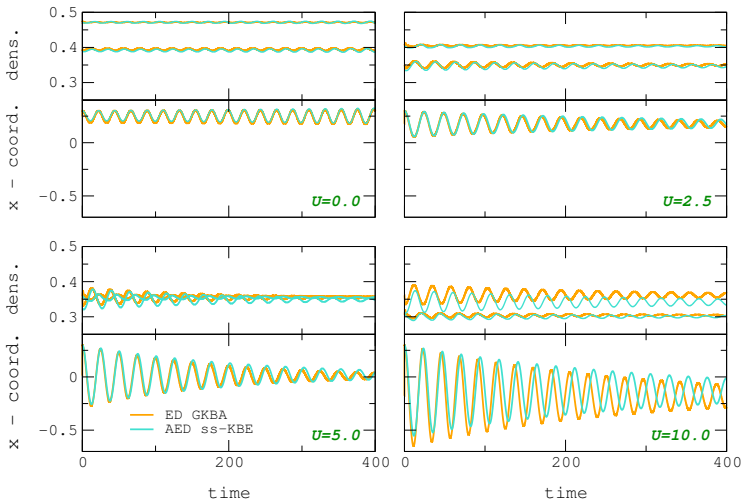


Figure 3.4: Adapted from paper IV. Comparison of the densities in the tunnel junction and x-coordinate coming from ED/GKBA dynamics (orange) and AED/ss-KBE dynamics (blue) for different strengths of the on-site interaction U . The parameters are chosen so that the junction is in the adiabatic regime. For higher interactions the AED deviates from the ED due to deviations of the GKBA from the KBE.

Chapter 4

Disorder vs. interactions and DFT characterization

In this chapter we again focus on systems with electron-electron interactions but this time, as additional ingredient, we consider the effect of disorder. A system with disorder and interactions will be described with standard methods - Exact Diagonalization and the NEGF. However, to interpret the joint effect of the disorder and the interactions we construct an exact independent particle picture by using the Kohn–Sham DFT. Such an auxiliary picture is helpful to understand the physics of competing disorder and interactions, since it allows to exactly quantify the screening of disorder due to interactions. This chapter presents background for the content of paper V.

4.1 Anderson Model and Anderson–Hubbard Model

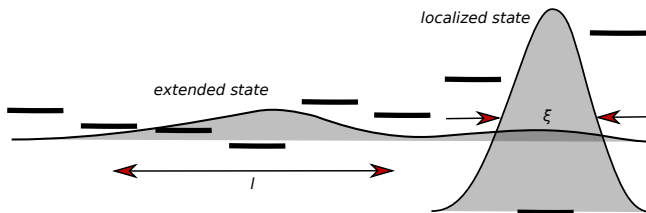


Figure 4.1: The Anderson localization of an electron with localization length ξ in the tight binding model with the disorder.

The Anderson model [61] is the tight binding model where the on-site energies v_i are drawn from a uniform and uncorrelated distribution $v_i \in [-W/2, W/2]$, and we refer to W as

the disorder strength. The disorder can induce a localization of some of the electrons, see Fig. 4.1. If the strength of the disorder is above a certain critical value, the disorder localizes all particles and the system undergoes the so-called Anderson transition; a metal-insulator transition driven purely by the disorder [61].

The Anderson–Hubbard model is the minimal model with the disorder and interactions both present:

$$\hat{H} = -t \sum_{\langle i,j \rangle, \sigma} \hat{c}_{i\sigma}^\dagger \hat{c}_{j\sigma} + \sum_{i, \sigma} v_i \hat{c}_{i\sigma}^\dagger \hat{c}_{i\sigma} + U \sum_i \hat{c}_{i\uparrow}^\dagger \hat{c}_{i\uparrow} \hat{c}_{i\downarrow}^\dagger \hat{c}_{i\downarrow}. \quad (4.1)$$

When disorder is not present the Anderson–Hubbard model reduces to the Hubbard model (2.2) which gives a different kind of metal-insulator transition. This so-called Mott–Hubbard transition [62] is driven by correlations. The Anderson–Hubbard model can be viewed either as an extension of the Anderson model or the Hubbard model.

The attractiveness of the Anderson–Hubbard model is boosted by ultracold gas experiments [63] where the model can be experimentally realized. Disordered and interacting lattices, where localization was present, were recently constructed [63, 64]. The experiments considered the strong disorder and the weak interaction regimes, i.e. regimes close to Anderson localization. This is referred to as many-body localization [65, 66]. However, this is not the only interesting regime, for example in a strongly correlated Mott regime the disorder can induce the emergence of a novel pseudogap metallic state [67]. Also, if strong correlations and strong disorder are present simultaneously, then a metallic behavior, i.e. a finite conductivity can be present [68]. Such behavior has also been indicated in small systems where conductances have a non-monotonic behavior [69, 70]. Hence there is a variety of phenomena due to the competition between disorder and interactions.

Here we discuss such competition in small finite systems and we propose an exact characterization with the help of the Kohn–Sham construction - an independent particle picture.

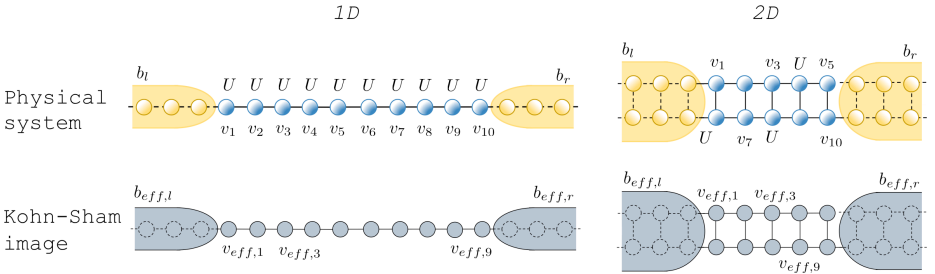


Figure 4.2: The physical system (top) and the corresponding Kohn–Sham image (bottom) for the 1D and 2D transport. The on-site interaction U , the one-body potential values v_i and KS potential values $v_{eff,i}$ are only shown at some representative sites. Further b_α is the bias and $b_{eff,\alpha}$ the effective bias in the lead α .

Specifically we consider two types of systems:

Transport setup. – we consider infinitely large systems in quantum transport geometries, see Fig.4.2. Disorder and interactions will be confined to a small region in space, which in turn is connected to macroscopic contacts. We drive the system out of equilibrium by applying an electric bias to the system.

Quantum rings. – We investigate a model of N electrons on a one-dimensional ring consisting of L lattice sites pierced by a homogeneous magnetic field. Such a system can have persistent steady-state currents, allowing us to study steady-state currents in a finite system. Under certain assumptions made on the properties of the magnetic field, the description can be hugely simplified by making use of the so-called Peierls substitution [71]. The approximation leads to a tight binding model in which the hopping terms are modified by complex numbers of modulus one. The Hamiltonian has a finite Hilbert space, which allows for finding the ground-state wave function by exact diagonalization:

$$\hat{H} = -t \sum_{i,j,\sigma} e^{i\phi_{ij}} \hat{c}_{i\sigma}^\dagger \hat{c}_{j\sigma} + \sum_{i,\sigma} v_i \hat{c}_{i\sigma}^\dagger \hat{c}_{i\sigma} + U \sum_i \hat{c}_{i\uparrow}^\dagger \hat{c}_{i\uparrow} \hat{c}_{i\downarrow}^\dagger \hat{c}_{i\downarrow}. \quad (4.2)$$

The first term corresponds to the kinetic energy, and we choose the elements of the hopping matrix as t for nearest neighbors, and 0 otherwise. The real numbers $\phi_{ij} = -\phi_{ji} = \phi/L$, the so-called Peierls phases are in principle determined by the magnetic vector potential, but here we simply take them as parameters of our model. The second term corresponds to the (diagonal) disorder and the third term corresponds to an on-site interaction.

4.2 Solvers: steady-state KBE and exact diagonalization

Quantum rings. – The Hamiltonian has a finite Hilbert space, which allows for finding the ground-state wave function by exact diagonalization. More specifically the method used is the implicitly restarted Lanczos method from the Scipy module, see Ref. [72]. After obtaining the ground-state wave function $|\psi\rangle$, we obtain the particle density per spin channel at site i as $n_i = \langle \psi | \hat{c}_{i\sigma}^\dagger \hat{c}_{i\sigma} | \psi \rangle$ (the system is spin-compensated). The bond current per spin channel I_{ij} between site i and j is non-zero only between nearest neighboring sites. Since

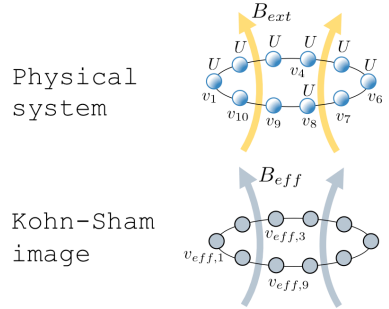


Figure 4.3: The physical system (top) and the corresponding Kohn-Sham image (bottom) for the ring. The on-site interaction U , the one-body potential values v_i and KS potential values $v_{eff,i}$ are shown only at some representative sites.

we are in a steady-state situation, $I_{i+1,i} = I$ is uniform and is given by

$$I = -2t \operatorname{Im} \left[e^{i\phi/L} \left\langle \psi \left| \hat{c}_{i+1,\sigma}^\dagger \hat{c}_{i,\sigma} \right| \psi \right\rangle \right]. \quad (4.3)$$

Transport setup. – The steady-state Green's function is determined from the steady-state KBE equations (3.22) discussed in the previous chapter, using the same approximations: 2B and TMA (see appendix C). The density per spin channel is obtained from

$$n_i = \int_{-\infty}^{\infty} \frac{d\omega}{2\pi i} G_{ii}^<(\omega), \quad (4.4)$$

while the current per spin channel is obtained from the Meir-Wingreen formula [73]

$$I = \int_{-\infty}^{\infty} \frac{d\omega}{2\pi i} \operatorname{Tr} \left[\Gamma_{emb}^l(\omega) (G^<(\omega) - 2\pi i f(\omega - \mu - b_l) A(\omega)) \right], \quad (4.5)$$

where l stands for the left lead ($\Gamma_{emb}^l = -2\operatorname{Im}\Sigma_{emb}^l$) and b_l the bias. Further, the spectral function is $A = i/(2\pi)(G^R - G^A)$, and $f(\omega) = \theta(-\omega)$ is the Fermi function at zero temperature.

4.3 DFT reconstruction procedure (reverse engineering)

In order to characterize the competition between disorder and interactions we consider the independent particle picture of Kohn–Sham theory as depicted in Fig. 4.3 and 4.2. Since the systems are in the steady-state there is a current present which means that the picture needs to reproduce not only the densities but also the current. The Kohn–Sham theory needs to be extended - we add an additional quantity - an effective phase in the case of the rings and an effective bias [74, 75, 76] in the case of the transport.

Quantum rings. – Here the reverse engineering is performed in the terms of the wave functions. We solve the KS equations [2]

$$(\tilde{t} + v_{\text{eff}})\varphi_\nu = \varepsilon_\nu \varphi_\nu, \quad (4.6)$$

where $(\tilde{t})_{ij} = t e^{i\phi_{ij}}$ contains the effective phase $\phi_{ij} = -\phi_{ji} = \phi_{\text{eff}}/L$, and ε_ν are the KS eigenvalues and φ_ν are the KS orbitals. The density per spin channel of the non-interacting KS system is given by the absolute square of the KS orbitals

$$n_i^{\text{KS}} = \sum_{\nu=1}^{N/2} |\varphi_\nu(i)|^2, \quad (4.7)$$

while the bond current per spin channel is given by Eq. (4.3), with the KS Slater determinant

$$I^{\text{KS}} = -2t \sum_{\nu=1}^{N/2} \text{Im} \left[e^{i\phi_{\text{eff}}/L} \varphi_{\nu}^*(i+1) \varphi_{\nu}(i) \right]. \quad (4.8)$$

The potential values $v_{\text{eff},i}$ and phase ϕ_{eff} are then chosen in order to reproduce the current and density of the original system. Note that we cannot attribute a physical significance to the KS orbitals or eigenvalues themselves, since the KS system is simply an auxiliary system designed to produce the correct density and current.

We now describe how we obtain v_{eff} and ϕ_{eff} via reverse engineering. We want a given density and current ($L + 1$ parameters) to be produced by the ground state of a non-interacting system with an effective potential and phase ($L + 1$ variables). Starting with an input guess, ϕ_{eff} and v_{eff} were obtained by numerically adjusting them until the KS system had the same current I and density n as the many-body system. Schematically, at the k -th iteration, the effective potential at the i -th site and the effective phase are updated with the criteria

$$\begin{aligned} [v_{\text{eff},i}^{(k+1)} - v_{\text{eff},i}^{(k)}][n_i^{\text{KS},(k)} - n_i] &> 0, \\ [\phi_{\text{eff}}^{(k+1)} - \phi_{\text{eff}}^{(k)}][I^{\text{KS},(k)} - I] &> 0. \end{aligned} \quad (4.9)$$

Transport setup. – The steady state Green’s functions are determined from the steady state KBE equations which have the form

$$\begin{aligned} G_{ij}^{R,\text{KS}} &= ((\omega - h - \Sigma_{\text{emb}}^R[b_{xc}] - V_{Hxc})^{-1})_{ij} \\ G_{ij}^{<,\text{KS}} &= \sum_{kl} G_{ik}^{R,\text{KS}} (\Sigma_{\text{emb}}^{<}[b_{xc}])_{kl} G_{lj}^{A,\text{KS}}, \end{aligned} \quad (4.10)$$

The density per spin channel is obtained from $G^{<,\text{KS}}$ as

$$n_i^{\text{KS}} = \int_{-\infty}^{\infty} \frac{d\omega}{2\pi i} G_{ii}^{<,\text{KS}}(\omega). \quad (4.11)$$

Since the KS system is an independent-particle system, the Meir-Wingreen formula, (4.5), reduces to the Landauer-Büttiker formula, which we write here as

$$I^{\text{KS}} = \int_{\mu}^{\mu+b_{\text{eff}}} \frac{d\omega}{2\pi} \mathcal{T}_r \left[\Gamma^{l,\text{KS}}(\omega) G^{R,\text{KS}}(\omega) \Gamma^{r,\text{KS}}(\omega) G^{A,\text{KS}}(\omega) \right], \quad (4.12)$$

where l/r stands for left/right. We wish to stress that even though (4.12) has the form of a transmission function for an independent-particle system, the current given by its integral still equals the true current.

Practically, the reverse-engineering algorithm to obtain b_{eff} and v_{eff} is very similar to the one used for the quantum ring setup. A modified update condition reads

$$\begin{aligned} [v_{eff,i}^{(k+1)} - v_{eff,i}^{(k)}][n_i^{KS,(k)} - n_i] &> 0, \\ [b_{eff}^{(k+1)} - b_{eff}^{(k)}][I^{KS,(k)} - I] &> 0. \end{aligned} \quad (4.13)$$

We use an iterative algorithm for b_{eff} and v_{eff} until the KS system yields the same current and density as the many-body system. For more details, see Ref. [76].

4.4 Effect of disorder and disorder screening

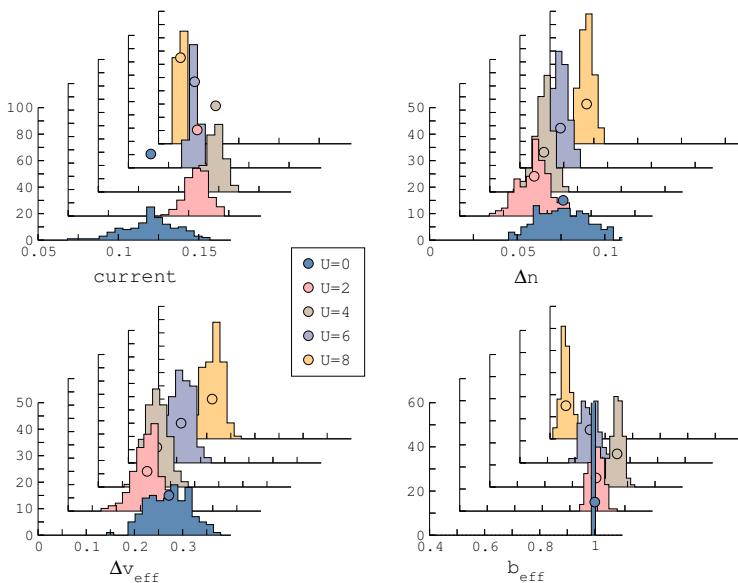


Figure 4.4: The results from the 1D transport setup of $M = 10$ sites. Histograms of the currents I , the spread of densities Δn , the spread of effective potential Δv_{eff} , and effective bias b_{eff} . The corresponding arithmetical averages are shown as dots. The corresponding statistical errors, $\sigma_x = \frac{\bar{x}}{\sqrt{M}}$, are of the same order or smaller than the dot sizes, and thus not shown.

Since the disorder in our systems is confined to a small region, the averages are not completely representative. Rather the statistical distribution, in the terms of typical values, of the physical quantity at hand gives a better description. To attain representative statistics we collected 150 disorder calculations in histograms. In these histograms, we show the distributions of the currents, spreads of densities Δn , spreads of effective potential Δv_{eff} , and effective biases b_{eff} . We also plot the arithmetic averages of these quantities in their

respective histograms. The results for a 1D transport setup of $M = 10$ sites can be seen in Fig. 4.4.

The effective potential v_{eff} is the quantity we elect to represent disorder screening. In a DFT language, this is the KS potential which can be split into contributions from the external potential and the Hartree-exchange-correlation potential. In our model, the external potential is the disorder, and thus we can write $v_{eff} = v + v_{Hxc}$. We then define a disorder-unscreened system to be when $v_{eff} \approx v$, and a fully screened one when v_{eff} is homogeneous. Note that, in this language, it is the Hartree-exchange-correlation potential that screens the disorder. Similarly, we write $b_{eff} = b + b_{xc}$, where b_{xc} is the exchange-correlation contribution to the bias. In our simulations, $b_{xc} < 0$, and thus also the applied bias is screened by interaction effects.

The currents through the system show a non-monotonic trend as a function of the interaction strength. The spread of densities and spread of effective potential instead decreases with the interaction strength. On the other hand b_{eff} , for low U , is almost equal to b , and thus the current through the system is increased for small U , since Δv_{eff} decreases. At larger U , however, the drop in b_{eff} is larger, and the corresponding current is smaller. We find that even though interactions smoothen the effective disordered landscape, this does not always lead to an increase of the current, due to the competition between disorder and interaction. This competition, in an independent-particle picture, is thus translated to a competition between the smoothness of the effective energy landscape and the reduced effective bias. Similar conclusions apply for the other systems - the 2D transport setup and the ring (see paper V).

Chapter 5

Competing Kondo and RKKY interactions and optimal control

In this chapter we consider a class of systems where the electron-electron interactions are localized at impurity sites, and the impurities are connected via noninteracting conduction electrons. Such systems with impurities with localized orbitals can exhibit magnetic effects once the temperature is lowered. Here, the conduction electrons will be considered in a general state carrying currents. We investigate how magnetic ordering is influenced by the currents and how to optimally manipulate the system between different magnetic regimes. This chapter presents background for the content of paper VI.

5.1 Single Kondo impurity and Kondo effect

The Kondo effect discovered in the 1930s by Haas et al. [77] is an effect induced by magnetic impurity scattering on the resistance of materials. As the temperature (energy scale) is lowered, the resistance reaches a minimum at a certain temperature. Such finite resistance in materials was puzzling for long time. In the beginning of 1960s it was suspected that the minimum is related to scattering from impurities. The first explanation of the minimum was provided by Kondo in 1964 [78], where the model of conduction electrons coupled to a local impurity, later called the Kondo model, was studied by means of perturbation theory. Perturbation theory was successful in the qualitative description of the minimum however, for $T \rightarrow 0$, the solution predicted a logarithmic divergence of the resistance. Such a breakdown of perturbation theory for lower temperatures was further discussed by Abrikosov [79], who showed that the higher order terms shift the divergence to a finite temperature, now known as the Kondo temperature.

In the mid 60s it was clear that the physics below the Kondo temperature cannot be described by perturbation theory, and in the following decade the problem attracted many theoreticians. A notable attempt to resolve the problem was done by Anderson in 1970 who devised a perturbative renormalization group method to show how the logarithmic divergences emerge [80]. The study also introduced the concept of renormalization and needs for nonperturbative solutions of the Kondo model. The answer came in 1975 by Kenneth Wilson [81] who invented a numerical algorithm for renormalization which was stable down to zero temperature. The method is now known as numerical renormalization group. Around the same time Nozières [82] developed an effective theory and pointed out that below the Kondo temperature the system behaves as a Fermi liquid - in this picture the spin of the impurity is screened by the spin of the conduction electrons and creates a Kondo singlet. We note that the results from the mid 70s were confirmed by exact solutions of the Kondo model by Andrei and Wiegmann [83, 84] in the beginning of 80s.

5.2 Dense Kondo impurities and RKKY interaction

In a system where the impurities are dense the physics will be different. An example of such system is a heavy-electron material - an inter-metallic compound, which contains elements with $4f$ or $5f$ electrons in unfilled electron bands. Here, the electrons can have higher effective mass than the free electron (up to 1000 times) [85]. The heavy fermion materials that were discovered first [86] exhibits a drastically lowered resistivity at low temperatures. This is opposed to the case of the dilute impurities where the finite resistance is expected from the Kondo effect.

In order to study such behavior a Kondo lattice model was proposed by Doniach [87]. In the Kondo lattice model, the Kondo impurities will spin-polarize the conduction electrons. However the polarization of the conduction electrons will induce an effective interaction between the local moments of the impurities, the so-called RKKY interaction [88, 89, 90] (named after Ruderman, Kittel, Kasuya, and Yoshida). Then the Kondo effect competes with the RKKY interaction. Doniach showed that depending on the product $J\rho_F$, where J is a coupling between the impurity and the conduction electrons, and ρ_F is the density of states at the Fermi energy, there will be either a lattice of Kondo singlets, or an antiferromagnetic ordering of the localized mo-

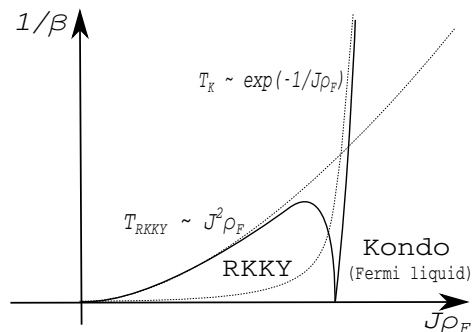


Figure 5.1: Doniach phase diagram showing a competition between RKKY interaction and Kondo effect.

ments, see Fig. 5.1. The RKKY regime below T_{RKKY} exhibits an antiferromagnetic ordering of local spins. In the Kondo regime there is a formation of Kondo singlets instead.

5.3 Single Impurity Anderson Model and Periodic Anderson Model

The Single Impurity Anderson Model (SIAM) describes a localized orbital of energy ϵ_f at site $i = i_{imp}$ with an on-site interaction U , which interacts with the mutually noninteracting conduction electrons through a hybridization V

$$H = -t \sum_{\langle i,j \rangle \sigma} (c_{i\sigma}^\dagger c_{j\sigma} + h.c.) + \epsilon_f \sum_{\sigma} f_{\sigma}^\dagger f_{\sigma} + U f_{\uparrow}^\dagger f_{\uparrow} f_{\downarrow}^\dagger f_{\downarrow} + V \sum_{\sigma} (c_{i_{imp}\sigma}^\dagger f_{\sigma} + h.c.). \quad (5.1)$$

The SIAM contains rich physics (Coulomb blockade, mixed valence regime, Kondo physics). Here, we are mainly interested in the Kondo limit. It was shown by Schrieffer and Wolff [91] that in the regime of strong correlation ($U/t \gg 1$), around a particle-hole symmetric point in small V limit, the Anderson and Kondo models are equivalent. The Anderson model in this regime shows the low-temperature behavior discussed for the Kondo model above.

For the competition between the RKKY and Kondo interactions, we can consider a model of the conduction electrons where each site is coupled to an Anderson impurity, known as a Periodic Anderson Model (PAM). Similarly to the single impurity case, the PAM can be mapped to the Kondo lattice model and thus it contains the possibility of Kondo vs. RKKY competition. Similarly to the Hubbard model, the PAM can also be seen as a minimalistic model which captures qualitatively the physics of strongly correlated materials [85].

5.4 Kondo and RKKY physics in finite systems

In 2000 [92] it was found experimentally that in cobalt clusters on short carbon nanotubes the Kondo physics can be altered due to finite size effects. The theoretical investigation in the so-called Kondo box [93] showed that a finite energy spacing can be used to tune the Kondo temperature. This led to several theoretical studies of finite size clusters with Kondo or Anderson impurity [94, 95, 96]; or dense impurity clusters [97, 98] which allowed to study Kondo vs. RKKY competition in finite site systems. The Kondo vs. RKKY competition has been recently reconsidered in multiple Kondo boxes [99, 100].

The physics of finite dense impurity clusters could be further tuned by controlled manufacturing of their geometry. An example is given by a quantum ring. In modern experiments [101] a nanoring with only a few electrons can be constructed. The ring topology is attractive

since the magnetic flux can be used to induce interesting phenomena such as the Aharonov Bohm effect [102]. Such nanorings were indeed used to study the Aharonov Bohm effect experimentally [103]. Moreover, with the advances which occurred in ultra-cold atoms experiments, the Aharonov Bohm effect can be constructed in optically engineered lattices as shown recently by Jimenez-Garcia et al. [104]. Additionally, the magnetic field can induce a stable current in the ring which can also lead to modified physics.

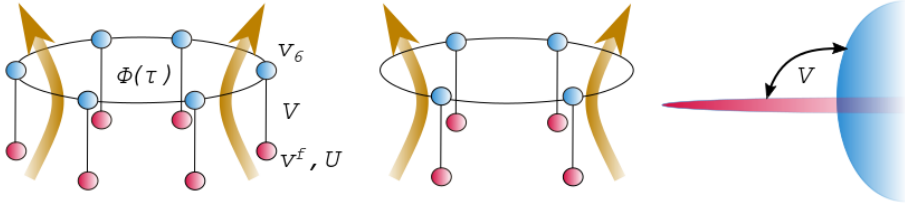


Figure 5.2: Typical clusters: a six-site PAM cluster (left) and a 4-site PAM cluster (center). A sketch of bands (right) representing the levels for conduction and impurity electrons, the bands can hybridize through the hopping term V .

We have investigated the Kondo vs. RKKY competition in a model of a one-dimensional PAM ring consisting of L lattice sites pierced by a homogeneous magnetic field. We generalize the standard PAM by adding a time-dependent Peierls phases to induce a time-varying current

$$\begin{aligned}
 H(\tau) = & -t \sum_{\langle i,j \rangle, \sigma} (c_{i\sigma}^\dagger c_{j\sigma} e^{i\phi_{ij}(\tau)} + h.c.) + \sum_{i,\sigma} v_i \hat{c}_{i\sigma}^\dagger \hat{c}_{i\sigma} + \sum_{i,\sigma} v_i^f f_{i\sigma}^\dagger f_{i\sigma} \\
 & + U \sum_i f_{i\uparrow}^\dagger f_{i\downarrow}^\dagger f_{i\downarrow} f_{i\uparrow} + V \sum_{i,\sigma} (c_{i\sigma}^\dagger f_{i\sigma} + h.c.). \quad (5.2)
 \end{aligned}$$

Here i, j label the sites of the PAM, f and c stands for operators of impurity or conduction electrons, the real numbers $\phi_{ij}(\tau)$ are the time-dependent Peierls phases. Further V is the hopping between the Anderson impurity and the conduction levels, U is the on-site interaction at the impurity, and ϵ_f is the on-site energy at the impurity. For homogeneous rings with the magnetic flux $\Phi(\tau)$ we get $\phi_{ij}(\tau) = -\phi_{ji}(\tau) = \phi(\tau) = \frac{\Phi(\tau)}{L}$, and we define the period for the phase as $\phi_0 = 2\pi/L$. We keep $v_i^f = -\frac{U}{2}$ in order to be at the particle-hole symmetric point (which represents the ideal condition for the Kondo regime).

5.5 Ground and equilibrium state

In order to address the Kondo vs. RKKY competition in the PAM clusters, the clusters need to be treated within a method which is nonperturbative in character. For the clusters of small size we can use the Exact Diagonalization method.

For the ground state, the exact diagonalization is computed with the implicitly restarted Lanczos method. The equilibrium ensemble can be written as

$$\langle \hat{O} \rangle = \sum_S \sum_{i_S=1}^{I_S} e^{-\beta E_{i_S}} \langle \psi_{i_S} | \hat{O} | \psi_{i_S} \rangle, \quad (5.3)$$

where S corresponds to the total spin, which defines the corresponding spin sector. Each spin sector can be diagonalized separately with the same method as for the ground state. In principle all the eigenstates in each sector should be taken into account. This would however require a very large diagonalization space. In practice, the sum can be truncated due to the exponential decay of the Boltzmann factor, so that only nonvanishing terms corresponding to low-lying excitations are counted $i_S^{max} < I_S$. In this case the convergence w.r.t the numbers i_S^{max} needs to be checked.

In Fig. 5.3 we show the result of the equilibrium state calculations. The surface represents the set of the parameters for which the Kondo and RKKY correlations are equal $\langle S_f S_{f+1} \rangle = \langle S_c S_f \rangle$. At the quantum flux $\phi = \frac{\pi}{2}$, the occupied conduction electron levels are pushed far from the unoccupied conduction electron levels. Here, it requires much higher temperature to make the electrons at the Fermi level free, so that the RKKY regime extends to the higher temperatures.

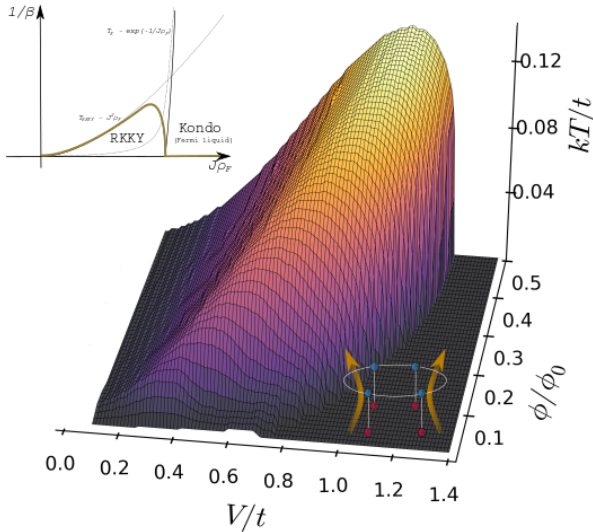


Figure 5.3: Adapted from paper VI. Extended Doniach phase diagram of a four-site ring. The volume beneath the surface corresponds to the regime where $\langle S_f S_{f+1} \rangle > \langle S_c S_f \rangle$, which means stronger RKKY correlations than Kondo correlations.

5.6 Time evolution and optimal control

Time evolution. – The method used for time evolution is based on the Lanczos method [105]; at each time step, the iterative Lanczos algorithm is used to find a small subspace where the Hamiltonian is diagonalized and then propagated.

Optimal control. – We adapt a Gradient Ascent Pulse Engineering (GRAPE) algorithm [106, 107] to the Lanczos time evolution explained in the previous paragraph. In the GRAPE algorithm the optimization routine builds on the fidelity function

$$\mathcal{F}(\alpha) = \sqrt{|\langle \psi_{\text{targ}} | \psi_T \rangle \langle \psi_T | \psi_{\text{targ}} \rangle|}, \quad (5.4)$$

and its gradient with respect to the control α ; ψ_T is the final state after the time evolution, and ψ_{targ} a target state. See appendix E for the details.

An example of an optimally controlled pulses is shown in figure 5.4. The initial and the target state is defined as

$$|\psi_{\text{init}}\rangle = |\psi_{\text{GS}, \phi=0}\rangle, \quad |\psi_{\text{targ}}\rangle = |\psi_{\text{GS}, \phi=\frac{\pi}{L}}\rangle. \quad (5.5)$$

Here we compare the effect of the optimal and linear pulse. For the optimal pulse, we observe the saturation of the correlations at the final time, whereas for the linear pulse there are induced oscillations of the correlation functions. The fidelity function is bigger when we drive the system from $\phi = 0$ to $\phi = \frac{\pi}{L}$ in the Kondo regime ($V/t = 1.3$) since the system is more homogeneous. Oppositely, in the RKKY regime ($V/t = 0.6$) it is much harder to drive the system from $\phi = 0$ to $\phi = \frac{\pi}{L}$ since the system ends at a strong RKKY anti-ferromagnetic configuration and the process thus requires stronger manipulation. Further, we show the possibility to cross from Kondo to RKKY regime ($V/t = 0.8, V/t = 1.0$).

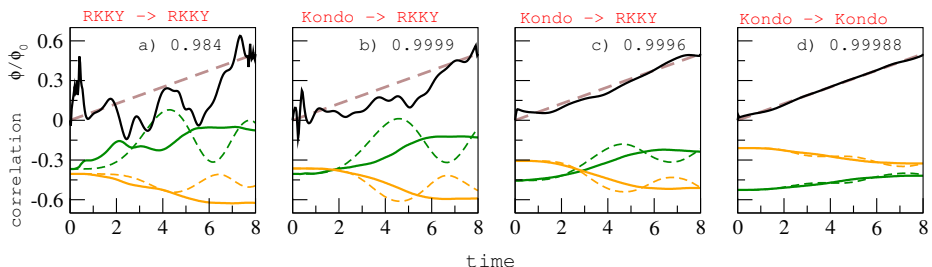


Figure 5.4: Adapted from paper VI. The time evolution of the Kondo (green) and RKKY (yellow) correlations in the 4-site ring for different ratios $\frac{V}{t} = 0.6, 0.8, 1.0, 1.3$. The results for a linear driving of phase $\frac{\phi}{\phi_0} = 0 \rightarrow \frac{\pi}{L}$ (dashed) and the results of the optimal driving (black solid) together with the fidelity are displayed.

References

- [1] P. Hohenberg and W. Kohn. Inhomogeneous Electron Gas. *Phys. Rev.*, 136:864–865, 1964.
- [2] W. Kohn and L. J. Sham. Self-Consistent Equations Including Exchange and Correlation Effects. *Phys. Rev.*, 140:1133–1138, 1965.
- [3] W. Metzner and D. Vollhardt. Correlated Lattice Fermions in $D = \infty$ Dimensions. *Phys. Rev. Lett.*, 62:324–327, 1989.
- [4] V. I. Anisimov, J. Zaanen, and O. K. Andersen. Band theory and Mott insulators: Hubbard U instead of Stoner I. *Phys. Rev. B*, 44:943–954, 1991.
- [5] V. I. Anisimov, A. I. Poteryaev, M. A. Korotin, A. O. Anokhin, and G. Kotliar. First-principles calculations of the electronic structure and spectra of strongly correlated systems: dynamical mean-field theory. *Journal of Physics: Condensed Matter*, 9:7359, 1997.
- [6] A. I. Lichtenstein and M. I. Katsnelson. *Ab initio* calculations of quasiparticle band structure in correlated systems: LDA++ approach. *Phys. Rev. B*, 57:6884–6895, Mar 1998.
- [7] S. Biermann, F. Aryasetiawan, and A. Georges. First-Principles Approach to the Electronic Structure of Strongly Correlated Systems: Combining the *GW* Approximation and Dynamical Mean-Field Theory. *Phys. Rev. Lett.*, 90:086402, 2003.
- [8] L. Hedin. New Method for Calculating the One-Particle Green’s Function with Application to the Electron-Gas Problem. *Phys. Rev.*, 139:A796–A823, 1965.
- [9] L. Boehnke, F. Nilsson, F. Aryasetiawan, and P. Werner. When strong correlations become weak: Consistent merging of *GW* and DMFT. *Phys. Rev. B*, 94:201106, 2016.
- [10] M. Hopjan and C. Verdozzi. Probing Strongly Correlated Materials in Non-equilibrium: Basic Concepts and Possible Future Trends in First Principle Approaches. *Top. In Curr. Chem.*, 347:347–384, 2014.

- [11] J. Hubbard. Electron correlations in narrow energy bands. *Proc. R. Soc. Lond. A*, 276:238–257, 1963.
- [12] K. Balzer and M. Bonitz. *Nonequilibrium Green's Functions Approach to Inhomogeneous Systems*. Springer Berlin Heidelberg, 2013.
- [13] G. Stefanucci and R. Leeuwen. *Nonequilibrium Many-Body Theory of Quantum Systems: A Modern Introduction*. Cambridge University Press, 2013.
- [14] J. Westergren. Many-body-based DFT treatment of fermions in optical lattices, 2017. Online at LUP Student Papers, Lund University.
- [15] L. P. Kadanoff and G. Baym. *Quantum Statistical Mechanics*. Benjamin, New York, 1962.
- [16] L. V. Keldysh. Diagram technique for nonequilibrium processes. *Sov. Phys. JETP*, 20:1018–26, 1965.
- [17] G. Baym and L. P. Kadanoff. Conservation Laws and Correlation Functions. *Phys. Rev.*, 124:287–299, 1961.
- [18] V. M. Galitskii. The Energy Spectrum of a Non-ideal Fermi Gas. *Sov. Phys. JETP*, 7:104, 1958.
- [19] P. Myöhänen, A. Stan, G. Stefanucci, and R. van Leeuwen. A many-body approach to quantum transport dynamics: Initial correlations and memory effects. *EPL*, 84:67001, 2008.
- [20] M. Puig von Friesen, C. Verdozzi, and C.-O. Almbladh. Successes and Failures of Kadanoff-Baym Dynamics in Hubbard Nanoclusters. *Phys. Rev. Lett.*, 103:176404, 2009.
- [21] Aoki, H. and Tsuji, N. and Eckstein, M. and Kollar, M. and Oka, T. and Werner, P. Nonequilibrium dynamical mean-field theory and its applications. *Rev. Mod. Phys.*, 86:779–837, 2014.
- [22] O. Gunnarsson and K. Schönhammer. Density-Functional Treatment of an Exactly Solvable Semiconductor Model. *Phys. Rev. Lett.*, 56:1968–1971, 1986.
- [23] K. Schönhammer and O. Gunnarsson. Discontinuity of the exchange-correlation potential in density functional theory. *J. Phys. C Solid State Phys.*, 20:3675, 1987.
- [24] K. Schönhammer, O. Gunnarsson, and R.M Noack. Density-functional theory on a lattice: Comparison with exact numerical results for a model with strongly interacting correlated electrons. *Phys. Rev. B*, 52:2504–2509, 1995.

- [25] N. A. Lima, L. N. Oliveira, and K. Capelle. Density-functional study of the Mott gap in the Hubbard model. *EPL (Europhysics Letters)*, 60:601, 2002.
- [26] E. Runge and E. K. U. Gross. Density-Functional Theory for Time-Dependent Systems. *Phys. Rev. Lett.*, 52:997–1000, 1984.
- [27] C. Verdozzi. Time-Dependent Density-Functional Theory and Strongly Correlated Systems: Insight from Numerical Studies. *Phys. Rev. Lett.*, 101:166401, 2008.
- [28] M. Farzanehpour and I. V. Tokatly. Time-dependent density functional theory on a lattice. *Phys. Rev. B*, 86:125130, 2012.
- [29] E. H. Lieb and F. Y. Wu. Absence of Mott Transition in an Exact Solution of the Short-Range, One-Band Model in One Dimension. *Phys. Rev. Lett.*, 20:1445–1448, 1968.
- [30] M. P. Tosi V. L. Campo Jr. G. Xianlong, M. Polini, K. Capelle, and M. Rigol. Bethe-Ansatz density-functional theory of ultracold repulsive fermions in one-dimensional optical lattices. *Phys. Rev. B*, 73(165120), 2006.
- [31] D. Karlsson, A. Privitera, and C. Verdozzi. Time-Dependent Density-Functional Theory Meets Dynamical Mean-Field Theory: Real-Time Dynamics for the 3D Hubbard Model. *Phys. Rev. Lett.*, 106:116401, 2011.
- [32] C. Verdozzi, D. Karlsson, M. Puig von Friesen, C.-O. Almbladh, and U. von Barth. Some open questions in TDDFT: Clues from lattice models and Kadanoff–Baym dynamics. *Chem. Phys.*, 391:37–49, 2011.
- [33] V. M. Galitskii and A. B. Migdal. Application of Quantum Field Theory Methods to the Many Body Problem. *Sov. Phys. JETP*, 7:96, 1958.
- [34] D. C. Langreth and J. W. Wilkins. Theory of Spin Resonance in Dilute Magnetic Alloys. *Phys. Rev. B*, 6:3189–3227, 1972.
- [35] E. Boström, M. Hopjan, A. Kartsev, C. Verdozzi, and C.-O. Almbladh. Nonequilibrium Green’s functions and atom-surface dynamics: Simple views from a simple model system. *J. Phys. Conf. Ser.*, 696:012007, 2016.
- [36] M. Hopjan, D. Karlsson, S. Ydman, C. Verdozzi, and C.-O. Almbladh. Merging Features from Green’s Functions and Time Dependent Density Functional Theory: A Route to the Description of Correlated Materials out of Equilibrium? *Phys. Rev. Lett.*, 116:236402, 2016.
- [37] W. Metzner and D. Vollhardt. Ground-state energy of the $D=1,2,3$ dimensional Hubbard model in the weak-coupling limit. *Phys. Rev. B*, 39:4462–4466, 1989.

- [38] J. P. F. LeBlanc, A. E. Antipov, F. Becca, I. W. Bulik, G. K.-L. Chan, Ch.-M. Chung, Y. Deng, M. Ferrero, T. M. Henderson, C.A. Jiménez-Hoyos, E. Kozik, X.-W. Liu, A. J. Millis, N. V. Prokof'ev, M. Qin, G. E. Scuseria, H. Shi, B. V. Svistunov, L. F. Tocchio, I. S. Tupitsyn, S. R. White, Sh. Zhang, B.-X. Zheng, Z. Zhu, and E. Gull. Solutions of the Two-Dimensional Hubbard Model: Benchmarks and Results from a Wide Range of Numerical Algorithms. *Phys. Rev. X*, 5:041041, 2015.
- [39] S. Ydman. Magnetization dynamics in nanorings, 2015. Online at LUP Student Papers, Lund University.
- [40] D. C. Sorensen R. B. Lehoucq and C. Yang. Three-dimensional dynamics of a fermionic Mott wedding-cake in clean and disordered optical lattices. *Sci. Rep.*, 3:2570, 2013.
- [41] N. Schlünzen, S. Hermanns, M. Bonitz, and C. Verdozzi. Dynamics of strongly correlated fermions: Ab initio results for two and three dimensions. *Phys. Rev. B*, 93:035107, 2016.
- [42] N. Schlünzen, J.-P. Joost, F. Heidrich-Meisner, and M. Bonitz. Nonequilibrium dynamics in the one-dimensional Fermi-Hubbard model: Comparison of the nonequilibrium Green-functions approach and the density matrix renormalization group method. *Phys. Rev. B*, 95:165139, 2017.
- [43] P. Gori-Giorgi, M. Seidl, and G. Vignale. Density-Functional Theory for Strongly Interacting Electrons. *Phys. Rev. Lett.*, 103:166402, 2009.
- [44] F. Malet and P. Gori-Giorgi. Strong Correlation in Kohn-Sham Density Functional Theory. *Phys. Rev. Lett.*, 109:246402, 2012.
- [45] L. J. Sham and M. Schlüter. Density-Functional Theory of the Energy Gap. *Phys. Rev. Lett.*, 51:1888–1891, 1983.
- [46] E. J. McEniry D. Dundas and T. N. Todorov. Current-driven atomic waterwheels. *Nat. Nanotechnol.*, 4:99–102, 2009.
- [47] M. Brandbyge. Computational nanoscience: Atomic waterwheels go to work. *Nat. Nanotechnol.*, 4:81–82, 2009.
- [48] N. Bode, S. V. Kusminskiy, R. Egger, and F. von Oppen. Scattering Theory of Current-Induced Forces in Mesoscopic Systems. *Phys. Rev. Lett.*, 107:036804, 2011.
- [49] N. Bode, S. V. Kusminskiy, R. Egger, and F. von Oppen. Current-induced forces in mesoscopic systems: A scattering-matrix approach. *F. Beilstein J. Nanotechnol.*, 3:144–162, 2011.

- [50] C. Verdozzi, G. Stefanucci, and C.-O. Almbladh. Classical Nuclear Motion in Quantum Transport. *Phys. Rev. Lett.*, 97:046603, 2006.
- [51] J.-T. Lü, M. Brandbyge, and P. Hedegård. Blowing the Fuse: Berry's Phase and Runaway Vibrations in Molecular Conductors. *Nano Letters*, 10:1657–1663, 2010.
- [52] Lü, Jing-Tao and Christensen, Rasmus B. and Wang, Jian-Sheng and Hedegård, Per and Brandbyge, Mads. Current-Induced Forces and Hot Spots in Biased Nanojunctions. *Phys. Rev. Lett.*, 114:096801, 2015.
- [53] R. Hussein, A. Metelmann, P. Zedler, and T. Brandes. Semiclassical dynamics of nanoelectromechanical systems. *Phys. Rev. B*, 82:165406, 2010.
- [54] A. Metelmann and T. Brandes. Adiabaticity in semiclassical nanoelectromechanical systems. *Phys. Rev. B*, 84:155455, 2011.
- [55] K. Balzer, N. Schlünzen, and M. Bonitz. Stopping dynamics of ions passing through correlated honeycomb clusters. *Phys. Rev. B*, 94:245118, 2016.
- [56] P. Lipavský, V. Špička, and B. Velický. Generalized Kadanoff-Baym ansatz for deriving quantum transport equations. *Phys. Rev. B*, 34:6933–6942, 1986.
- [57] S. Hermanns, N. Schlünzen, and M. Bonitz. Hubbard nanoclusters far from equilibrium. *Phys. Rev. B*, 90:125111, 2014.
- [58] S. Latini, E. Perfetto, A.-M. Uimonen, R. van Leeuwen, and G. Stefanucci. Charge dynamics in molecular junctions: Nonequilibrium Green's function approach made fast. *Phys. Rev. B*, 89:075306, 2014.
- [59] S. Hermanns, K. Balzer, and M. Bonitz. The non-equilibrium Green function approach to inhomogeneous quantum many-body systems using the generalized Kadanoff–Baym ansatz. *Physica Scripta*, 2012:014036, 2012.
- [60] E. Wigner. On the Quantum Correction For Thermodynamic Equilibrium. *Phys. Rev.*, 40:749–759, 1932.
- [61] P. W. Anderson. Absence of Diffusion in Certain Random Lattices. *Phys. Rev.*, 109:1492–1505, 1958.
- [62] N. F. Mott. The Basis of the Electron Theory of Metals, with Special Reference to the Transition Metals. *Proc. Phys. Soc. A*, 62:416, 1949.
- [63] J. Dalibard I. Bloch and S. Nascimbène. Quantum simulations with ultracold quantum gases. *Nat. Phys.*, 8:267–276, 2012.

- [64] J.-y. Choi, S. Hild, J. Zeiher, P. Schauß, A. Rubio-Abadal, T. Yefsah, V. Khemani, D. A. Huse, I. Bloch, and Ch. Gross. Exploring the many-body localization transition in two dimensions. *Science*, 352:1547–1552, 2016.
- [65] D. M. Basko, I. L. Aleiner, and B. L. Altshuler. Metal–insulator transition in a weakly interacting many-electron system with localized single-particle states. *Ann. Phys. (N. Y.)*, 321:1126 – 1205, 2006.
- [66] I. V. Gornyi, A. D. Mirlin, and D. G. Polyakov. Interacting Electrons in Disordered Wires: Anderson Localization and Low- T Transport. *Phys. Rev. Lett.*, 95:206603, 2005.
- [67] Elias Lahoud, O. Nganba Meetei, K. B. Chaska, A. Kanigel, and Nandini Trivedi. Emergence of a Novel Pseudogap Metallic State in a Disordered 2D Mott Insulator. *Phys. Rev. Lett.*, 112:206402, 2014.
- [68] N. D. Patel, A. Mukherjee, N. Kaushal, A. Moreo, and E. Dagotto. Non-Fermi Liquid Behavior and Continuously Tunable Resistivity Exponents in the Anderson-Hubbard Model at Finite Temperature. *Phys. Rev. Lett.*, 119:086601, 2017.
- [69] T. Vojta, F. Epperlein, and M. Schreiber. Do Interactions Increase or Reduce the Conductance of Disordered Electrons? It Depends! *Phys. Rev. Lett.*, 81:4212–4215, 1998.
- [70] D. Karlsson and C. Verdozzi. Transport of correlated electrons through disordered chains: A perspective on entanglement, conductance, and disorder averaging. *Phys. Rev. B*, 90:201109, 2014.
- [71] R. Peierls. On the theory of diamagnetism of conduction electrons. *Z. Phys.*, 80:763–791, 2012.
- [72] D. C. Sorensen R. B. Lehoucq and C. Yang. *ARPACK USERS GUIDE: Solution of Large Scale Eigenvalue Problems by Implicitly Restarted Arnoldi Methods*. SIAM, 1998.
- [73] Yigal Meir and Ned S. Wingreen. Landauer formula for the current through an interacting electron region. *Phys. Rev. Lett.*, 68:2512–2515, 1992.
- [74] P. Schmitteckert, M. Dzierzawa, and P. Schwab. Exact time-dependent density functional theory for impurity models. *Phys. Chem. Chem. Phys.*, 15:5477–5481, 2013.
- [75] G. Stefanucci and S. Kurth. Steady-State Density Functional Theory for Finite Bias Conductances. *Nano Lett.*, 15:8020–8025, 2015.
- [76] D. Karlsson and C. Verdozzi. Effective bias and potentials in steady-state quantum transport: A NEGF reverse-engineering study. *J. Phys. Conf. Ser.*, 696:012018, 2016.

- [77] W.J. de Haas, J. de Boer, and G.J. van den Berg. The electrical resistance of gold, copper and lead at low temperatures. *Physica*, 1:1115 – 1124, 1934.
- [78] J. Kondo. Resistance Minimum in Dilute Magnetic Alloys. *Progr. Theor. Phys.*, 32:37–49, 1964.
- [79] A. A. Abrikosov. Electron Scattering on Magnetic Impurities in Metals and Anomalous Resistivity Effects. *Physics*, 2(5), 1965.
- [80] P. W. Anderson. A poor man’s derivation of scaling laws for the Kondo problem. *J. Phys. C Solid State Phys.*, 3:2436, 1970.
- [81] K. G. Wilson. The renormalization group: Critical phenomena and the Kondo problem. *Rev. Mod. Phys.*, 47:773–840, 1975.
- [82] P. Nozières. A “fermi-liquid” description of the Kondo problem at low temperatures. *Jour. Low Temp. Phys.*, 17:31–42, 1974.
- [83] N. Andrei. Diagonalization of the Kondo Hamiltonian. *Phys. Rev. Lett.*, 45:379–382, 1980.
- [84] P. B. Wiegmann. Exact solution of the s-d exchange model (Kondo problem). *J. Phys. C Solid State Phys.*, 14:1463, 1981.
- [85] A. C. Hewson. *The Kondo Problem to Heavy Fermions*. Cambridge University Press, 1993.
- [86] K. Andres, J. E. Graebner, and H. R. Ott. $4f$ -Virtual-Bound-State Formation in CeAl_3 at Low Temperatures. *Phys. Rev. Lett.*, 35:1779–1782, 1975.
- [87] S. Doniach. The Kondo lattice and weak antiferromagnetism. *Physica B+C*, 91:231 – 234, 1977.
- [88] M. A. Ruderman and C. Kittel. Indirect Exchange Coupling of Nuclear Magnetic Moments by Conduction Electrons. *Phys. Rev.*, 96:99–102, 1954.
- [89] T. Kasuya. A Theory of Metallic Ferro- and Antiferromagnetism on Zener’s Model. *Progr. Theor. Phys.*, 16:45–57, 1956.
- [90] K. Yosida. Magnetic Properties of Cu-Mn Alloys. *Phys. Rev.*, 106:893–898, 1957.
- [91] J. R. Schrieffer and P. A. Wolff. Relation between the Anderson and Kondo Hamiltonians. *Phys. Rev.*, 149:491–492, 1966.
- [92] T. W. Odom, J.-L. Huang, Ch. L. Cheung, and Ch. M. Lieber. Magnetic Clusters on Single-Walled Carbon Nanotubes: The Kondo Effect in a One-Dimensional Host. *Science*, 290:1549–1552, 2000.

- [93] W. B. Thimm, J. Kroha, and J. von Delft. Kondo Box: A Magnetic Impurity in an Ultrasmall Metallic Grain. *Phys. Rev. Lett.*, 82:2143–2146, 1999.
- [94] H. Hu, G.-M. Zhang, and L. Yu. Mesoscopic Kondo Screening Effect in a Single-Electron Transistor Embedded in a Metallic Ring. *Phys. Rev. Lett.*, 86:5558–5561, 2001.
- [95] Bing Dong and X. L. Lei. Nonequilibrium Kondo effect in a multilevel quantum dot near the singlet-triplet transition. *Phys. Rev. B*, 66:113310, 2002.
- [96] P. Simon and I. Affleck. Finite-Size Effects in Conductance Measurements on Quantum Dots. *Phys. Rev. Lett.*, 89:206602, 2002.
- [97] C. Verdozzi, Y. Luo, and Nicholas Kioussis. Disordered Kondo nanoclusters: Effect of energy spacing. *Phys. Rev. B*, 70:132404, 2004.
- [98] Yan Luo, C. Verdozzi, and Nicholas Kioussis. Tunable Doniach phase diagram for strongly-correlated nanoclusters. *Phys. Rev. B*, 71:033304, 2005.
- [99] A. Schwabe, D. Gütersloh, and M. Potthoff. Competition between Kondo Screening and Indirect Magnetic Exchange in a Quantum Box. *Phys. Rev. Lett.*, 109:257202, 2012.
- [100] A. Schwabe, M. Hänsel, M. Potthoff, and A. K. Mitchell. Screening mechanisms in magnetic nanostructures. *Phys. Rev. B*, 92:155104, 2015.
- [101] Axel Lorke, R. Johannes Luyken, Alexander O. Govorov, Jörg P. Kotthaus, J. M. Garcia, and P. M. Petroff. Spectroscopy of Nanoscopic Semiconductor Rings. *Phys. Rev. Lett.*, 84:2223–2226, 2000.
- [102] Y. Aharonov and D. Bohm. Significance of Electromagnetic Potentials in the Quantum Theory. *Phys. Rev.*, 115:485–491, 1959.
- [103] S. Kasai, E. Saitoh, and H. Miyajima. Quantum transport properties in ferromagnetic nanorings at low temperature. *J. Appl. Phys.*, 93:8427–8429, 2003.
- [104] K. Jiménez-García, L. J. LeBlanc, R. A. Williams, M. C. Beeler, A. R. Perry, and I. B. Spielman. Peierls Substitution in an Engineered Lattice Potential. *Phys. Rev. Lett.*, 108:225303, 2012.
- [105] Tae Jun Park and J. C. Light. Unitary quantum time evolution by iterative Lanczos reduction. *J. Chem. Phys.*, 85:5870–5876, 1986.
- [106] S. Machnes, U. Sander, S. J. Glaser, P. de Fouquières, A. Gruslys, S. Schirmer, and T. Schulte-Herbrüggen. Comparing, optimizing, and benchmarking quantum-control algorithms in a unifying programming framework. *Phys. Rev. A*, 84:022305, 2011.

- [107] P. de Fouquieres, S. G. Schirmer, S. J. Glaser, and I. Kuprov. Second order gradient ascent pulse engineering. *J. Magn. Reson.*, 212:412 – 417, 2011.

Part III

Appendix

Appendix A

Derivation of gradient expansion rules

A.1 Derivative

The first expression which appears in the KBE and which needs to be transformed to the Wigner space [60] is a time derivative. The derivative written in the Wigner times reads

$$\partial_{t'} = \frac{\partial T}{\partial t'} \partial_T + \frac{\partial \tau}{\partial t'} \partial_\tau = 1/2 \partial_T - \partial_\tau. \quad (\text{A.1})$$

Let us to apply the derivative to two time function

$$\begin{aligned} \partial_{t'} f(t, t') &= (1/2 \partial_T - \partial_\tau) f(T, \tau) = (1/2 \partial_T - \partial_\tau) \int \frac{d\omega}{2\pi} e^{-i\omega\tau} f(T, \omega) = \\ &= \int \frac{d\omega}{2\pi} (1/2 \partial_T + i\omega) e^{-i\omega\tau} f(T, \omega), \end{aligned} \quad (\text{A.2})$$

so the derivative from the KBE will be translated as $-i\partial_{t'} \rightarrow (-i/2\partial_T + \omega)$.

A.2 Time integral

We start with an integral of two double times functions (e.g. the KBE scattering term)

$$C(t, t') = \int d\bar{t} A(t, \bar{t}) B(\bar{t}, t') \quad (\text{A.3})$$

and we write down the definition of C

$$\begin{aligned}
C(T, \omega) &= \int d\tau e^{i\omega\tau} C(T, \tau) = \int d\tau e^{i\omega\tau} C(T + \tau/2, T - \tau/2) = \\
&= \int d\tau e^{i\omega\tau} \int d\bar{t} A(T + \tau/2, \bar{t}) B(\bar{t}, T - \tau/2) = \\
&= \frac{1}{2} \int d\tau d\bar{\tau} e^{i\omega\tau} A(T + \tau/2, T + \bar{\tau}/2) B(T + \bar{\tau}/2, T - \tau/2).
\end{aligned} \tag{A.4}$$

Switching from the function inside the integral to its Wigner function

$$C(T, \omega) = \frac{1}{2} \int d\tau d\bar{\tau} e^{i\omega\tau} A(T + (\tau + \bar{\tau})/4, (\tau - \bar{\tau})/2) B(T - (\tau - \bar{\tau})/4, (\tau + \bar{\tau})/2). \tag{A.5}$$

Now, we employ the following substitutions

$$\tau_A = (\tau - \bar{\tau})/2, \quad \tau_B = (\tau + \bar{\tau})/2, \quad \tau = \tau_A + \tau_B, \quad d\tau d\bar{\tau} = 2d\tau_A d\tau_B, \tag{A.6}$$

so the integral is transformed to

$$C(T, \omega) = \int d\tau_A d\tau_B e^{i\omega(\tau_A + \tau_B)} A(T + \tau_B/2, \tau_A) B(T - \tau_A/2, \tau_B). \tag{A.7}$$

We note that the shift of the function can be written as an exponent

$$\begin{aligned}
A(T + \tau_B/2, \tau_A) &= \sum_{n=0}^{\infty} \frac{1}{n!} (\tau_B/2)^n (\partial/\partial T)^n A(T, \tau_A) = e^{\frac{\tau_B}{2} \frac{\partial}{\partial T}} A(T, \tau_A), \\
B(T - \tau_A/2, \tau_B) &= e^{-\frac{\tau_A}{2} \frac{\partial}{\partial T}} B(T, \tau_B),
\end{aligned} \tag{A.8}$$

and we also know that the multiplication of the function is connected with the derivative

$$\int d\tau e^{i\omega\tau} \tau f(\tau) = -i\partial_{\omega} \int d\tau e^{i\omega\tau} f(\tau). \tag{A.9}$$

Finally, using the relations (A.8) and (A.9) in (A.7) we can pull out the exponential in front of the integral

$$C(T, \omega) = e^{-\frac{i}{2} \frac{\partial}{\partial \omega'} \frac{\partial}{\partial T} + \frac{i}{2} \frac{\partial}{\partial \omega} \frac{\partial}{\partial T'}} \int d\tau_A e^{i\omega\tau_A} A(T, \tau_A) \int d\tau_B e^{i\omega'\tau_B} B(T', \tau_B) |_{\omega=\omega', T=T'} \tag{A.10}$$

which leads to final expression in the Wigner space

$$C(T, \omega) = e^{-\frac{i}{2} \frac{\partial}{\partial \omega'} \frac{\partial}{\partial T} + \frac{i}{2} \frac{\partial}{\partial \omega} \frac{\partial}{\partial T'}} A(T, \omega) B(T', \omega') |_{\omega=\omega', T=T'}. \tag{A.11}$$

After the expansion up to first order in the time derivative the expression reads

$$C(T, \omega) \approx A(T, \omega) B(T, \omega) + i/2 [\partial_{\omega} A(T, \omega) \partial_T B(T, \omega) - \partial_T A(T, \omega) \partial_{\omega} B(T, \omega)]. \tag{A.12}$$

A.3 Multiplication

Let us also consider multiplication of the double time function with one time function which can appear in the KBE. This can be reduced to the problem of previous section

$$A(t, t')b(t') = \int d\bar{t}A(t, \bar{t})b(\bar{t})\delta(\bar{t}, t') = \int d\bar{t}A(t, \bar{t})B(\bar{t}, t') = C(t, t'), \quad (\text{A.13})$$

with $B(t, t') = b(t)\delta(t-t')$. The Dirac delta is independent of T then for Wigner function applies

$$B(T, \tau) = b(T)\delta(\tau) = b(T)\delta(\tau), \quad (\text{A.14})$$

and thus the by Fourier transform we find that B is independent of ω

$$B(T, \omega) = \int d\tau e^{i\omega\tau}b(T)\delta(\tau) = b(T). \quad (\text{A.15})$$

Using the rule (A.12) for gradient expansion derived above, the multiplication will be translated up to first order in the time derivative according to

$$A(t, t')b(t') \rightarrow A(T, \omega)b(T) + i/2\partial_\omega A(T, \omega)\partial_T b(T). \quad (\text{A.16})$$

Appendix B

Generalized Kadanoff–Baym Ansatz

B.1 KBE - differential form

The electron dynamics of the time ordered Green's function is governed by the Kadanoff–Baym equation [15] which in the matrix notation reads

$$[i\partial_t - h_{HF}(t)]G(t, t') = \delta(t, t') + \int_{\gamma} d\bar{t} \Sigma(t, \bar{t}) G(\bar{t}, t'), \quad (\text{B.1})$$

where $\Sigma = \Sigma_{emb} + \Sigma_c$ and γ is the extended Schwinger–Keldysh contour [13, 20] which includes the initial correlated state. An alternative way to include initial correlations is via adiabatic switching of the correlations on the original Schwinger–Keldysh contour [16], denoted as \mathcal{K}

$$[i\partial_t - h_{HF}(t)]G(t, t') = \delta(t, t') + \int_{\mathcal{K}} d\bar{t} \Sigma(t, \bar{t}) G(\bar{t}, t'). \quad (\text{B.2})$$

We will use the latter formulation in this appendix as it is more convenient for the discussion of the Generalized Kadanoff–Baym Ansatz [56]. The Langreth–Wilkins rules [34] translate the Schwinger–Keldysh contour KBE into the equation for the lesser (greater) component

$$[i\partial_t - h_{HF}(t)]G^{\lessgtr}(t, t') = \int d\bar{t} (\Sigma^{\lessgtr}(t, \bar{t}) G^A(\bar{t}, t') + \Sigma^R(t, \bar{t}) G^{\lessgtr}(\bar{t}, t')), \quad (\text{B.3})$$

and for the retarded (advanced) component

$$[i\partial_t - h_{HF}(t)]G^{R/A}(t, t') = \delta(t, t') + \int d\bar{t} \Sigma^{R/A}(t, \bar{t}) G^{R/A}(\bar{t}, t'). \quad (\text{B.4})$$

where the integrals run over the real axis. The equations in this section are the KBE in their differential form. However for further discussion it is more convenient to transform the equations into their integral form.

B.2 KBE - integral form

The differential equations of the previous section can be formally solved by an integration starting from the initial uncorrelated Hartree–Fock ground state. The integral equation for the lesser (greater) function can be schematically written as

$$G^{\lessgtr} = G_{HF}^{\lessgtr} + G_{HF}^{\lessgtr} \Sigma^A G^A + G_{HF}^R \Sigma^{\lessgtr} G^A + G_{HF}^R \Sigma^R G^{\lessgtr}, \quad (\text{B.5})$$

or, alternatively, in the more symmetric way

$$G^{\lessgtr} = (1 + G^R \Sigma^R) G_{HF}^{\lessgtr} (1 + \Sigma^A G^A) + G^R \Sigma^{\lessgtr} G^A, \quad (\text{B.6})$$

where all the selfenergies $\Sigma[G]$ are functionals of G , and the multiplication is to be understood in the sense of the matrix multiplication and the time integral over the real time axis. The integral equation for the retarded (advanced) function should in a similar way be written as

$$G^{R/A} = G_{HF}^{R/A} + G_{HF}^{R/A} \Sigma^{R/A} G^{R/A}. \quad (\text{B.7})$$

Consistency check.– The Green’s function from integral equations above must be consistent with the key relation (this is just consequence of the definitions of the particular Green’s function component)

$$G^> - G^< = G^R - G^A, \quad (\text{B.8})$$

when a similar relation applies also for the selfenergies (as the consequence of Langreth–Wilkins rules)

$$\Sigma^> - \Sigma^< = \Sigma^R - \Sigma^A. \quad (\text{B.9})$$

A consistency check starts with the symmetric form of the equations (B.6). We take a difference of the left hand sides

$$G^> - G^< = (1 + G^R \Sigma^R) (G_{HF}^> - G_{HF}^<) (1 + \Sigma^A G^A) + G^R (\Sigma^> - \Sigma^<) G^A. \quad (\text{B.10})$$

Now we can use that for the Hartree–Fock Green’s functions the similar equation as (B.8) applies (this can be easily shown since the Hartree–Fock is constructed from the Slater determinants)

$$G_{HF}^> - G_{HF}^< = G_{HF}^R - G_{HF}^A. \quad (\text{B.11})$$

and with this we can perform a substitution in the equation (B.10)

$$G^> - G^< = (1 + G^R \Sigma^R) (G_{HF}^R - G_{HF}^A) (1 + \Sigma^A G^A) + G^R (\Sigma^R - \Sigma^A) G^A, \quad (\text{B.12})$$

and after an expansion of the first term we get the rather long expression

$$\begin{aligned} G^> - G^< = & (1 + G^R \Sigma^R) G_{HF}^R - G_{HF}^A (1 + \Sigma^A G^A) + G^R (\Sigma^R - \Sigma^A) G^A + \\ & + (1 + G^R \Sigma^R) G_{HF}^R \Sigma^A G^A - G^R \Sigma^R G_{HF}^A (1 + \Sigma^A G^A). \end{aligned} \quad (\text{B.13})$$

This expression is, however, reduced by using the equation (B.7) for retarded (advanced) functions

$$G^> - G^< = G^R - G^A + G^R \Sigma^R G^A - G^R \Sigma^A G^A + G^R \Sigma^A G^A - G^R \Sigma^R G^A \quad (\text{B.14})$$

and after cancellations of some terms we finally arrive to the desired relation

$$G^> - G^< = G^R - G^A. \quad (\text{B.15})$$

In this way we have shown that equations (B.6) and (B.7) gives the consistent evolution of the Green's function.

B.3 KBE - integral form - long-time limit

Let us briefly discuss the long-time limit of equation (B.6). In the long-time limit, the first term of equation (B.6) (which corresponds to a memory from initial correlations) can be disregarded since it decays to zero [13]. This leads to simplified integral equations

$$G^{\lessgtr} = G^R \Sigma^{\lessgtr} G^A, \quad (\text{B.16})$$

known as long-time KBE. In this case we can modify the consistency check of the previous section. We start with the difference of equations (B.16) to obtain

$$G^> - G^< = G^R (\Sigma^> - \Sigma^<) G^A = G^R (\Sigma^R - \Sigma^A) G^A. \quad (\text{B.17})$$

where we used the property (B.9). Further we use the equation (B.7) in its differential form

$$\Sigma^{R/A} = (G_{HF})^{-1} - (G^{R/A})^{-1}, \quad (\text{B.18})$$

and by substitution we derive that

$$G^> - G^< = G^R (-(G^R)^{-1} + (G^A)^{-1}) G^A = G^R - G^A. \quad (\text{B.19})$$

In this way we have checked the consistency of equation (B.16) with the property (B.8) in the long time limit.

B.4 KBE - time-diagonal equation

The Generalized Kadanoff–Baym Ansatz is formulated for a time-diagonal equation. It is thus instructive to present a derivation of the time-diagonal equation from the differential KBE (B.3)

$$[i\partial_t - b_{HF}(t)] G^<(t, t') = \int d\bar{t} (\Sigma^<(t, \bar{t}) G^A(\bar{t}, t') + \Sigma^R(t, \bar{t}) G^<(\bar{t}, t')), \quad (\text{B.20})$$

where we will use a short notation for the collision integral on the right hand side

$$[i\partial_t - h_{HF}(t)]G^<(t, t') = I^<(t, t'). \quad (\text{B.21})$$

The time-diagonal equation can be derived with help of the Wigner space coordinates (T, ω) [60]. Following the rules of the appendix A, we can transform the equation of motion for $G^<$

$$(i/2\partial_T + \omega)G^< - h_{HF}G^< + i/2\partial_T h_{HF}\partial_\omega G^< + \dots = I^<, \quad (\text{B.22})$$

where the dots stand for the terms of the expansion. Taking the time-diagonal $(t, t') \rightarrow (t, t)$ in the double time space is equivalent to integrate over the omega variable in the Wigner space. Focusing on the left hand side of the equation (B.22) we get

$$i/2\partial_T \int \frac{d\omega}{2\pi} G^< + \int \frac{d\omega}{2\pi} \omega G^< - h_{HF} \int \frac{d\omega}{2\pi} G^< + i/2\partial_T h_{HF} \int \frac{d\omega}{2\pi} \partial_\omega G^< + \dots \quad (\text{B.23})$$

Performing the integral of the higher order terms of the expansion will give zero contribution since the Green's function $G^<$ and its derivatives decay to zero in the infinity. We further use the definition of the density matrix to rewrite the left hand side as

$$i/2\partial_T(-i\rho) + \int \frac{d\omega}{2\pi} \omega G^< - h_{HF}(-i\rho), \quad (\text{B.24})$$

to finally obtain the time-diagonal equation

$$1/2\partial_T \rho + i h_{HF} \rho - \int \frac{d\omega}{2\pi} \omega G^<(T, \omega) = - \int \frac{d\omega}{2\pi} I^<(T, \omega). \quad (\text{B.25})$$

Similarly one can derive the time-diagonal equation of the adjoint of the equation (B.3)

$$-1/2\partial_T \rho + i\rho h_{HF} - \int \frac{d\omega}{2\pi} G^<(T, \omega)\omega = \int \frac{d\omega}{2\pi} (I^<)^\dagger(T, \omega). \quad (\text{B.26})$$

A symmetric form of the time-diagonal equation is obtained from a difference of the two equations above

$$\partial_T \rho + i[h_{HF}, \rho] = - \int \frac{d\omega}{2\pi} [I^< + (I^<)^\dagger]. \quad (\text{B.27})$$

We have derived the time-diagonal equation in the Wigner space. However, this equation can be now expressed back in the double-time space (t, t') . Since we are on the time diagonal where $t = t'$, one can identify that the central time is equivalent to the time in the double-time space $T = t = t'$. The equation for the time diagonal in the double-time space is

$$\partial_t \rho(t) + i[h_{HF}(t), \rho(t)] = -(I^<(t, t) + h.c.) \quad (\text{B.28})$$

where the collision term reads

$$I^<(t, t) = \int d\bar{t} [\Sigma^<(t, \bar{t}) G^A(\bar{t}, t) + \Sigma^R(t, \bar{t}) G^<(\bar{t}, t)]. \quad (\text{B.29})$$

This equation is still an exact equation with no approximation involved.

B.5 GKBA - time-diagonal equation

Now we are ready to introduce the Generalized Kadanoff–Baym Ansatz (GKBA) which is an approximation for the collision term

$$I^<(t, t) = \int d\bar{t} (\Sigma^<[G](t, \bar{t}) G^A(\bar{t}, t) + \Sigma^R[G](t, \bar{t}) G^<(\bar{t}, t)). \quad (\text{B.30})$$

The GKBA suggests to replace the functional dependence of the collision term on the full Green's function as $I[G] \rightarrow I[\tilde{G}]$: more explicitly,

$$I^<(t, t) \approx \int d\bar{t} (\Sigma^<[\tilde{G}](t, \bar{t}) \tilde{G}^A(\bar{t}, t) + \Sigma^R[\tilde{G}](t, \bar{t}) \tilde{G}^<(\bar{t}, t)), \quad (\text{B.31})$$

where the ansatz [56] is following

$$\tilde{G}^<(t, t') = -\tilde{G}^R(t, t')\rho(t') + \rho(t)\tilde{G}^A(t, t'), \quad (\text{B.32})$$

$$\tilde{G}^>(t, t') = \tilde{G}^R(t, t')(1 - \rho(t')) - (1 - \rho(t))\tilde{G}^A(t, t'). \quad (\text{B.33})$$

Auxiliary lesser and greater Green's functions are constructed from the density matrix ρ and an auxiliary retarded (advanced) Green's function which is determined from an independent equation of motion

$$(i\partial_t - h_{HF}(t))\tilde{G}^R(t, t') = \delta(t - t') + \int d\bar{t} \tilde{\Sigma}^R(t, \bar{t})\tilde{G}^R(\bar{t}, t'). \quad (\text{B.34})$$

Typically we choose $\tilde{\Sigma}^R(t, \bar{t}) = \tilde{\Sigma}^R(t)\delta(t - \bar{t})$ time local in order to keep the computational cost as low as possible. The interesting and important property of the GKBA is the following relation

$$\tilde{G}^> - \tilde{G}^< = \tilde{G}^R - \tilde{G}^A, \quad (\text{B.35})$$

which is fulfilled by the construction (B.32) and (B.33). Another interesting property is the fulfillment of the relation for the selfenergies

$$\Sigma^>[\tilde{G}] - \Sigma^<[\tilde{G}] = \Sigma^R[\tilde{G}] - \Sigma^A[\tilde{G}], \quad (\text{B.36})$$

even if the approximate Green's functions \tilde{G} are used for the construction. The formal proof of this relation is similar to the proof of relation (B.9) for the full Green's function dependence. The relation (B.9) is connected to the Langreth–Wilkins rules for the construction of the selfenergies. To derive the Langreth–Wilkins rules the property (B.8) is used. For the relation (B.36) we use instead the property (B.35). Beside, for the second Born approximation, we have verified equation (B.36) analytically (the proof is not be shown here) and numerically.

B.6 Extended GKBA

The GKBA is formulated for a time-diagonal equation and it aims directly at the time evolution of the density matrix. In this way we loose the part of information contained in the Green's function, notably the spectral function, which may be used for the construction of the ground state. Hence we wish now to investigate what will happen if we extend the GKBA approximation to the off-diagonal equation. This corresponds to use $I[G] \rightarrow I[\tilde{G}]$ in the collision part of the KBE equations for G^{\lessgtr} , see Fig. B.1.

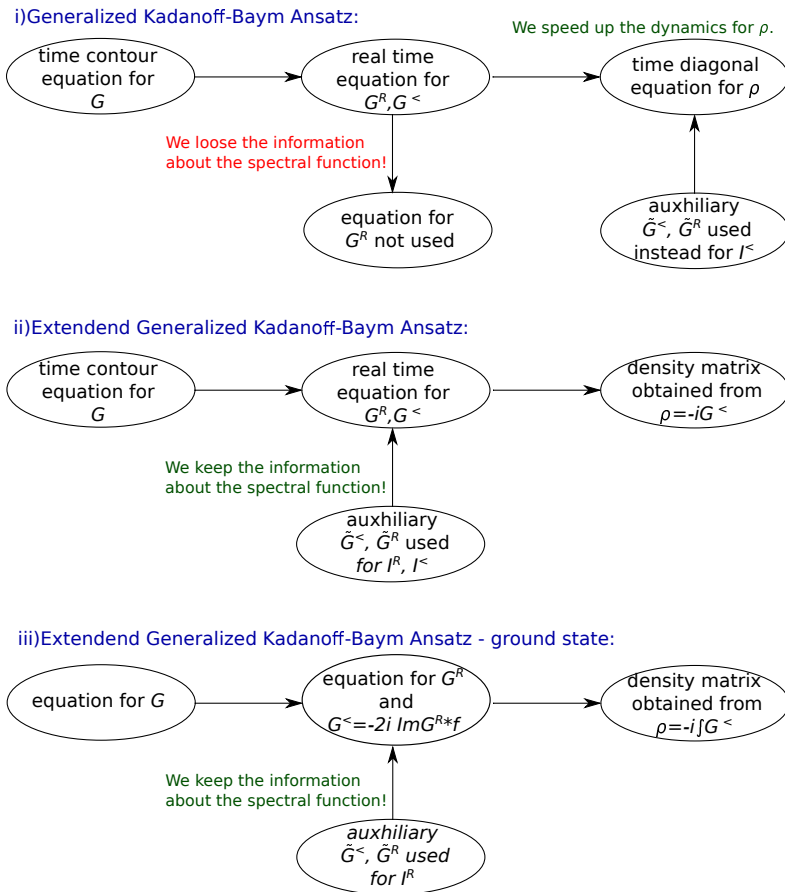


Figure B.1: A flowchart showing the loss of the spectral information within the Generalized Kadanoff–Baym Ansatz. The information will be restored if the ansatz is applied in the real time equations for G^R and $G^<$. Such Extended Generalized Kadanoff–Baym Ansatz (EGKBA) is used in groundstate calculations, where the equation for G^R is to be solved.

Extended GKBA.– In the Extended Generalized Kadanoff–Baym Ansatz (EGKBA), we approximate the collision part of the KBE

$$(i\partial_t - h_{HF}(t))G^{\lessgtr}(t, t') = \int d\bar{t}(\Sigma^{\lessgtr}[\tilde{G}](t, \bar{t})\tilde{G}^A(\bar{t}, t') + \Sigma^R[\tilde{G}](t, \bar{t})\tilde{G}^{\lessgtr}(\bar{t}, t')). \quad (\text{B.37})$$

This differential equations can be formally solved by integration starting from the initial uncorrelated Hartree–Fock ground state

$$G^{\lessgtr} = G_{HF}^{\lessgtr} + G_{HF}^{\lessgtr}\Sigma^A[\tilde{G}]\tilde{G}^A + G_{HF}^R\Sigma^{\lessgtr}[\tilde{G}]\tilde{G}^A + G_{HF}^R\Sigma^R[\tilde{G}]\tilde{G}^{\lessgtr}. \quad (\text{B.38})$$

How to evolve the retarded (advanced) Green's in order to be consistent with (B.8)? We will now show that the corresponding evolution of retarded (advanced) Green's function must obey to

$$(i\partial_t - h_{HF}(t))G^{R/A}(t, t') = \delta(t, t') + \int d\bar{t}\Sigma^{R/A}[\tilde{G}](t, \bar{t})\tilde{G}^{R/A}(\bar{t}, t'). \quad (\text{B.39})$$

This is formally solved by integration starting from the initial uncorrelated Hartree–Fock ground state

$$G^{R/A} = G_{HF}^{R/A} + G_{HF}^{R/A}\Sigma^{R/A}[\tilde{G}]\tilde{G}^{R/A}. \quad (\text{B.40})$$

Notice that this equation is not a standard Dyson equation.

Consistency check.– We start by the difference of the left hand sides of (B.38), so we have

$$\begin{aligned} G^> - G^< &= (G_{HF}^> - G_{HF}^<) + (G_{HF}^> - G_{HF}^<)\Sigma^A\tilde{G}^A \\ &+ G_{HF}^R(\Sigma^> - \Sigma^<)\tilde{G}^A + G_{HF}^R\Sigma^R(\tilde{G}^> - \tilde{G}^<), \end{aligned} \quad (\text{B.41})$$

and using the relations (B.11), (B.35) and (B.36) discussed above

$$\begin{aligned} G^> - G^< &= (G_{HF}^R - G_{HF}^A) + (G_{HF}^R - G_{HF}^A)\Sigma^A\tilde{G}^A \\ &+ G_{HF}^R(\Sigma^R - \Sigma^A)\tilde{G}^A + G_{HF}^R\Sigma^R(\tilde{G}^R - \tilde{G}^A). \end{aligned} \quad (\text{B.42})$$

By cancellation of some terms we get

$$G^> - G^< = G_{HF}^R - G_{HF}^A - G_{HF}^A\Sigma^A\tilde{G}^A + G_{HF}^R\Sigma^R\tilde{G}^R = G^R - G^A \quad (\text{B.43})$$

where we used equation (B.40). Thus, we have consistently extended the GKBA idea to double time domain. We will discuss a use of the EGKBA for obtaining the correlated ground state in the next section.

B.7 GKBA - correlated ground state

The correlated ground state is usually obtained by the adiabatic switching procedure [16, 57] starting from the uncorrelated Hartree–Fock state, i.e. the time evolution is truly performed. However it would be useful to have a direct procedure to compute the correlated ground state. If we follow the same logic as in the KBE case the crucial equation for us is

$$G^>(t, t') - G^<(t, t') = G^R(t, t') - G^A(t, t'). \quad (\text{B.44})$$

which must be fulfilled at all times. Assuming that in the long time limit the functions depend only on the time difference,

$$G^>(t - t') - G^<(t - t') = G^R(t - t') - G^A(t - t'), \quad (\text{B.45})$$

we can use the Fourier transform to express the equation in the omega space

$$G^>(\omega) - G^<(\omega) = G^R(\omega) - G^A(\omega). \quad (\text{B.46})$$

If we assume that except for the adiabatic switching there is no external force during the evolution then after the evolution the adiabatically prepared state is the equilibrium [16]. The equilibrium state can be represented by the Green's function (on the Matsubara imaginary time segment) which should fulfill the Kubo-Martin-Schwinger conditions and which can be analytically continued to real times. The analytically continued Green's function satisfy the same boundary conditions [13]. Then we can express the lesser Green's function as

$$G^<(\omega) = -2i\text{Im}G^R(\omega)f(\omega). \quad (\text{B.47})$$

This relation is known as fluctuation-dissipation theorem. The density is given by

$$\rho = \int \frac{d\omega}{2\pi} (-i)G^<(\omega) = - \int \frac{d\omega}{\pi} \text{Im}G^R(\omega)f(\omega). \quad (\text{B.48})$$

This should correspond to the density reached by the preparation of the correlated ground state by the adiabatic switching $\rho_{HF} \rightarrow \rho$. In the EGKBA approximation (see the previous section) the retarded Green's function is computed via

$$G^R(\omega) = G_{HF}^R(\omega) + G_{HF}^R(\omega)\Sigma^R[\tilde{G}](\omega)\tilde{G}^R(\omega). \quad (\text{B.49})$$

This rather interesting equation does not have the standard Dyson structure. The resulting Green's function is not guaranteed to have a positive spectral function, even if Σ generates the positive spectral function in the standard KBE. The mentioned analytic behavior of the retarded Green's function can lead to practical problems during the iteration of the ground state equations due to the numerically delicate evaluation of ρ .

B.8 GKBA - approximate correlated ground state

In isolated systems the auxiliary Green's function is usually the Hartree–Fock Green's function $\tilde{G}^R(\omega) = G_{HF}^R(\omega)$. Then the equation (B.49) becomes

$$G^R(\omega) = G_{HF}^R(\omega) + G_{HF}^R(\omega)\Sigma^R[G_{HF}](\omega)G_{HF}^R(\omega). \quad (\text{B.50})$$

This equation can be still problematic to solve since the spectral features mentioned above persist. However, we can make an observation about an approximate retarded Green's function given by

$$G_{\text{appr.}}^R \approx G_{HF}^R + G_{HF}^R\Sigma^R G^R = G_{HF}^R + G_{HF}^R\Sigma^R G_{HF}^R + G_{HF}^R\Sigma^R G_{HF}^R\Sigma^R G_{HF}^R \dots \quad (\text{B.51})$$

If the second and higher orders of the expansion are negligible, the approximate Green's function will be the same as in (B.50). The advantage of this equation is that it has the Dyson structure and gives less numerically delicate evaluation of ρ . The error between the approximate Green's function and the Green's function is of the second order in the interaction expansion

$$G_{\text{appr.}}^R - G^R = G_{HF}^R\Sigma^R G_{HF}^R\Sigma^R G_{HF}^R + \dots \quad (\text{B.52})$$

An example.— The solution of the approximate correlated ground state will be illustrated using a Hubbard dimer. In figure B.2 we show a comparison of the GKBA time evolution

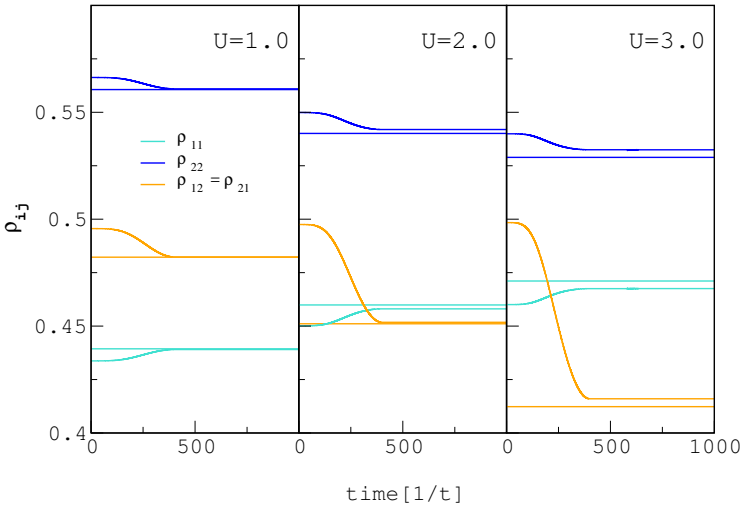


Figure B.2: The density matrix elements for the Hubbard dimer $v_1 - v_2 = 0.4t$ where $t = 1$ is the hopping and v_i are the onsite energies, for the different strengths of the on-site interactions. Time is measured in inverse of the hopping t . A comparison of the GKBA time evolution with the approximate correlated ground state (straight lines).

with the direct solution of the approximate correlated ground state given by the equation (B.51). From the results we can clearly see that for strong enough interactions there is a deviation, since we compute the ground state only approximately. Here, the higher order terms given by (B.52) are not negligible. However, for lower interaction strengths where we can neglect these terms, the approximation is remarkably good.

Appendix C

Selfenergy approximations for steady state KBE

C.1 Second Born approximation

We use the Langreth–Wilkins rules [34] for the second order Feynman diagram (for the local interaction only one diagram can be considered due to cancellations) which is then formulated in terms of $G^{R,ss}$ and $G^{<,ss}$. The retarded selfenergy - correlation part reads

$$\begin{aligned}
 (\Sigma_c^{R,ss})_{ij}(\omega) = U_i U_j \int \int \frac{d\omega' d\omega''}{(2\pi)^2} & \left(G_{ij}^{R,ss}(\omega') G_{ji}^{<,ss}(\omega'') G_{ij}^{<,ss}(\omega - \omega' + \omega'') + \right. \\
 & + G_{ij}^{R,ss}(\omega') G_{ji}^{<,ss}(\omega'') G_{ij}^{R,ss}(\omega - \omega' + \omega'') - \\
 & - G_{ij}^{R,ss}(\omega') G_{ji}^{<,ss}(\omega'') (G_{ji}^{R,ss})^*(\omega - \omega' + \omega'') + \\
 & + G_{ij}^{<,ss}(\omega') (G_{ij}^{R,ss})^*(\omega'') G_{ij}^{<,ss}(\omega - \omega' + \omega'') + \\
 & \left. + G_{ij}^{<,ss}(\omega') G_{ji}^{<,ss}(\omega'') G_{ij}^{R,ss}(\omega - \omega' + \omega'') \right), \tag{C.1}
 \end{aligned}$$

and the lesser selfenergy - correlation part reads

$$\begin{aligned}
 (\Sigma_c^{<,ss})_{ij}(\omega) = U_i U_j \int \int \frac{d\omega' d\omega''}{(2\pi)^2} & \left(G_{ij}^{<,ss}(\omega') G_{ji}^{<,ss}(\omega'') G_{ij}^{<,ss}(\omega - \omega' + \omega'') + \right. \\
 & + G_{ij}^{<,ss}(\omega') G_{ji}^{R,ss}(\omega'') G_{ij}^{<,ss}(\omega - \omega' + \omega'') - \\
 & - G_{ij}^{<,ss}(\omega') (G_{ij}^{R,ss})^*(\omega'') G_{ij}^{<,ss}(\omega - \omega' + \omega'') \left. \right). \tag{C.2}
 \end{aligned}$$

C.2 T-matrix approximation

Here, we first construct a two-particle propagator

$$\begin{aligned}\mathcal{G}_{ij}^{R,ss}(\omega) &= \int \frac{d\omega'}{2\pi} (G_{ij}^{R,ss}(\omega) G_{ij}^{<,ss}(\omega - \omega') + G_{ij}^{R,ss}(\omega) G_{ij}^{R,ss}(\omega - \omega') - \\ &\quad - G_{ij}^{R,ss}(\omega) (G_{ji}^{R,ss})^*(\omega - \omega') + G_{ij}^{<,ss}(\omega) G_{ij}^{R,ss}(\omega - \omega')), \quad (\text{C.3}) \\ \mathcal{G}_{ij}^{<,ss}(\omega) &= \int \frac{d\omega'}{2\pi} G_{ij}^{<,ss}(\omega) G_{ij}^{<,ss}(\omega - \omega').\end{aligned}$$

Then we find the retarded T-matrix from a Dyson-like equation by inversion:

$$\begin{aligned}(U * \mathcal{G}^R)_{ij}(\omega) &= \sum_l U_{il} \mathcal{G}_{lj}^{R,ss}(\omega), \\ T_{ij}^{R,ss}(\omega) &= -i \sum_l ((\delta - iU * \mathcal{G}^R(\omega))^{-1})_{il} U_{lj},\end{aligned}\quad (\text{C.4})$$

and the lesser T-matrix is determined by

$$T_{ij}^{<,ss}(\omega) = \sum_{kl} T_{ik}^{R,ss}(\omega) G_{kl}^{<,ss}(\omega) (T_{jl}^{R,ss})^*(\omega). \quad (\text{C.5})$$

The TMA selfenergy is then found by closing the T-matrix equation with the Green's function

$$\begin{aligned}(\Sigma_{HFc}^{R,ss})_{ij}(\omega) &= \int \frac{d\omega'}{2\pi} (T_{ij}^{R,ss}(\omega + \omega') G_{ji}^{<,ss}(\omega') + T_{ij}^{<,ss}(\omega + \omega') (G_{ij}^{R,ss})^*(\omega')), \\ (\Sigma_c^{<,ss})_{ij}(\omega) &= \int \frac{d\omega'}{2\pi} (T_{ij}^{<,ss}(\omega + \omega') G_{ji}^{<,ss}(\omega') + T_{ij}^{<,ss}(\omega + \omega') G_{ji}^{R,ss}(\omega') \\ &\quad - T_{ij}^{<,ss}(\omega + \omega') (G_{ij}^{R,ss})^*(\omega')).\end{aligned}\quad (\text{C.6})$$

Note that in the retarded selfenergy the Hartree–Fock part is already included in this formulation. To obtain pure correlation part one subtracts the Hartree–Fock part

$$(\Sigma_c^{R,ss})_{ij}(\omega) = (\Sigma_{HFc}^{R,ss})_{ij}(\omega) - (\Sigma_{HF}^{R,ss})_{ij} = (\Sigma_{HFc}^{R,ss})_{ij}(\omega) - \delta_{ij} U_i n_i^{ss}. \quad (\text{C.7})$$

Appendix D

Gradient expansion

D.1 Retarded Green's function

We start with the equation of motion for the retarded Green's function in differential form

$$-i\partial_{t'} G^R(t, t') - G^R(t, t')h(t') = \delta(t - t') + \int dt_1 G^R(t, t_1)\Sigma^R(t_1, t'), \quad (\text{D.1})$$

and apply the gradient expansion rules derived above so that we obtain the expression

$$(-i/2\partial_T + \omega)G^R - G^R h - i/2\partial_\omega G^R \partial_T h \approx 1 + G^R \Sigma^R + i/2(\partial_\omega G^R \partial_T \Sigma^R - \partial_T G^R \partial_\omega \Sigma^R). \quad (\text{D.2})$$

After some algebra we get

$$G^R(\omega - h - \Sigma^R) \approx 1 + i/2\partial_T G^R(1 - \partial_\omega \Sigma^R) + i/2\partial_\omega G^R \partial_T (h + \Sigma^R). \quad (\text{D.3})$$

which by multiplication can be transformed to

$$G^R \approx [1 + i/2\partial_T G^R(1 - \partial_\omega \Sigma^R) + i/2\partial_\omega G^R \partial_T (h + \Sigma^R)] \cdot (\omega - h - \Sigma^R)^{-1}. \quad (\text{D.4})$$

Further we can use $G^R \approx (\omega - h - \Sigma^R)^{-1}$ in terms already containing time derivative

$$G^R \approx (\omega - h - \Sigma^R)^{-1} + i/2[\partial_T G^R(1 - \partial_\omega \Sigma^R)G^R + \partial_\omega G^R \partial_T (h + \Sigma^R)G^R]. \quad (\text{D.5})$$

For the terms already containing time derivative where $G^R \approx (\omega - h - \Sigma^R)^{-1}$ we can derive

$$\partial_\omega(G^R G^{R-1}) = \partial_\omega(G^R(\omega - h - \Sigma^R)) = \partial_\omega G^R G^{R-1} + G^R(1 - \partial_\omega \Sigma^R) = 0, \quad (\text{D.6})$$

and thus from the last equivalence we get

$$\partial_\omega G^R = -G^R(1 - \partial_\omega \Sigma^R)G^R. \quad (\text{D.7})$$

Similarly to the derivative with respect to ω we can derive the time derivative

$$\partial_T G^R = G^R \partial_T (h + \Sigma^R) G^R. \quad (\text{D.8})$$

We can derive another useful relation

$$\partial_T G^R (1 - \partial_\omega \Sigma^R) G^R \approx G^R \partial_T (h + \Sigma^R) G^R (1 - \partial_\omega \Sigma^R) G^R \approx -G^R \partial_T (h + \Sigma^R) \partial_\omega G^R. \quad (\text{D.9})$$

The relation (D.9) can be used in the relation for retarded function (D.5) so that the final result up to linear order is in symmetric form

$$G^R \approx (\omega - h - \Sigma^R)^{-1} + i/2[\partial_\omega G^R \partial_T (h + \Sigma^R) G^R - G^R \partial_T (h + \Sigma^R) \partial_\omega G^R]. \quad (\text{D.10})$$

D.2 Lesser Green's function

We start with the equation of motion for the lesser Green's function in integral form

$$G^<(t, t') = \int \int d\bar{t} d\bar{t}' G^R(t, \bar{t}) \Sigma^<(\bar{t}, \bar{t}') G^A(\bar{t}', t') = \int d\bar{t} G^R(t, \bar{t}) I^<(\bar{t}, t'), \quad (\text{D.11})$$

where $I^<(t, t') = \int d\bar{t} \Sigma^<(t, \bar{t}) G^A(\bar{t}, t')$ is the scattering integral. In this form we can apply the gradient expansion rule (A.16) twice to get

$$\begin{aligned} G^< &\approx G^R I^< + i/2(\partial_\omega G^R \partial_T I^< - \partial_T G^R \partial_\omega I^<), \\ I^< &\approx \Sigma^< G^A + i/2(\partial_\omega \Sigma^< \partial_T G^A - \partial_T \Sigma^< \partial_\omega G^A). \end{aligned} \quad (\text{D.12})$$

Plugging the expansion of $I^<$ into the expansion of $G^<$ we get

$$\begin{aligned} G^< &\approx G^R [\Sigma^< G^A + i/2(\partial_\omega \Sigma^< \partial_T G^A - \partial_T \Sigma^< \partial_\omega G^A)] + \\ &+ i/2(\partial_\omega G^R \partial_T [\Sigma^< G^A \dots] - \partial_T G^R \partial_\omega [\Sigma^< G^A \dots]). \end{aligned} \quad (\text{D.13})$$

Neglecting the higher order terms in velocity and the higher order derivatives, we arrive at

$$\begin{aligned} G^< &\approx G^R \Sigma^< G^A + i/2[G^R \partial_\omega \Sigma^< \partial_T G^A - G^R \partial_T \Sigma^< \partial_\omega G^A + \partial_\omega G^R \partial_T \Sigma^< G^A \\ &+ \partial_\omega G^R \Sigma^< \partial_T G^A - \partial_T G^R \partial_\omega \Sigma^< G^A - \partial_T G^R \Sigma^< \partial_\omega G^A]. \end{aligned} \quad (\text{D.14})$$

In the term $G^R \Sigma^< G^A$ we use the retarded Green's function expression (D.10) to pull out the terms linear in time derivatives (the same for the advanced Green's function)

$$\begin{aligned}
G^< &\approx (\omega - h - \Sigma^R)^{-1} \Sigma^< (\omega - h - \Sigma^A)^{-1} + \\
&+ i/2 [\partial_\omega G^R \partial_T (h + \Sigma^R) G^R - G^R \partial_T (h + \Sigma^R) \partial_\omega G^R] \cdot \Sigma^< \cdot (\omega - h - \Sigma^A)^{-1} + \\
&+ (\omega - h - \Sigma^R)^{-1} \cdot \Sigma^< \cdot i/2 [\partial_\omega G^A \partial_T (h + \Sigma^A) G^A - G^A \partial_T (h + \Sigma^A) \partial_\omega G^A] + \\
&+ i/2 [G^R \partial_\omega \Sigma^< \partial_T G^A - G^R \partial_T \Sigma^< \partial_\omega G^A + \partial_\omega G^R \partial_T \Sigma^< G^A + \\
&+ \partial_\omega G^R \Sigma^< \partial_T G^A - \partial_T G^R \partial_\omega \Sigma^< G^A - \partial_T G^R \Sigma^< \partial_\omega G^A].
\end{aligned} \tag{D.15}$$

Now we can write $(\omega - h - \Sigma^{R/A})^{-1} \approx G^{R/A}$ in the terms proportional to time derivatives

$$\begin{aligned}
G^< &\approx (\omega - h - \Sigma^R)^{-1} \Sigma^< (\omega - h - \Sigma^A)^{-1} + \\
&+ i/2 [\partial_\omega G^R \partial_T (h + \Sigma^R) G^R \Sigma^< G^A - G^R \partial_T (h + \Sigma^R) \partial_\omega G^R \Sigma^< G^A] + \\
&+ i/2 [G^R \Sigma^< \partial_\omega G^A \partial_T (h + \Sigma^A) G^A - G^R \Sigma^< G^A \partial_T (h + \Sigma^A) \partial_\omega G^A] + \\
&+ i/2 [G^R \partial_\omega \Sigma^< \partial_T G^A - G^R \partial_T \Sigma^< \partial_\omega G^A + \partial_\omega G^R \partial_T \Sigma^< G^A + \\
&+ \partial_\omega G^R \Sigma^< \partial_T G^A - \partial_T G^R \partial_\omega \Sigma^< G^A - \partial_T G^R \Sigma^< \partial_\omega G^A].
\end{aligned} \tag{D.16}$$

Next we use that $G^R \Sigma^< G^A \approx G^<$ in the terms proportional to time derivatives, collect and sort all terms linear in velocity:

$$\begin{aligned}
G^< &\approx (\omega - h - \Sigma^R)^{-1} \Sigma^< (\omega - h - \Sigma^A)^{-1} + i/2 [\partial_\omega G^R \partial_T \Sigma^< G^A - \\
&- G^R \partial_T \Sigma^< \partial_\omega G^A + \partial_\omega G^R \partial_T (h + \Sigma^R) G^< - G^< \partial_T (h + \Sigma^A) \partial_\omega G^A + \\
&+ G^R \Sigma^< \partial_\omega G^A \partial_T (h + \Sigma^A) G^A + G^R \partial_\omega \Sigma^< \partial_T G^A + \partial_\omega G^R \Sigma^< \partial_T G^A - \\
&- G^R \partial_T (h + \Sigma^R) \partial_\omega G^R \Sigma^< G^A - \partial_T G^R \partial_\omega \Sigma^< G^A - \partial_T G^R \Sigma^< \partial_\omega G^A].
\end{aligned} \tag{D.17}$$

We further work with the last two lines, where we would like to replace $\partial_T G^{R/A}$ with the relation (D.9):

$$\begin{aligned}
G^< &\approx (\omega - h - \Sigma^R)^{-1} \Sigma^< (\omega - h - \Sigma^A)^{-1} + i/2 [\partial_\omega G^R \partial_T \Sigma^< G^A - \\
&- G^R \partial_T \Sigma^< \partial_\omega G^A + \partial_\omega G^R \partial_T (h + \Sigma^R) G^< - G^< \partial_T (h + \Sigma^A) \partial_\omega G^A + \\
&+ (G^R \Sigma^< \partial_\omega G^A + G^R \partial_\omega \Sigma^< G^A + \partial_\omega G^R \Sigma^< G^A) \partial_T (h + \Sigma^A) G^A - \\
&- G^R \partial_T (h + \Sigma^R) (\partial_\omega G^R \Sigma^< G^A - G^R \partial_\omega \Sigma^< G^A - G^R \Sigma^< \partial_\omega G^A)].
\end{aligned} \tag{D.18}$$

Each of the last two lines can be rewritten with help of $\partial_\omega G^< \approx \partial_\omega (G^R \Sigma^< G^A)$, so that the final expression up to linear order is

$$\begin{aligned}
G^< &\approx (\omega - h - \Sigma^R)^{-1} \Sigma^< (\omega - h - \Sigma^A)^{-1} + i/2 [\partial_\omega G^R \partial_T \Sigma^< G^A - \\
&- G^R \partial_T \Sigma^< \partial_\omega G^A + \partial_\omega G^R \partial_T (h + \Sigma^R) G^< - G^< \partial_T (h + \Sigma^A) \partial_\omega G^A + \\
&+ \partial_\omega G^< \partial_T (h + \Sigma^A) G^A - G^R \partial_T (h + \Sigma^R) \partial_\omega G^<].
\end{aligned} \tag{D.19}$$

Appendix E

Optimal control - details

The GRAPE algorithm optimizes a time-discretized version of the controls $\alpha^i(T)$ in the interval $(0, T)$ where $T = n\Delta\tau$. Then the controls are described by vectors $\alpha^i = (\alpha_1^i, \alpha_2^i, \dots, \alpha_n^i)$ where α_n^i is the value of control i on the interval between $(n-1)\Delta\tau$ and $n\Delta\tau$. In the case of a single control field, in our case the Peierls phase, the Hamiltonian can be described as $H(T) = H_0 + V(\alpha(T))$, and the overlap of the discretized control can be written

$$\langle \psi_{\text{targ}} | \psi_T \rangle = \langle \psi_{\text{targ}} | \hat{U}(T, 0) | \psi_{\text{init}} \rangle. \quad (\text{E.1})$$

Here $\hat{U}(T, 0) = \hat{T}\{e^{-i\sum_k H(\alpha^k)\Delta\tau}\}$ is the evolution operator. The evolution operator $\hat{U}(T, 0)$ can be expanded as

$$\langle \psi_{\text{targ}} | \hat{U}(T, t_{m+1}) e^{-i[H_0 + V(\alpha_m)]\Delta\tau} \hat{U}(t_{m-1}, 0) | \psi_{\text{init}} \rangle \equiv \langle m | e^{-i[H_0 + V(\alpha_m)]\Delta\tau} | m-1 \rangle, \quad (\text{E.2})$$

where we introduced a short notation showing the dependence on α_m . With this notation the elements of the gradient of the fidelity function are proportional to

$$\partial_{\alpha_m} \langle \psi_{\text{targ}} | \psi_T \rangle = \langle m | \partial_{\alpha_m} e^{-i[H_0 + V(\alpha_m)]\Delta\tau} | m-1 \rangle. \quad (\text{E.3})$$

The derivative of the overlap with respect to α_m can be described exactly using the spectral theorem. This method[106] is suitable for obtaining very accurate results for small systems, but it scales very badly, as it requires a full eigen-decomposition. Instead it is much easier to use a subspace method. However, using the Lanczos method, the derivative in the equation (E.3) needs to be approximated. For short time-steps we find adequate to use a split operator method to calculate this derivative

$$\begin{aligned} \partial_{\alpha_m} e^{-i[H_0 + V]\Delta\tau} &\approx \partial_{\alpha_m} \left(e^{-iH_0 \frac{\Delta\tau}{2}} e^{-iV(\alpha_m)\Delta\tau} e^{-iH_0 \frac{\Delta\tau}{2}} \right) = \\ &= -i\Delta\tau e^{-iH_0 \frac{\Delta\tau}{2}} \partial_{\alpha_m} V e^{-iV\Delta\tau} e^{-iH_0 \frac{\Delta\tau}{2}}, \end{aligned} \quad (\text{E.4})$$

where $\partial_{\alpha_m} V$ can be placed ambiguously as it commutes with $e^{-iV\Delta\tau}$. The gradient element m can be finally expressed as

$$\partial_{\alpha_m} \langle \psi_{\text{target}} | \psi_T \rangle = -i\Delta\tau \langle \psi_{m+1} | e^{-iH_0 \frac{\Delta\tau}{2}} \partial_{\alpha_m} V e^{-iV(\alpha_m)\Delta\tau} e^{-iH_0 \frac{\Delta\tau}{2}} | \psi_{m-1} \rangle. \quad (\text{E.5})$$

After the evolution is performed, and the fidelity and its gradient are computed, the results are fit into the optimizing procedure.

The whole control algorithm can be summarized in 5 steps:

- i) Make an initial guess of the control amplitudes $\alpha^{(0)}$.
- ii) Calculate the fidelity function, $\mathcal{F}(\alpha)$, and the gradient of the fidelity function with respect to the control amplitudes, $\nabla\mathcal{F}(\alpha)$.
- iii) Escape the loop if the fidelity has reached some threshold value, or if the gradient is very close to 0.
- iv) Calculate $\alpha^{(j+1)}$ using some optimization procedure (in our case Limited memory Broyden–Fletcher–Goldfarb–Shanno).
- v) Continue at ii).

